DOE/ER/40762-009
UMD-PP#02-011
YITP-SB-01-51

Theory of deeply virtual Compton scattering on the nucleon

A.V. Belitsky[a,b,c], **D. Müller**[c,d], **A. Kirchner**[d]

[a] *Department of Physics*
University of Maryland at College Park
MD 20742-4111, College Park, USA

[b] *C.N. Yang Institute for Theoretical Physics*
State University of New York at Stony Brook
NY 11794-3840, Stony Brook, USA

[c] *Fachbereich Physik, Universität Wuppertal*
D-42097 Wuppertal, Germany

[d] *Institut für Theoretische Physik, Universität Regensburg*
D-93040 Regensburg, Germany

Abstract

We compute the cross section for leptoproduction of the real photon off the nucleon, which is sensitive to the deeply virtual Compton scattering amplitude with power accuracy. Our considerations go beyond the leading twist and involve the complete analysis in the twist-three approximation. We discuss consequences of the target and lepton beam polarizations for accessing the generalized parton distributions from experimental measurements of the azimuthal angular dependence of the final state photon or nucleon. We introduce several sets of asymmetries, defined as Fourier moments with respect to the azimuthal angle, which allow for a clear separation of the twist-two and -three sectors. Relying on a simple ansatz for the generalized parton distributions, we give quantitative estimates for azimuthal and spin asymmetries, discuss the uncertainties of these predictions brought in by radiative corrections, and compare them with experimental data as well as other theoretical expectations. Furthermore, we derive a general parametrization of the DVCS amplitudes in the region of small Bjorken variable.

Contents

1 Introduction

The complicated long distance dynamics of hadron constituents, not controllable by well-defined methods of perturbative QCD, was studied over decades by means of experimental measurements with inclusive lepton-hadron and hadron-hadron scattering. Information on the nucleon's parton structure, originating from them, can be used to access inclusive properties of hadrons, like parton distributions. However, they are insufficient to constrain the detailed picture of the hadron wave function in full diversity of its manifestations.

The parton distributions and correlation functions encode the long-distance dynamics of inclusive cross sections. The former accompany the interaction of a hard probe with a single parton, while the latter are involved in the rescattering off a multi-parton system. Both of them are given by the interference of light-cone wave functions with equal or different numbers of constituents in the amplitude and its conjugate, but the same total momentum flowing through each of them. This obviously simplifies the theoretical description on the one hand and, however, lacks a plethora of important features of strong interaction dynamics on the other one.

As has been recently understood, a straightforward generalization of the aforementioned parton densities via new nonperturbative nucleon characteristics arises in exclusive two-photon processes in the generalized Bjorken region [1], e.g., in the Compton scattering with highly virtual incoming γ-quantum [2, 3, 4], and in the hard photoproduction of mesons [5]. These are genuinely exclusive processes. Here one finds off-forward matrix elements, as distinguished from the forward ones in inclusive reactions, of certain non-local quark and gluon composite operators, which give rise to the so-called generalized parton distribution (GPDs). They carry information on parton distributions, distribution amplitudes, and form factors and are of interest in their own right. Moreover, they can shed some light on the intriguing spin structure of the proton as they provide a way to get access to the parton's angular momentum unreachable elsewhere [2].

The deeply virtual Compton scattering (DVCS) is the hard photoproduction of a real photon, i.e., $\gamma^* N \to \gamma N'$. Being a process involving a single hadron, it is one of the cleanest tools in the problem of constraining GPDs from data. The theoretical efforts and achievements are supported by pioneering experimental results from HERMES [6], HERA [7, 8], and CLAS [9] collaborations, and encouraging future plans [10, 11, 12].

This paper is a culmination of our previous studies initiated in Ref. [13] and completes the

theoretical background of the theory of DVCS by an exhaustive set of analytical results for the cross section to the twist-three accuracy for all possible hadron and lepton polarizations involved. Numerical studies performed here are done in the so-called Wandzura-Wilczek (WW) approximation for the twist-three GPDs, developed by two of us in Ref. [14]. Our present consideration is compatible with the one performed earlier in a fully numerical manner [15], see also Ref. [16]. We also comment on the effect of multi-particle correlations, provided we cease using the WW relations. The knowledge of power corrections to the leading twist-two results, with the twist-three terms being the first of them, is indispensable because the hard momentum of the incoming photon is not in the deep Euclidean domain for the present experiments. Therefore, the higher-twist contributions may affect the understanding of lowest order results. There is a number of theoretical uncertainties in phenomenological predictions for DVCS. Apart from the basically unconstrained shape of GPDs, which one models on the ground of previous theoretical considerations, these are higher-twist and -order effects, which alter the handbag approximation. The former include the dynamical and target mass corrections, see [17] for a partial result. While the latter have been computed in next-to-leading order (NLO) of perturbation theory in the strong coupling constant, see Refs. [18, 19, 20] for coefficient functions and Refs. [21, 22] for evolution kernels. Their numerical significance was studied in Refs. [23, 24, 25]. We will elaborate on these issues in the present study as well.

Our presentation is organized as follows. The next section recapitulates basic results for the DVCS amplitude to the twist-three accuracy and introduces the WW relations for the twist-three quark GPDs. In section 3 we briefly discuss the gluon double helicity-flip distributions, vanishing in the forward scattering off spin-1/2 targets. Their peculiar properties propagate into a genuinely distinguishable angular dependence in physical observables. This allows to access them, uncontaminated by leading twist quark GPDs. The differential leptoproduction cross section is extensively analyzed with power accuracy in section 4 for all polarization options of the lepton beam and target. Based on these results, we discuss a way to unravel GPDs from cross sections and then turn to appropriate definitions of the most favorable physical observables, i.e., asymmetries. These asymmetries allow to extract separate components of the angular dependence of the cross section, and in this manner to project out distributions carrying information on the orbital momentum of constituents in the nucleon. In section 6, we address the models for GPDs and discuss their diverse properties. We then study the magnitude of radiative corrections to the Compton form factors (CFFs). Next in section 7, fitting the model parameters to the recent H1 data in the small Bjorken-variable region, we give phenomenological predictions for the HERMES and CLAS kinematics. Finally, we conclude.

2 DVCS amplitude in twist-three approximation

Let us give a few basic definitions required for understanding of the Compton amplitude with power accuracy. Here we mainly recapitulate the results of our previous studies, where we have introduced the WW-approximation [14] for the twist-three GPDs, and used it for preliminary studies of appropriate physical observables [13].

The DVCS hadronic tensor is given by the time-ordered product of the electromagnetic currents $j_\mu = e\sum_i Q_i\bar\psi_i\gamma_\mu\psi_i$ of quarks, having fractional charge Q_i, which is sandwiched between hadronic states with different momenta. In leading order (LO) of perturbation theory it reads [14]

$$\begin{aligned} T_{\mu\nu}(q,P,\Delta) &= \frac{i}{e^2}\int dx \mathrm{e}^{ix\cdot q}\langle P_2|Tj_\mu(x/2)j_\nu(-x/2)|P_1\rangle \\ &= -\mathcal{P}_{\mu\sigma}g_{\sigma\tau}\mathcal{P}_{\tau\nu}\frac{q\cdot V_1}{P\cdot q} + (\mathcal{P}_{\mu\sigma}P_\sigma\mathcal{P}_{\rho\nu}+\mathcal{P}_{\mu\rho}P_\sigma\mathcal{P}_{\sigma\nu})\frac{V_{2\,\rho}}{P\cdot q} - \mathcal{P}_{\mu\sigma}i\epsilon_{\sigma\tau q\rho}\mathcal{P}_{\tau\nu}\frac{A_{1\,\rho}}{P\cdot q}\,, \end{aligned} \tag{1}$$

where we have kept all contributions up to twist-three accuracy. The three independent four-momenta are $P = P_1+P_2$, $\Delta = P_2-P_1$, and $q = (q_1+q_2)/2$, where the vectors P_1 (q_1) and P_2 (q_2) refer to the incoming and outgoing proton (photon) momentum, respectively. The decomposition (1) is similar to the one used in deeply inelastic scattering. Indeed, the twist-two part of the generalized structure functions V_1 and A_1 corresponds to the conventional one F_1 and g_1 (see the first paper of [13]). The current conservation in the tensor decomposition (1) is ensured by means of the projection operator

$$\mathcal{P}_{\mu\nu} = g_{\mu\nu} - \frac{q_{1\mu}q_{2\nu}}{q_1\cdot q_2}\,. \tag{2}$$

This is consistent with an explicit calculation of the amplitude (1) to twist-three accuracy [26, 14], see also Refs. [27, 28] for spinless targets.

In Eq. (1) we have used conventional conditions on the kinematical invariants in the Bjorken limit, $-q^2 \sim P\cdot q =$ large, $\Delta^2 =$ small, a generalized Bjorken variable $\xi = -q^2/q\cdot P =$ fixed. If both photons are virtual, we would have an extra scaling variable $\eta = \Delta\cdot q/P\cdot q$, the skewedness [1]. The reality of the outgoing photon implies the presence of only one scaling variable ξ, namely, for $q_2^2 = 0$ one has

$$\eta = -\xi\left(1+\frac{\Delta^2}{2\mathcal{Q}^2}\right)^{-1}\,.$$

It is convenient to introduce variables closely related to the ones used in deeply inelastic scattering, namely, the incoming photon virtuality and conventional Bjorken variable

$$\mathcal{Q}^2 \equiv -q_1^2\,, \qquad x_{\rm B} \equiv \frac{\mathcal{Q}^2}{2P_1\cdot q_1}\,, \tag{3}$$

with the latter related to ξ via

$$\xi = x_{\rm B} \frac{1+\frac{\Delta^2}{2\mathcal{Q}^2}}{2-x_{\rm B}+x_{\rm B}\frac{\Delta^2}{\mathcal{Q}^2}}\,. \tag{4}$$

In the above Eq. (1), $V_{2\,\rho}$ is expressed in terms of the vector $V_{1\,\rho}$ and axial-vector $A_{1\,\rho}$ functions[1],

$$V_{2\,\rho} = \xi V_{1\,\rho} - \frac{\xi}{2}\frac{P_\rho}{P\cdot q} q\cdot V_1 + \frac{i}{2}\frac{\epsilon_{\rho\sigma\Delta q}}{P\cdot q} A_{1\,\sigma}\,. \tag{5}$$

The amplitudes V_1 and A_1 depend on the scaling variable ξ, momentum transfer Δ^2, and hard momentum of the probe $\mathcal{Q}^2$. The latter dependence is logarithmic and is governed by a generalized off-forward evolution equation [30, 31], which is presently known to two-loop order [21, 22]. In order to simplify notations considerably, we will drop the dependence on Δ^2 and $\mathcal{Q}^2$ when it is not essential for the presentation and restore them in sections dealing with the modeling of GPDs and numerical estimates.

A general decomposition of the vector and axial-vector amplitudes, in a complete basis of CFFs to twist-three accuracy, reads

$$V_{1\,\rho} = P_\rho \frac{q\cdot h}{q\cdot P}\mathcal{H} + P_\rho \frac{q\cdot e}{q\cdot P}\mathcal{E} + \Delta^\perp_\rho \frac{q\cdot h}{q\cdot P}\mathcal{H}^3_+ + \Delta^\perp_\rho \frac{q\cdot e}{q\cdot P}\mathcal{E}^3_+ + \widetilde{\Delta}^\perp_\rho \frac{q\cdot \widetilde{h}}{q\cdot P}\widetilde{\mathcal{H}}^3_- + \widetilde{\Delta}^\perp_\rho \frac{q\cdot \widetilde{e}}{q\cdot P}\widetilde{\mathcal{E}}^3_-\,, \tag{6}$$

$$A_{1\,\rho} = P_\rho \frac{q\cdot \widetilde{h}}{q\cdot P}\widetilde{\mathcal{H}} + P_\rho \frac{q\cdot \widetilde{e}}{q\cdot P}\widetilde{\mathcal{E}} + \Delta^\perp_\rho \frac{q\cdot \widetilde{h}}{q\cdot P}\widetilde{\mathcal{H}}^3_+ + \Delta^\perp_\rho \frac{q\cdot \widetilde{e}}{q\cdot P}\widetilde{\mathcal{E}}^3_+ + \widetilde{\Delta}^\perp_\rho \frac{q\cdot h}{q\cdot P}\mathcal{H}^3_- + \widetilde{\Delta}^\perp_\rho \frac{q\cdot e}{q\cdot P}\mathcal{E}^3_-\,, \tag{7}$$

where $\Delta^\perp_\rho \equiv \Delta_\rho + \xi P_\rho$, $\widetilde{\Delta}^\perp_\rho \equiv i\epsilon_{\rho\Delta Pq}/P\cdot q$, and the Dirac bilinears are conventionally defined by

$$\begin{aligned} h_\rho &= \bar{U}(P_2,S_2)\gamma_\rho U(P_1,S_1)\,, & e_\rho &= \bar{U}(P_2,S_2) i\sigma_{\rho\sigma}\frac{\Delta_\sigma}{2M} U(P_1,S_1)\,,\\ \widetilde{h}_\rho &= \bar{U}(P_2,S_2)\gamma_\rho\gamma_5 U(P_1,S_1)\,, & \widetilde{e}_\rho &= \frac{\Delta_\rho}{2M}\bar{U}(P_2,S_2)\gamma_5 U(P_1,S_1)\,, \end{aligned} \tag{8}$$

with U being the nucleon bispinor normalized as $\bar{U}(P_1)U(P_1) = 2M$.

The CFFs introduced in Eqs. (6,7) are given by a convolution of perturbatively calculable coefficient functions $C^{(\pm)}$ and a set of twist-two and -three GPDs via

$$\begin{aligned} \left\{\mathcal{H},\mathcal{E},\mathcal{H}^3_+,\mathcal{E}^3_+,\widetilde{\mathcal{H}}^3_-,\widetilde{\mathcal{E}}^3_-\right\}(\xi) &= \int_{-1}^1 dx\, C^{(-)}(\xi,x)\left\{H,E,H^3_+,E^3_+,\widetilde{H}^3_-,\widetilde{E}^3_-\right\}(x,\eta)_{|\eta=-\xi}\,,\\ \left\{\widetilde{\mathcal{H}},\widetilde{\mathcal{E}},\widetilde{\mathcal{H}}^3_+,\widetilde{\mathcal{E}}^3_+,\mathcal{H}^3_-,\mathcal{E}^3_-\right\}(\xi) &= \int_{-1}^1 dx\, C^{(+)}(\xi,x)\left\{\widetilde{H},\widetilde{E},\widetilde{H}^3_+,\widetilde{E}^3_+,H^3_-,E^3_-\right\}(x,\eta)_{|\eta=-\xi}\,, \end{aligned} \tag{9}$$

where $1/\mathcal{Q}^2$-power suppressed effects have been neglected, i.e., $\eta = -\xi$. The GPDs $\{H,\ldots,\widetilde{E}^3_-\}$ and $\{\widetilde{H},\ldots,E^3_-\}$ are related to the off-forward matrix elements of the vector and axial quark

[1] We use the conventions for Dirac and Lorentz tensors from Itzykson and Zuber [29], e.g., $\epsilon^{0123} = +1$.

operators, see Eqs. (116) and (117), respectively. We have implied that there is a summation on the right-hand side of the above equations over the quark species, so that they have to be understood as follows

$$C^{(\mp)}F \to \sum_{i=u,d,s} C_i^{(\mp)} F_i \,, \tag{10}$$

with $C^{(\mp)}$ having perturbative expansion

$$C^{(\mp)} = C^{(\mp)}_{(0)} + \frac{\alpha_s}{2\pi} C^{(\mp)}_{(1)} + \mathcal{O}(\alpha_s^2)\,.$$

To reduce the number of equations we have introduced unifying conventions F and $F^3_\pm$ for all twist-two and -three functions, which run over H, E, $\widetilde{H}$, and $\widetilde{E}$ species as in Eq. (9). At LO in the QCD coupling constant the coefficient functions read for the even $(-)$ and odd $(+)$ parity sectors

$$\xi\, C^{(\mp)}_{(0)i}\,(\xi, x) = \frac{Q_i^2}{1 - x/\xi - i0} \mp \frac{Q_i^2}{1 + x/\xi - i0}\,. \tag{11}$$

According to [14], all twist-three GPDs are decomposed into the so-called WW term $F^{WW}_\pm$ (later recalculated in Ref. [32]) and a function $F^{qGq}_\pm$ that contains new dynamical information arising from antiquark-gluon-quark correlations:

$$F^3_\pm = F^{WW}_\pm + F^{qGq}_\pm\,. \tag{12}$$

The WW parts are expressed solely in terms of the twist-two functions $F = \{H, E, \widetilde{H}, \widetilde{E}\}$ and have the following form

$$\begin{aligned}
F^{WW}_+(x,\xi) &= \int_{-1}^1 \frac{dy}{\xi}\, W_+\left(\frac{x}{\xi}, \frac{y}{\xi}\right)\left(y\frac{\overleftarrow{\partial}}{\partial y} - \xi\frac{\overrightarrow{\partial}}{\partial \xi}\right) F(y,\xi) - \frac{1}{\xi}F(x,\xi) - \frac{4M^2\, F^\perp_+(x,\xi)}{(1-\xi^2)(\Delta^2 - \Delta^2_{\rm min})}\,,\\
F^{WW}_-(x,\xi) &= -\int_{-1}^1 \frac{dy}{\xi}\, W_-\left(\frac{x}{\xi}, \frac{y}{\xi}\right)\left(y\frac{\overleftarrow{\partial}}{\partial y} - \xi\frac{\overrightarrow{\partial}}{\partial \xi}\right) F(y,\xi) - \frac{4M^2\, F^\perp_-(x,\xi)}{(1-\xi^2)(\Delta^2 - \Delta^2_{\rm min})}\,,
\end{aligned} \tag{13}$$

for the '+' and '−' component of the twist-three GPDs in the WW-approximation, respectively. The minimum value of the momentum transfer squared $\Delta^2_{\rm min}$ is given below in Eq. (31). The functions $F^\perp_\pm$ specifically appear for the spin-1/2 targets, cf. Refs. [14, 34, 28, 33, 35, 36] for the pion target, and read

$$\begin{aligned}
H^\perp_\pm(x,\xi) &= \mp\frac{\Delta^2}{4M^2}\int_{-1}^1 dy \left\{\xi W_\pm\left(\frac{x}{\xi}, \frac{y}{\xi}\right)(H+E)\,(y,\xi) - W_\mp\left(\frac{x}{\xi}, \frac{y}{\xi}\right)\widetilde{H}(y,\xi)\right\},\\
E^\perp_\pm(x,\xi) &= \pm\int_{-1}^1 dy \left\{\xi W_\pm\left(\frac{x}{\xi}, \frac{y}{\xi}\right)(H+E)\,(y,\xi) - W_\mp\left(\frac{x}{\xi}, \frac{y}{\xi}\right)\widetilde{H}(y,\xi)\right\},\\
\widetilde{H}^\perp_\pm(x,\xi) &= \pm\int_{-1}^1 dy \left\{\xi\left(1 - \frac{\Delta^2}{4M^2}\right) W_\pm\left(\frac{x}{\xi}, \frac{y}{\xi}\right)\widetilde{H}(y,\xi) + \frac{\Delta^2}{4M^2} W_\mp\left(\frac{x}{\xi}, \frac{y}{\xi}\right)(H+E)\,(y,\xi)\right\},\\
\widetilde{E}^\perp_\pm(x,\xi) &= \pm\frac{1}{\xi}\int_{-1}^1 dy \left\{W_\pm\left(\frac{x}{\xi}, \frac{y}{\xi}\right)\widetilde{H}(y,\xi) - \xi W_\mp\left(\frac{x}{\xi}, \frac{y}{\xi}\right)(H+E)\,(y,\xi)\right\}.
\end{aligned} \tag{14}$$

The W-kernels introduced in these formulae are defined by

$$W_\pm\left(\frac{x}{\xi},\frac{y}{\xi}\right)=\frac{1}{2\xi}\left\{W\left(\frac{x}{\xi},\frac{y}{\xi}\right)\pm W\left(-\frac{x}{\xi},-\frac{y}{\xi}\right)\right\},\qquad W(x,y)=\frac{\theta(1+x)-\theta(x-y)}{1+y}\,. \tag{15}$$

The antiquark-gluon-quark contributions,

$$F_\pm^{qGq}=-\int_{-1}^1\frac{dy}{\xi}\int_{-1}^1 du\frac{1-u}{2}\left\{W\left(-\frac{x}{\xi},-\frac{y}{\xi}\right)\frac{\overleftarrow{\partial^2}}{\partial y^2}S_F^+(y,u,-\xi)\pm W\left(\frac{x}{\xi},\frac{y}{\xi}\right)\frac{\overleftarrow{\partial^2}}{\partial y^2}S_F^-(y,-u,-\xi)\right\},$$

can be read off from the parametrization of the corresponding operators and result in eight independent functions

$$S_\rho^\pm=\Delta_\rho^\perp\frac{q\cdot h}{q\cdot P}S_H^\pm+\Delta_\rho^\perp\frac{q\cdot e}{q\cdot P}S_E^\pm\pm\widetilde{\Delta}_\rho^\perp\frac{q\cdot\widetilde{h}}{q\cdot P}S_{\widetilde{H}}^\pm\pm\widetilde{\Delta}_\rho^\perp\frac{q\cdot\widetilde{e}}{q\cdot P}S_{\widetilde{E}}^\pm\,, \tag{16}$$

(see Ref. [14] for details).

It turns out that only the difference $\mathcal{F}_+^3-\mathcal{F}_-^3$ enters the DVCS amplitude [34, 28, 33, 13], where, again similar to the previous definitions, the CFF $\mathcal{F}$ in Eq. (9) stands for $\mathcal{H}$, $\mathcal{E}$, $\widetilde{\mathcal{H}}$, and $\widetilde{\mathcal{E}}$ species. Therefore, only four new GPDs remain at twist-three level. In the WW-approximation, i.e., neglecting the antiquark-gluon-quark correlation, all the twist-three CFFs are entirely determined by the four twist-two GPDs H, E, $\widetilde{H}$, and $\widetilde{E}$.

3 DVCS amplitude with gluon transversity

Apart from the conventional vector and axial composite quark operators, whose matrix elements define the GPDs discussed in the previous section, there is a specific gluon operator that requires the helicity of the hadron to be flipped by two units. It can show up in the scattering off a spin-1/2 target due to a non-zero angular momentum of partons in the nucleon. The latter is a result of the non-vanishing t-channel momentum transfer Δ in the present settings. The corresponding operator forms the $(1,1)$ representation of the Lorentz group and reads in terms of the gluon field strength tensors

$${}^G\mathcal{O}_{\mu\nu}^T(\kappa_1,\kappa_2)=G_{+\rho}(\kappa_2 n)\tau_{\mu\nu;\rho\sigma}^\perp G_{\sigma+}(\kappa_1 n)\,, \tag{17}$$

with the omitted gauge link. Here the totally symmetric and traceless tensor is

$$\tau_{\mu\nu;\rho\sigma}^\perp=\frac{1}{2}\left(g_{\mu\rho}^\perp g_{\nu\sigma}^\perp+g_{\mu\sigma}^\perp g_{\nu\rho}^\perp-g_{\mu\nu}^\perp g_{\rho\sigma}^\perp\right)\,. \tag{18}$$

The two-dimensional metric $g^\perp_{\mu\nu} = g_{\mu\nu} - n_\mu n^*_\nu - n^*_\mu n_\nu$ is defined in terms of two light-like vectors n and n^*, such that $n^2 = n^{*2} = 0$ and $n \cdot n^* = 1$. The off-forward matrix element of this operator is parametrized via four GPDs [37] (see [38, 39] for an earlier discussion)

$$\begin{aligned} G^T_{\mu\nu}(x,\xi,\Delta^2) &\equiv 4(P\cdot n)^{-1}\int\frac{d\kappa}{2\pi}\mathrm{e}^{ix\kappa(P\cdot n)}\langle P_2|^G\mathcal{O}^T_{\mu\nu}(\kappa,-\kappa)|P_1\rangle \\ &= \frac{\tau^\perp_{\mu\nu;\alpha\beta}}{2M}\Delta_\alpha\bar{U}(P_2)\Big\{H_T(x,\xi,\Delta^2)\frac{q_\gamma}{P\cdot q}\,i\sigma_{\gamma\beta} + \widetilde{H}_T(x,\xi,\Delta^2)\frac{\Delta_\beta}{2M^2} \\ &\qquad + E_T(x,\xi,\Delta^2)\frac{1}{2M}\left(\frac{\gamma\cdot q}{P\cdot q}\Delta_\beta - \eta\,\gamma_\beta\right) - \widetilde{E}_T(x,\xi,\Delta^2)\frac{\gamma_\beta}{2M}\Big\}U(P_1)\,, \end{aligned} \tag{19}$$

The traceless symmetric projector $\tau^\perp$ in Eq. (19) possesses the properties

$$\tau^\perp_{\mu\nu;\rho\sigma}\tau^\perp_{\mu\nu;\rho'\sigma'} = \tau^\perp_{\rho\sigma;\rho'\sigma'}\,, \qquad \tau^\perp_{\mu\nu;\rho\sigma} = \tau^\perp_{\rho\sigma;\mu\nu}\,, \qquad \tau^\perp_{\mu\mu;\rho\sigma} = 0\,, \qquad \tau^\perp_{\mu\nu;\mu\nu} = 2\,.$$

A simple calculation of one-loop diagrams [38, 39] gives us the following result for the real final-state photon DVCS amplitude

$$T_{\mu\nu} = \frac{\alpha_s}{2\pi}T_F\sum_{i=u,d,s}\int_{-1}^{1}dx\; C^{(+)}_{(0)i}(x,\xi)\,G^T_{\mu\nu}(x,\xi,\Delta^2)\,, \tag{20}$$

with $T_F = 1/2$ and the coefficient function $C^{(+)}_{i(0)}$ defined in Eq. (11). Substituting Eq. (19) into the above expression gives the amplitude, which we will use in our computation of the cross section. We define the CFFs similarly to Eqs. (9) via

$$\left\{\mathcal{H}_T,\mathcal{E}_T,\widetilde{\mathcal{H}}_T,\widetilde{\mathcal{E}}_T\right\}(\xi) = \frac{\alpha_s}{2\pi}T_F\sum_{i=u,d,s}\int_{-1}^{1}dx\,C^{(+)}_{(0)i}(\xi,x)\left\{H_T,E_T,\widetilde{H}_T,\widetilde{E}_T\right\}(x,\xi)\,. \tag{21}$$

Below we will use unifying conventions for these CFFs, i.e., $\mathcal{F}_T = \{\mathcal{H}_T,\ldots,\widetilde{\mathcal{E}}_T\}$.

4 Angular dependence of the cross section

Now we are in a position to turn to physical observables, which give direct access to GPDs in a measurement of the five-fold cross section for the process $e(k)h(P_1) \to e(k')h(P_2)\gamma(q_2)$,

$$\frac{d\sigma}{dx_{\rm B}dyd|\Delta^2|d\phi d\varphi} = \frac{\alpha^3 x_{\rm B} y}{16\,\pi^2\,\mathcal{Q}^2\sqrt{1+\epsilon^2}}\left|\frac{\mathcal{T}}{e^3}\right|^2\,. \tag{22}$$

This cross section depends on the Bjorken variable $x_{\rm B}$, the squared momentum transfer $\Delta^2 = (P_2 - P_1)^2$, the lepton energy fraction $y = P_1\cdot q_1/P_1\cdot k$, with $q_1 = k - k'$, and, in general, two azimuthal angles. We use throughout our presentation the convention

$$\epsilon \equiv 2x_{\rm B}\frac{M}{\mathcal{Q}}\,.$$

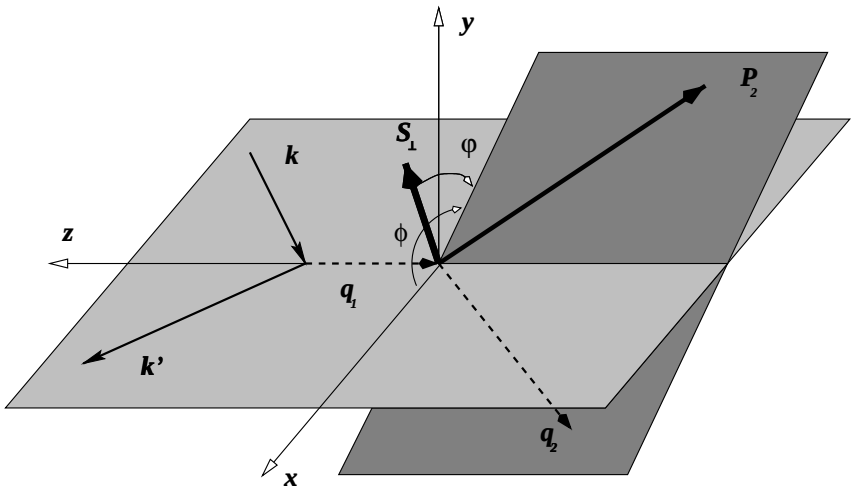

Figure 1: The kinematics of the leptoproduction in the target rest frame. The z-direction is chosen counter-along the three-momentum of the incoming virtual photon. The lepton three-momenta form the lepton scattering plane, while the recoiled proton and outgoing real photon define the hadron scattering plane. In this reference system the azimuthal angle of the scattered lepton is $\phi_l = 0$, while the azimuthal angle between the lepton plane and the recoiled proton momentum is $\phi_N = \phi$. When the hadron is transversely polarized (in this reference frame) $S_\perp = (0, \cos\Phi, \sin\Phi, 0)$, the angle between the polarization vector and the scattered hadron is denoted as $\varphi = \Phi - \phi_N$.

In Eq. (22), $\phi = \phi_N - \phi_l$ is the angle between the lepton and hadron scattering planes and $\varphi = \Phi - \phi_N$ is the difference of the azimuthal angle Φ of the transverse part of the nucleon polarization vector S, i.e., $S_\perp = (0, \cos\Phi, \sin\Phi, 0)$, and the azimuthal angle ϕ_N of the recoiled hadron. Our frame is rotated with respect to the laboratory one in such a way that the virtual photon four-momentum has no transverse components, see Fig. 1. We fix our kinematics by choosing the z-component of the virtual photon momentum to be negative and the positive x-component of the incoming lepton: $k = (E, E\sin\theta_l, 0, E\cos\theta_l)$, $q_1 = (q_1^0, 0, 0, -|q_1^3|)$. Other vectors are $P_1 = (M, 0, 0, 0)$ and $P_2 = (E_2, |\boldsymbol{P}_2|\cos\phi\sin\theta_N, |\boldsymbol{P}_2|\sin\phi\sin\theta_N, |\boldsymbol{P}_2|\cos\theta_N)$. The longitudinal part of the polarization vector is $S_{\rm LP} = (0, 0, 0, \Lambda)$.

The amplitude $\mathcal{T}$ is the sum of the DVCS $\mathcal{T}_{\rm DVCS}$ and Bethe-Heitler (BH) $\mathcal{T}_{\rm BH}$ amplitudes. The latter one is real (to the lowest order in the QED fine structure constant) and is parametrized in terms of electromagnetic form factors, which we assume to be known from other measurements. The azimuthal angular dependence of each of the three terms in

$$\mathcal{T}^2 = |\mathcal{T}_{\rm BH}|^2 + |\mathcal{T}_{\rm DVCS}|^2 + \mathcal{I}\,, \tag{23}$$

with the interference term

$$\mathcal{I} = \mathcal{T}_{\rm DVCS}\mathcal{T}^*_{\rm BH} + \mathcal{T}^*_{\rm DVCS}\mathcal{T}_{\rm BH}\,, \tag{24}$$

arises from the contraction of leptonic and handronic tensors (see also [42]). In our frame these contractions yield finite sums of Fourier harmonics, whose maximal frequencies are defined by the the rank-m of the corresponding leptonic tensor in the incoming lepton momentum k_μ. Note, however, that in the polarized part of the leptonic tensors, proportional to λ times the ϵ-tensor, one has one four-vector k_μ less than in the unpolarized part. Thus, the highest harmonic which is proportional to λ will be $\cos\,/\,\sin([m-1]\phi)$ instead of $\cos\,/\,\sin(m\phi)$. The parity and time reversal invariance provide further constraints on the Fourier coefficients.

The BH term $|\mathcal{T}_{\rm BH}|^2$, squared DVCS amplitude $|\mathcal{T}_{\rm DVCS}|^2$, and interference term $\mathcal{I}$ read

$$|\mathcal{T}_{\rm BH}|^2 = \frac{e^6}{x_{\rm B}^2 y^2(1+\epsilon^2)^2\Delta^2\,\mathcal{P}_1(\phi)\mathcal{P}_2(\phi)}\left\{c_0^{\rm BH} + \sum_{n=1}^{2} c_n^{\rm BH}\,\cos\left(n\phi\right) + s_1^{\rm BH}\,\sin\left(\phi\right)\right\}\,, \tag{25}$$

$$|\mathcal{T}_{\rm DVCS}|^2 = \frac{e^6}{y^2\mathcal{Q}^2}\left\{c_0^{\rm DVCS} + \sum_{n=1}^{2}\Big[c_n^{\rm DVCS}\cos(n\phi) + s_n^{\rm DVCS}\sin(n\phi)\Big]\right\}\,, \tag{26}$$

$$\mathcal{I} = \frac{\pm e^6}{x_{\rm B} y^3\mathcal{P}_1(\phi)\mathcal{P}_2(\phi)\Delta^2}\left\{c_0^{\mathcal{I}} + \sum_{n=1}^{3}\Big[c_n^{\mathcal{I}}\cos(n\phi) + s_n^{\mathcal{I}}\sin(n\phi)\Big]\right\}\,, \tag{27}$$

where the $+$ $(-)$ sign in the interference stands for the negatively (positively) charged lepton beam[2]. The results for the Fourier coefficients, presented below, show that the generation of new harmonics in the azimuthal angular dependence is terminated at the twist-three level. The coefficients $c_1^{\mathcal{I}}, s_1^{\mathcal{I}}$ as well as $c_0^{\rm DVCS}$ arise at the twist-two level, and their dependence on GPDs has been elaborated in Refs. [42, 43]. The rest provides an additional angular dependence and is given in terms of twist-two, i.e., $c_0^{\mathcal{I}}$, and twist-three, i.e., $c_1^{\rm DVCS}$, $s_1^{\rm DVCS}$, $c_2^{\mathcal{I}}$, and $s_2^{\mathcal{I}}$, GPDs. The harmonics proportional to $\cos\left(3\phi\right)$ $[\cos\left(2\phi\right)]$ or $\sin\left(3\phi\right)$ $[\sin\left(2\phi\right)]$ in the interference [squared DVCS] term stem from the twist-two double helicity-flip gluonic GPDs alone. They are not contaminated by twist-two quark amplitudes, however, will be affected by twist-four power corrections [44]. We neglect in our consequent considerations the effects of dynamical higher-twist (larger than three) contributions. They will give power-suppressed corrections to the Fourier coefficients, we discussed.

There is an important difference between the interference term and the squared DVCS amplitude. The former has a contaminating ϕ-dependence due to the lepton BH propagators,

$$\mathcal{Q}^2\mathcal{P}_1 \equiv (k-q_2)^2 = \mathcal{Q}^2 + 2k\cdot\Delta\,, \qquad \mathcal{Q}^2\mathcal{P}_2 \equiv (k-\Delta)^2 = -2k\cdot\Delta + \Delta^2\,, \tag{28}$$

[2]Note that only in the case of massless leptons, a partial cancellation of propagators occurs in the squared BH term [41].

where

$$k\cdot\Delta=-\frac{\mathcal{Q}^2}{2y(1+\epsilon^2)}\left\{1+2K\cos\phi-\frac{\Delta^2}{\mathcal{Q}^2}\left(1-x_{\rm B}(2-y)+\frac{y\epsilon^2}{2}\right)+\frac{y\epsilon^2}{2}\right\}. \tag{29}$$

The $1/\mathcal{Q}$-power suppressed kinematical factor K appearing here also shows up in the Fourier series (25-27),

$$K^2=-\frac{\Delta^2}{\mathcal{Q}^2}(1-x_{\rm B})\left(1-y-\frac{y^2\epsilon^2}{4}\right)\left(1-\frac{\Delta^2_{\rm min}}{\Delta^2}\right)\left\{\sqrt{1+\epsilon^2}+\frac{4x_{\rm B}(1-x_{\rm B})+\epsilon^2}{4(1-x_{\rm B})}\frac{\Delta^2-\Delta^2_{\rm min}}{\mathcal{Q}^2}\right\}, \tag{30}$$

(with the plus sign taken for the square root in Eq. (29)). It vanishes at the kinematical boundary $\Delta^2=\Delta^2_{\rm min}$, determined by the minimal value

$$-\Delta^2_{\rm min}=\mathcal{Q}^2\frac{2(1-x_{\rm B})\left(1-\sqrt{1+\epsilon^2}\right)+\epsilon^2}{4x_{\rm B}(1-x_{\rm B})+\epsilon^2}\approx\frac{M^2x_{\rm B}^2}{1-x_{\rm B}+x_{\rm B}M^2/\mathcal{Q}^2}\,, \tag{31}$$

as well as at

$$y(x,\mathcal{Q}^2)=y_{\rm max}\equiv 2\frac{\sqrt{1+\epsilon^2}-1}{\epsilon^2}\approx 1-\frac{M^2x_{\rm B}^2}{\mathcal{Q}^2}\,.$$

The square of the transverse momentum transfer is given by

$$\Delta^2_\perp\approx(1-\xi^2)(\Delta^2-\Delta^2_{\rm min})\,,$$

up to corrections suppressed by the hard-photon virtuality.

According to Eqs. (28) and (29), we introduce the following parametrization:

$$\mathcal{P}_1=-\frac{1}{y(1+\epsilon^2)}\left\{J+2K\cos(\phi)\right\}\,,\qquad \mathcal{P}_2=\frac{1}{y(1+\epsilon^2)}\left\{1+J+\frac{\Delta^2}{\mathcal{Q}^2}+2K\cos(\phi)\right\}\,, \tag{32}$$

where

$$J=\left(1-y-\frac{y\epsilon^2}{2}\right)\left(1+\frac{\Delta^2}{\mathcal{Q}^2}\right)-(1-x)(2-y)\frac{\Delta^2}{\mathcal{Q}^2}\,.$$

As we see, the denominator of the u-channel lepton propagator, i.e., $\mathcal{P}_1$, can be of order $1/\mathcal{Q}^2$ at large y. In the Bjorken limit it behaves like $(1-y)$. Moreover, if the outgoing photon is collinear to the incoming lepton, it vanishes. Of course, the photon then lies in the lepton scattering plane, i.e., $\phi_\gamma=\phi+\pi=0$, and both polar angles coincide with each other. The latter condition is fulfilled if

$$y=y_{\rm col}\equiv\frac{\mathcal{Q}^2+\Delta^2}{\mathcal{Q}^2+x\Delta^2}\approx 1+(1-x_{\rm B})\frac{\Delta^2}{\mathcal{Q}^2}\,,$$

(with $y_{\rm col} \leq y_{\rm max}$) and this leads to the equality

$$\begin{aligned} J_{|y=y_{\rm col}} &= 2K_{|y=y_{\rm col}} \\ &= -\frac{2(1-x_{\rm B})\Delta^2}{\mathcal{Q}^2+x\Delta^2}\left(1-\frac{\Delta^2_{\rm min}}{\Delta^2}\right)\left\{\sqrt{1+\epsilon^2}+\frac{4x_{\rm B}(1-x_{\rm B})+\epsilon^2}{4(1-x_{\rm B})}\frac{\Delta^2-\Delta^2_{\rm min}}{\mathcal{Q}^2}\right\}. \end{aligned} \tag{33}$$

Obviously, for large y the squared BH (25) and interference (27) terms are enhanced with respect to the squared DVCS one (26). Furthermore, the expansion of $\mathcal{P}_1$ in $\mathcal{Q}$ is not justified, and, thus, the Fourier analysis of experimental data must be modified. For small y it is legitimate to expand $\mathcal{P}_1$ and $\mathcal{P}_2$ in power series with respect to $1/\mathcal{Q}$. This generates higher harmonics suppressed by powers of K.

The computation of the Fourier coefficients in Eq. (25-27) is tedious, however, relatively straightforward (see Refs. [3, 42, 43]). After an extensive algebra we come to the Fourier harmonics summarized in the following sections. We will employ the conventional definition of the lepton helicity, i.e., $\lambda = +1$ if the spin is aligned with the direction of the lepton three-momentum. To have a compact notation, we write the cross section for a polarized target as

$$d\sigma = d\sigma_{\rm unp} + \cos(\theta)\, d\sigma_{\rm LP}(\Lambda) + \sin(\theta)\, d\sigma_{\rm TP}(\varphi)\,, \tag{34}$$

where the polar angle θ appears in the decomposition of the spin vector $S = \cos(\theta)S_{\rm LP}(\Lambda) + \sin(\theta)S_{\perp}(\Phi)$. The same decomposition will be used for the Fourier coefficients.

4.1 Bethe-Heitler amplitude squared

This part of the leptoproduction cross section is expressed solely in terms of $F_1(\Delta^2)$ and $F_2(\Delta^2)$, the known Dirac and Pauli form factors of the nucleon. For diverse target polarizations the Fourier coefficients are:

- Unpolarized target:

$$\begin{aligned} c^{\rm BH}_{0,{\rm unp}} &= 8K^2\left\{\left(2+3\epsilon^2\right)\frac{\mathcal{Q}^2}{\Delta^2}\left(F_1^2-\frac{\Delta^2}{4M^2}F_2^2\right)+2x_{\rm B}^2\left(F_1+F_2\right)^2\right\} \\ &+ (2-y)^2\Bigg\{\left(2+\epsilon^2\right)\left[\frac{4x_{\rm B}^2M^2}{\Delta^2}\left(1+\frac{\Delta^2}{\mathcal{Q}^2}\right)^2+4(1-x_{\rm B})\left(1+x_{\rm B}\frac{\Delta^2}{\mathcal{Q}^2}\right)\right]\left(F_1^2-\frac{\Delta^2}{4M^2}F_2^2\right) \\ &+ 4x_{\rm B}^2\left[x_{\rm B}+\left(1-x_{\rm B}+\frac{\epsilon^2}{2}\right)\left(1-\frac{\Delta^2}{Q^2}\right)^2-x_{\rm B}(1-2x_{\rm B})\frac{\Delta^4}{Q^4}\right]\left(F_1+F_2\right)^2\Bigg\} \\ &+ 8\left(1+\epsilon^2\right)\left(1-y-\frac{\epsilon^2y^2}{4}\right)\left\{2\epsilon^2\left(1-\frac{\Delta^2}{4M^2}\right)\left(F_1^2-\frac{\Delta^2}{4M^2}F_2^2\right)\right. \end{aligned} \tag{35}$$

$$-x_{\rm B}^2\left(1-\frac{\Delta^2}{Q^2}\right)^2(F_1+F_2)^2\Big\},$$

$$c_{1,\rm unp}^{\rm BH}=8K(2-y)\Big\{\left(\frac{4x_{\rm B}^2M^2}{\Delta^2}-2x_{\rm B}-\epsilon^2\right)\left(F_1^2-\frac{\Delta^2}{4M^2}F_2^2\right)+2\,x_{\rm B}^2\left(1-(1-2x_{\rm B})\frac{\Delta^2}{\mathcal{Q}^2}\right)(F_1+F_2)^2\Big\}, \tag{36}$$

$$c_{2,\rm unp}^{\rm BH}=8x_{\rm B}^2K^2\left\{\frac{4M^2}{\Delta^2}\left(F_1^2-\frac{\Delta^2}{4M^2}F_2^2\right)+2\,(F_1+F_2)^2\right\}. \tag{37}$$

- Longitudinally polarized target:

$$\begin{aligned}c_{0,\rm LP}^{\rm BH}=&\,8\lambda\Lambda x_{\rm B}(2-y)y\frac{\sqrt{1+\epsilon^2}}{1-\frac{\Delta^2}{4M^2}}(F_1+F_2)\left\{\frac{1}{2}\left[\frac{x_{\rm B}}{2}\left(1-\frac{\Delta^2}{\mathcal{Q}^2}\right)-\frac{\Delta^2}{4M^2}\right]\left[2-x_{\rm B}\right.\right.\\&-2(1-x_{\rm B})^2\frac{\Delta^2}{\mathcal{Q}^2}+\epsilon^2\left(1-\frac{\Delta^2}{\mathcal{Q}^2}\right)-x_{\rm B}(1-2x_{\rm B})\frac{\Delta^4}{\mathcal{Q}^4}\Big](F_1+F_2)\\&\left.+\left(1-(1-x_{\rm B})\frac{\Delta^2}{\mathcal{Q}^2}\right)\left[\frac{x_{\rm B}^2M^2}{\Delta^2}\left(1+\frac{\Delta^2}{\mathcal{Q}^2}\right)^2+(1-x_{\rm B})\left(1+x_{\rm B}\frac{\Delta^2}{\mathcal{Q}^2}\right)\right]\left(F_1+\frac{\Delta^2}{4M^2}F_2\right)\right\},\end{aligned} \tag{38}$$

$$\begin{aligned}c_{1,\rm LP}^{\rm BH}=&-8\lambda\Lambda x_{\rm B}yK\frac{\sqrt{1+\epsilon^2}}{1-\frac{\Delta^2}{4M^2}}(F_1+F_2)\left\{\left[\frac{\Delta^2}{2M^2}-x_{\rm B}\left(1-\frac{\Delta^2}{\mathcal{Q}^2}\right)\right]\left(1-x_{\rm B}+x_{\rm B}\frac{\Delta^2}{\mathcal{Q}^2}\right)(F_1+F_2)\right.\\&\left.+\left[1+x_{\rm B}-(3-2x_{\rm B})\left(1+x_{\rm B}\frac{\Delta^2}{\mathcal{Q}^2}\right)-\frac{4x_{\rm B}^2M^2}{\Delta^2}\left(1+\frac{\Delta^4}{\mathcal{Q}^4}\right)\right]\left(F_1+\frac{\Delta^2}{4M^2}F_2\right)\right\}.\end{aligned} \tag{39}$$

- Transversely polarized target:

$$\begin{aligned}c_{0,\rm TP}^{\rm BH}=&-8\lambda\cos(\varphi)(2-y)y\frac{\mathcal{Q}}{M}\frac{\sqrt{1+\epsilon^2}K}{\sqrt{1-y-\frac{\epsilon^2y^2}{4}}}(F_1+F_2)\left\{\frac{x_{\rm B}^3M^2}{\mathcal{Q}^2}\left(1-\frac{\Delta^2}{\mathcal{Q}^2}\right)(F_1+F_2)\right.\\&\left.+\left(1-(1-x_{\rm B})\frac{\Delta^2}{\mathcal{Q}^2}\right)\left[\frac{x_{\rm B}^2M^2}{\Delta^2}\left(1-\frac{\Delta^2}{\mathcal{Q}^2}\right)F_1+\frac{x_{\rm B}}{2}F_2\right]\right\},\end{aligned} \tag{40}$$

$$\begin{aligned}c_{1,\rm TP}^{\rm BH}=&-16\lambda\cos(\varphi)x_{\rm B}y\sqrt{1-y-\frac{\epsilon^2y^2}{4}}\frac{M}{\mathcal{Q}}\sqrt{1+\epsilon^2}(F_1+F_2)\left\{\frac{2K^2\mathcal{Q}^2}{\Delta^2\left(1-y-\frac{\epsilon^2y^2}{4}\right)}\left[x_{\rm B}\left(1-\frac{\Delta^2}{\mathcal{Q}^2}\right)F_1\right.\right.\\&\left.\left.+\frac{\Delta^2}{4M^2}F_2\right]+(1+\epsilon^2)x_{\rm B}\left(1-\frac{\Delta^2}{\mathcal{Q}^2}\right)\left(F_1+\frac{\Delta^2}{4M^2}F_2\right)\right\},\end{aligned} \tag{41}$$

$$s_{1,\rm TP}^{\rm BH}=16\lambda\sin(\varphi)yx_{\rm B}^2\sqrt{1-y-\frac{\epsilon^2y^2}{4}}\frac{M}{\mathcal{Q}}\sqrt{(1+\epsilon^2)^3}\left(1-\frac{\Delta^2}{\mathcal{Q}^2}\right)(F_1+F_2)\left(F_1+\frac{\Delta^2}{4M^2}F_2\right). \tag{42}$$

4.2 DVCS amplitude squared

$|\mathcal{T}_{\rm DVCS}|^2$ is bilinear in the CFFs, and its coefficients read in terms of $\mathcal{C}^{\rm DVCS}$ functions, which are specified in section 4.4:

- Unpolarized target:

$$c_{0,\mathrm{unp}}^{\mathrm{DVCS}} = 2(2-2y+y^2)\mathcal{C}_{\mathrm{unp}}^{\mathrm{DVCS}}\left(\mathcal{F},\mathcal{F}^*\right), \tag{43}$$

$$\begin{Bmatrix} c_{1,\mathrm{unp}}^{\mathrm{DVCS}} \\ s_{1,\mathrm{unp}}^{\mathrm{DVCS}} \end{Bmatrix} = \frac{8K}{2-x_{\mathrm{B}}} \begin{Bmatrix} 2-y \\ -\lambda y \end{Bmatrix} \begin{Bmatrix} \Re\mathrm{e} \\ \Im\mathrm{m} \end{Bmatrix} \mathcal{C}_{\mathrm{unp}}^{\mathrm{DVCS}}\left(\mathcal{F}^{\mathrm{eff}},\mathcal{F}^*\right), \tag{44}$$

$$c_{2,\mathrm{unp}}^{\mathrm{DVCS}} = -\frac{4\mathcal{Q}^2K^2}{M^2(2-x_{\mathrm{B}})}\Re\mathrm{e}\,\mathcal{C}_{T,\mathrm{unp}}^{\mathrm{DVCS}}\left(\mathcal{F}_T,\mathcal{F}^*\right). \tag{45}$$

- Longitudinally polarized target:

$$c_{0,\mathrm{LP}}^{\mathrm{DVCS}} = 2\lambda\Lambda y(2-y)\mathcal{C}_{\mathrm{LP}}^{\mathrm{DVCS}}\left(\mathcal{F},\mathcal{F}^*\right), \tag{46}$$

$$\begin{Bmatrix} c_{1,\mathrm{LP}}^{\mathrm{DVCS}} \\ s_{1,\mathrm{LP}}^{\mathrm{DVCS}} \end{Bmatrix} = -\frac{8\Lambda K}{2-x_{\mathrm{B}}} \begin{Bmatrix} -\lambda y \\ 2-y \end{Bmatrix} \begin{Bmatrix} \Re\mathrm{e} \\ \Im\mathrm{m} \end{Bmatrix} \mathcal{C}_{\mathrm{LP}}^{\mathrm{DVCS}}\left(\mathcal{F}^{\mathrm{eff}},\mathcal{F}^*\right), \tag{47}$$

$$s_{2,\mathrm{LP}}^{\mathrm{DVCS}} = -\frac{4\Lambda\mathcal{Q}^2K^2}{M^2(2-x_{\mathrm{B}})}\Im\mathrm{m}\,\mathcal{C}_{T,\mathrm{LP}}^{\mathrm{DVCS}}\left(\mathcal{F}_T,\mathcal{F}^*\right). \tag{48}$$

- Transversely polarized target:

$$c_{0,\mathrm{TP}}^{\mathrm{DVCS}} = -\frac{\mathcal{Q}K}{M\sqrt{1-y}}\left[-\lambda y(2-y)\cos(\varphi)\mathcal{C}_{\mathrm{TP}+}^{\mathrm{DVCS}} + (2-2y+y^2)\sin(\varphi)\Im\mathrm{m}\,\mathcal{C}_{\mathrm{TP}-}^{\mathrm{DVCS}}\right]\left(\mathcal{F},\mathcal{F}^*\right), \tag{49}$$

$$\begin{Bmatrix} c_{1,\mathrm{TP}}^{\mathrm{DVCS}} \\ s_{1,\mathrm{TP}}^{\mathrm{DVCS}} \end{Bmatrix} = -\frac{4\mathcal{Q}K^2}{M(2-x_{\mathrm{B}})\sqrt{1-y}} \tag{50}$$

$$\times \left[\cos(\varphi) \begin{Bmatrix} -\lambda y \\ 2-y \end{Bmatrix} \begin{Bmatrix} \Re\mathrm{e} \\ \Im\mathrm{m} \end{Bmatrix} \mathcal{C}_{\mathrm{TP}+}^{\mathrm{DVCS}} + \sin(\varphi) \begin{Bmatrix} 2-y \\ \lambda y \end{Bmatrix} \begin{Bmatrix} \Im\mathrm{m} \\ \Re\mathrm{e} \end{Bmatrix} \mathcal{C}_{\mathrm{TP}-}^{\mathrm{DVCS}}\right]\left(\mathcal{F}^{\mathrm{eff}},\mathcal{F}^*\right),$$

$$\begin{Bmatrix} c_{2,\mathrm{TP}}^{\mathrm{DVCS}} \\ s_{2,\mathrm{TP}}^{\mathrm{DVCS}} \end{Bmatrix} = -\frac{4\mathcal{Q}\sqrt{1-y}K}{M(2-x_{\mathrm{B}})}\Im\mathrm{m} \begin{Bmatrix} \sin(\varphi)\,\mathcal{C}_{T,\mathrm{TP}-}^{\mathrm{DVCS}} \\ \cos(\varphi)\,\mathcal{C}_{T,\mathrm{TP}+}^{\mathrm{DVCS}} \end{Bmatrix}\left(\mathcal{F}_T,\mathcal{F}^*\right). \tag{51}$$

The harmonic c_0^{DVCS} is given in terms of twist-two CFFs $\mathcal{F} = \{\mathcal{H},\mathcal{E},\widetilde{\mathcal{H}},\widetilde{\mathcal{E}}\}$, defined in Eq. (9). The twist-three coefficients c_1^{DVCS} and s_1^{DVCS} arise from the interference of twist-two CFFs with 'effective' twist-three ones,

$$\mathcal{F}^{\mathrm{eff}} \equiv -2\xi\left(\frac{1}{1+\xi}\mathcal{F} + \mathcal{F}_+^3 - \mathcal{F}_-^3\right), \tag{52}$$

where $\mathcal{F}_\pm^3$ are defined in Eqs. (13-16). These Fourier harmonics have the same functional dependence on CFFs as the leading twist-two ones [43]. However, this is not the case for the Fourier coefficients c_2^{DVCS} and s_2^{DVCS}, induced by the gluon transversity CFFs (21).

4.3 Interference of Bethe-Heitler and DVCS amplitudes

For the phenomenology of GPDs, $\mathcal{I}$ is the most interesting quantity since it is linear in CFFs. This simplifies their disentanglement from experimental measurements. The Fourier harmonics have the form:

- Unpolarized target:

$$c^{\mathcal{I}}_{0,\mathrm{unp}} = -8(2-y)\Re\mathrm{e}\left\{\frac{(2-y)^2}{1-y}K^2\mathcal{C}^{\mathcal{I}}_{\mathrm{unp}}\left(\mathcal{F}\right)+\frac{\Delta^2}{\mathcal{Q}^2}(1-y)(2-x_{\mathrm{B}})\left(\mathcal{C}^{\mathcal{I}}_{\mathrm{unp}}+\Delta\mathcal{C}^{\mathcal{I}}_{\mathrm{unp}}\right)\left(\mathcal{F}\right)\right\}, \tag{53}$$

$$\begin{Bmatrix} c^{\mathcal{I}}_{1,\mathrm{unp}} \\ s^{\mathcal{I}}_{1,\mathrm{unp}} \end{Bmatrix} = 8K\begin{Bmatrix} -(2-2y+y^2) \\ \lambda y(2-y) \end{Bmatrix}\begin{Bmatrix} \Re\mathrm{e} \\ \Im\mathrm{m} \end{Bmatrix}\mathcal{C}^{\mathcal{I}}_{\mathrm{unp}}\left(\mathcal{F}\right), \tag{54}$$

$$\begin{Bmatrix} c^{\mathcal{I}}_{2,\mathrm{unp}} \\ s^{\mathcal{I}}_{2,\mathrm{unp}} \end{Bmatrix} = \frac{16K^2}{2-x_{\mathrm{B}}}\begin{Bmatrix} -(2-y) \\ \lambda y \end{Bmatrix}\begin{Bmatrix} \Re\mathrm{e} \\ \Im\mathrm{m} \end{Bmatrix}\mathcal{C}^{\mathcal{I}}_{\mathrm{unp}}\left(\mathcal{F}^{\mathrm{eff}}\right), \tag{55}$$

$$c^{\mathcal{I}}_{3,\mathrm{unp}} = -\frac{8\mathcal{Q}^2K^3}{M^2(2-x_{\mathrm{B}})^2}\Re\mathrm{e}\,\mathcal{C}^{\mathcal{I}}_{T,\mathrm{unp}}\left(\mathcal{F}_T\right). \tag{56}$$

- Longitudinally polarized target:

$$c^{\mathcal{I}}_{0,\mathrm{LP}} = -8\lambda\Lambda y\Re\mathrm{e}\left\{\left(\frac{(2-y)^2}{1-y}+2\right)K^2\mathcal{C}^{\mathcal{I}}_{\mathrm{LP}}\left(\mathcal{F}\right)+\frac{\Delta^2}{\mathcal{Q}^2}(1-y)(2-x_{\mathrm{B}})\left(\mathcal{C}^{\mathcal{I}}_{\mathrm{LP}}+\Delta\mathcal{C}^{\mathcal{I}}_{\mathrm{LP}}\right)\left(\mathcal{F}\right)\right\}, \tag{57}$$

$$\begin{Bmatrix} c^{\mathcal{I}}_{1,\mathrm{LP}} \\ s^{\mathcal{I}}_{1,\mathrm{LP}} \end{Bmatrix} = 8\Lambda K\begin{Bmatrix} -\lambda y(2-y) \\ 2-2y+y^2 \end{Bmatrix}\begin{Bmatrix} \Re\mathrm{e} \\ \Im\mathrm{m} \end{Bmatrix}\mathcal{C}^{\mathcal{I}}_{\mathrm{LP}}\left(\mathcal{F}\right), \tag{58}$$

$$\begin{Bmatrix} c^{\mathcal{I}}_{2,\mathrm{LP}} \\ s^{\mathcal{I}}_{2,\mathrm{LP}} \end{Bmatrix} = \frac{16\Lambda K^2}{2-x_{\mathrm{B}}}\begin{Bmatrix} -\lambda y \\ 2-y \end{Bmatrix}\begin{Bmatrix} \Re\mathrm{e} \\ \Im\mathrm{m} \end{Bmatrix}\mathcal{C}^{\mathcal{I}}_{\mathrm{LP}}\left(\mathcal{F}^{\mathrm{eff}}\right), \tag{59}$$

$$s^{\mathcal{I}}_{3,\mathrm{LP}} = \frac{8\Lambda\mathcal{Q}^2K^3}{M^2(2-x_{\mathrm{B}})^2}\Im\mathrm{m}\,\mathcal{C}^{\mathcal{I}}_{T,\mathrm{LP}}\left(\mathcal{F}_T\right). \tag{60}$$

- Transversely polarized target:

$$\begin{aligned} c^{\mathcal{I}}_{0,\mathrm{TP}} = \frac{8M\sqrt{1-y}K}{\mathcal{Q}}\Bigg[&-\lambda y\cos(\varphi)\,\Re\mathrm{e}\left\{\left(\frac{(2-y)^2}{1-y}+2\right)\mathcal{C}^{\mathcal{I}}_{\mathrm{TP}+}\left(\mathcal{F}\right)+\Delta\mathcal{C}^{\mathcal{I}}_{\mathrm{TP}+}\left(\mathcal{F}\right)\right\} \\ &+(2-y)\sin(\varphi)\,\Im\mathrm{m}\left\{\frac{(2-y)^2}{1-y}\mathcal{C}^{\mathcal{I}}_{\mathrm{TP}-}\left(\mathcal{F}\right)+\Delta\mathcal{C}^{\mathcal{I}}_{\mathrm{TP}-}\left(\mathcal{F}\right)\right\}\Bigg], \end{aligned} \tag{61}$$

$$\begin{aligned} \begin{Bmatrix} c^{\mathcal{I}}_{1,\mathrm{TP}} \\ s^{\mathcal{I}}_{1,\mathrm{TP}} \end{Bmatrix} = &\frac{8M\sqrt{1-y}}{\mathcal{Q}} \\ &\times\left[\cos(\varphi)\begin{Bmatrix} -\lambda y(2-y) \\ 2-2y+y^2 \end{Bmatrix}\begin{Bmatrix} \Re\mathrm{e} \\ \Im\mathrm{m} \end{Bmatrix}\mathcal{C}^{\mathcal{I}}_{\mathrm{TP}+}+\sin(\varphi)\begin{Bmatrix} 2-2y+y^2 \\ \lambda y(2-y) \end{Bmatrix}\begin{Bmatrix} \Im\mathrm{m} \\ \Re\mathrm{e} \end{Bmatrix}\mathcal{C}^{\mathcal{I}}_{\mathrm{TP}-}\right]\left(\mathcal{F}\right), \end{aligned} \tag{62}$$

$$\left\{\begin{matrix} c^{\mathcal{I}}_{2,\mathrm{TP}} \\ s^{\mathcal{I}}_{2,\mathrm{TP}} \end{matrix}\right\} = \frac{16M\sqrt{1-y}K}{\mathcal{Q}(2-x_{\mathrm{B}})} \tag{63}$$
$$\times \left[\cos(\varphi)\left\{\begin{matrix} -\lambda y \\ 2-y \end{matrix}\right\}\left\{\begin{matrix} \Re\mathrm{e} \\ \Im\mathrm{m} \end{matrix}\right\}\mathcal{C}^{\mathcal{I}}_{\mathrm{TP}+} + \sin(\varphi)\left\{\begin{matrix} 2-y \\ \lambda y \end{matrix}\right\}\left\{\begin{matrix} \Im\mathrm{m} \\ \Re\mathrm{e} \end{matrix}\right\}\mathcal{C}^{\mathcal{I}}_{\mathrm{TP}-}\right]\left(\mathcal{F}^{\mathrm{eff}}\right) ,$$
$$s^{\mathcal{I}}_{3,\mathrm{TP}} = \frac{8\mathcal{Q}\sqrt{1-y}K^2}{M(2-x_{\mathrm{B}})^2}\cos(\varphi)\Im\mathrm{m}\,\mathcal{C}^{\mathcal{I}}_{T,\mathrm{TP}+}\left(\mathcal{F}_T\right) , \tag{64}$$
$$c^{\mathcal{I}}_{3,\mathrm{TP}} = \frac{8\mathcal{Q}\sqrt{1-y}K^2}{M(2-x_{\mathrm{B}})^2}\sin(\varphi)\Im\mathrm{m}\,\mathcal{C}^{\mathcal{I}}_{T,\mathrm{TP}-}\left(\mathcal{F}_T\right) . \tag{65}$$

The higher twist-three harmonics, i.e., $c_2^{\mathcal{I}}$ and $s_2^{\mathcal{I}}$ have again the same functional dependence as the twist-two ones. However, this is not the case for $c_0^{\mathcal{I}}$, which depends only on twist-two CFFs $\mathcal{F}$, and for $c_3^{\mathcal{I}}$ and $s_3^{\mathcal{I}}$, induced by $\mathcal{F}_T$ CFFs.

4.4 Angular harmonics in terms of GPDs

The Fourier coefficients displayed above are expressed in terms of the coefficients $\mathcal{C}$. They depend on GPDs, integrated over the momentum fraction, and are functions of the kinematical variables x_{B}, Δ^2, and $\mathcal{Q}^2$. For the harmonics involving H, E, $\widetilde{H}$, and $\widetilde{E}$-type GPDs they are:

- Squared DVCS amplitude:

$$\mathcal{C}^{\mathrm{DVCS}}_{\mathrm{unp}}\left(\mathcal{F},\mathcal{F}^*\right) = \frac{1}{(2-x_{\mathrm{B}})^2}\Bigg\{4(1-x_{\mathrm{B}})\left(\mathcal{H}\mathcal{H}^* + \widetilde{\mathcal{H}}\widetilde{\mathcal{H}}^*\right) - x_{\mathrm{B}}^2\Big(\mathcal{H}\mathcal{E}^* + \mathcal{E}\mathcal{H}^* + \widetilde{\mathcal{H}}\widetilde{\mathcal{E}}^* + \widetilde{\mathcal{E}}\widetilde{\mathcal{H}}^*\Big)$$
$$- \left(x_{\mathrm{B}}^2 + (2-x_{\mathrm{B}})^2\frac{\Delta^2}{4M^2}\right)\mathcal{E}\mathcal{E}^* - x_{\mathrm{B}}^2\frac{\Delta^2}{4M^2}\widetilde{\mathcal{E}}\widetilde{\mathcal{E}}^*\Bigg\}, \tag{66}$$

$$\mathcal{C}^{\mathrm{DVCS}}_{\mathrm{LP}}\left(\mathcal{F},\mathcal{F}^*\right) = \frac{1}{(2-x_{\mathrm{B}})^2}\Bigg\{4(1-x_{\mathrm{B}})\left(\mathcal{H}\widetilde{\mathcal{H}}^* + \widetilde{\mathcal{H}}\mathcal{H}^*\right) - x_{\mathrm{B}}^2\Big(\mathcal{H}\widetilde{\mathcal{E}}^* + \widetilde{\mathcal{E}}\mathcal{H}^* + \widetilde{\mathcal{H}}\mathcal{E}^* + \mathcal{E}\widetilde{\mathcal{H}}^*\Big)$$
$$-x_{\mathrm{B}}\left(\frac{x_{\mathrm{B}}^2}{2} + (2-x_{\mathrm{B}})\frac{\Delta^2}{4M^2}\right)\left(\mathcal{E}\widetilde{\mathcal{E}}^* + \widetilde{\mathcal{E}}\mathcal{E}^*\right)\Bigg\}, \tag{67}$$

$$\mathcal{C}^{\mathrm{DVCS}}_{\mathrm{TP}+}\left(\mathcal{F},\mathcal{F}^*\right) = \frac{1}{(2-x_{\mathrm{B}})^2}\Bigg\{2x_{\mathrm{B}}(\mathcal{H}\widetilde{\mathcal{E}}^* + \widetilde{\mathcal{E}}\mathcal{H}^*) - 2(2-x_{\mathrm{B}})(\widetilde{\mathcal{H}}\mathcal{E}^* + \widetilde{\mathcal{H}}^*\mathcal{E}) + x_{\mathrm{B}}^2(\mathcal{E}\widetilde{\mathcal{E}}^* + \widetilde{\mathcal{E}}\mathcal{E}^*)\Bigg\},$$
$$\mathcal{C}^{\mathrm{DVCS}}_{\mathrm{TP}-}\left(\mathcal{F},\mathcal{F}^*\right) = \frac{2}{(2-x_{\mathrm{B}})^2}\Bigg\{(2-x_{\mathrm{B}})(\mathcal{H}\mathcal{E}^* - \mathcal{E}\mathcal{H}^*) - x_{\mathrm{B}}(\widetilde{\mathcal{H}}\widetilde{\mathcal{E}}^* - \widetilde{\mathcal{E}}\widetilde{\mathcal{H}}^*)\Bigg\}. \tag{68}$$

- Interference of Bethe-Heitler and DVCS amplitudes:

Here a part of the result at the twist-two level is expressed in terms of the functions, which show up in the lowest twist approximation, and they read [43]

$$\mathcal{C}^{\mathcal{I}}_{\rm unp} = F_1\mathcal{H} + \frac{x_{\rm B}}{2-x_{\rm B}}(F_1+F_2)\widetilde{\mathcal{H}} - \frac{\Delta^2}{4M^2}F_2\mathcal{E}\,, \tag{69}$$

$$\mathcal{C}^{\mathcal{I}}_{\rm LP} = \frac{x_{\rm B}}{2-x_{\rm B}}(F_1+F_2)\left(\mathcal{H}+\frac{x_{\rm B}}{2}\mathcal{E}\right) + F_1\widetilde{\mathcal{H}} - \frac{x_{\rm B}}{2-x_{\rm B}}\left(\frac{x_{\rm B}}{2}F_1 + \frac{\Delta^2}{4M^2}F_2\right)\widetilde{\mathcal{E}}\,, \tag{70}$$

$$\begin{aligned}\mathcal{C}^{\mathcal{I}}_{\rm TP+} = {} & (F_1+F_2)\left\{\frac{x_{\rm B}^2}{2-x_{\rm B}}\left(\mathcal{H}+\frac{x_{\rm B}}{2}\mathcal{E}\right) + \frac{x_{\rm B}\Delta^2}{4M^2}\mathcal{E}\right\} - \frac{x_{\rm B}^2}{2-x_{\rm B}}F_1\left(\widetilde{\mathcal{H}}+\frac{x_{\rm B}}{2}\widetilde{\mathcal{E}}\right)\\ & + \frac{\Delta^2}{4M^2}\left\{4\frac{1-x_{\rm B}}{2-x_{\rm B}}F_2\widetilde{\mathcal{H}} - \left(x_{\rm B}F_1 + \frac{x_{\rm B}^2}{2-x_{\rm B}}F_2\right)\widetilde{\mathcal{E}}\right\}\,,\end{aligned} \tag{71}$$

$$\begin{aligned}\mathcal{C}^{\mathcal{I}}_{\rm TP-} = {} & \frac{1}{2-x_{\rm B}}\left(x_{\rm B}^2F_1 - (1-x_{\rm B})\frac{\Delta^2}{M^2}F_2\right)\mathcal{H} + \left\{\frac{\Delta^2}{4M^2}\left((2-x_{\rm B})F_1 + \frac{x_{\rm B}^2}{2-x_{\rm B}}F_2\right)\right.\\ & \left. + \frac{x_{\rm B}^2}{2-x_{\rm B}}F_1\right\}\mathcal{E} - \frac{x_{\rm B}^2}{2-x_{\rm B}}(F_1+F_2)\left(\widetilde{\mathcal{H}}+\frac{\Delta^2}{4M^2}\widetilde{\mathcal{E}}\right)\,.\end{aligned}$$

The addenda arising in power-suppressed contributions are defined as

$$\Delta\mathcal{C}^{\mathcal{I}}_{\rm unp} = -\frac{x_{\rm B}}{2-x_{\rm B}}(F_1+F_2)\left\{\frac{x_{\rm B}}{2-x_{\rm B}}(\mathcal{H}+\mathcal{E}) + \widetilde{\mathcal{H}}\right\}\,, \tag{72}$$

$$\Delta\mathcal{C}^{\mathcal{I}}_{\rm LP} = -\frac{x_{\rm B}}{2-x_{\rm B}}(F_1+F_2)\left\{\mathcal{H} + \frac{x_{\rm B}}{2}\mathcal{E} + \frac{x_{\rm B}}{2-x_{\rm B}}\left(\widetilde{\mathcal{H}}+\frac{x_{\rm B}}{2}\widetilde{\mathcal{E}}\right)\right\}\,, \tag{73}$$

$$\Delta\mathcal{C}^{\mathcal{I}}_{\rm TP+} = -\frac{\Delta^2}{M^2}\left\{F_2\widetilde{\mathcal{H}} - \frac{x_{\rm B}}{2-x_{\rm B}}\left(F_1+\frac{x_{\rm B}}{2}F_2\right)\widetilde{\mathcal{E}}\right\}\,, \tag{74}$$

$$\Delta\mathcal{C}^{\mathcal{I}}_{\rm TP-} = \frac{\Delta^2}{M^2}\left(F_2\mathcal{H} - F_1\mathcal{E}\right)\,. \tag{75}$$

Let us now list the coefficients involving the gluon transversity:

- Squared DVCS amplitude:

$$\begin{aligned}\mathcal{C}^{\rm DVCS}_{T,\rm unp} = {} & \frac{1}{(2-x_{\rm B})^2}\left\{\mathcal{H}_T\left[(2-x_{\rm B})\mathcal{E}^* - x_{\rm B}\widetilde{\mathcal{E}}^*\right] - 2(2-x_{\rm B})\widetilde{\mathcal{H}}_T\left[\mathcal{H}^* + \frac{\Delta^2}{4M^2}\mathcal{E}^*\right]\right.\\ & \left. - \mathcal{E}_T\left[(2-x_{\rm B})\mathcal{H}^* - x_{\rm B}\widetilde{\mathcal{H}}^*\right] + \widetilde{\mathcal{E}}_T\left[x_{\rm B}(\mathcal{H}^*+\mathcal{E}^*) - (2-x_{\rm B})\widetilde{\mathcal{H}}^*\right]\right\},\end{aligned} \tag{76}$$

$$\begin{aligned}\mathcal{C}^{\rm DVCS}_{T,\rm LP} = {} & \frac{1}{(2-x_{\rm B})^2}\left\{\mathcal{H}_T\left[(2-x_{\rm B})\mathcal{E}^* - x_{\rm B}\widetilde{\mathcal{E}}^*\right] + \widetilde{\mathcal{H}}_T\left[2(2-x_{\rm B})\widetilde{\mathcal{H}}^* - x_{\rm B}\left(x_{\rm B} - \frac{\Delta^2}{2M^2}\right)\widetilde{\mathcal{E}}^*\right]\right.\\ & - \mathcal{E}_T\left[x_{\rm B}\mathcal{H}^* - (2-x_{\rm B})\widetilde{\mathcal{H}}^* + \frac{x_{\rm B}^2}{2}\left(\mathcal{E}^*+\widetilde{\mathcal{E}}^*\right)\right]\\ & \left. + \widetilde{\mathcal{E}}_T\left[(2-x_{\rm B})\left(\mathcal{H}^* + \frac{x_{\rm B}}{2}\mathcal{E}^*\right) - x_{\rm B}\left(\widetilde{\mathcal{H}}^* + \frac{x_{\rm B}}{2}\widetilde{\mathcal{E}}^*\right)\right]\right\},\end{aligned} \tag{77}$$

$$\mathcal{C}^{\rm DVCS}_{T,\rm TP+} = \frac{1}{(2-x_{\rm B})^2}\left\{\left[4(1-x_{\rm B})\mathcal{H}_T - x_{\rm B}^2\mathcal{E}_T + x_{\rm B}(2-x_{\rm B})\widetilde{\mathcal{E}}_T\right]\left(\mathcal{H}^* + \widetilde{\mathcal{H}}^*\right)\right. \tag{78}$$

$$
\begin{aligned}
&-\widetilde{\mathcal{H}}_T\left(x_{\rm B}^2+(1-x_{\rm B})\frac{\Delta^2}{M^2}\right)(2\widetilde{\mathcal{H}}^*+x_{\rm B}\widetilde{\mathcal{E}}^*)\\
&-x_{\rm B}\left[x_{\rm B}\mathcal{H}_T+\left(\frac{x_{\rm B}^2}{2}+(2-x_{\rm B})\frac{\Delta^2}{4M^2}\right)\mathcal{E}_T\right](\mathcal{E}^*+\widetilde{\mathcal{E}}^*)\\
&+\widetilde{\mathcal{E}}_T\left[(2-x_{\rm B})\left(\frac{x_{\rm B}^2}{2}+(2-x_{\rm B})\frac{\Delta^2}{4M^2}\right)\mathcal{E}^*-x_{\rm B}^2\left(\frac{x_{\rm B}}{2}-\frac{\Delta^2}{4M^2}\right)\widetilde{\mathcal{E}}^*\right]\Bigg\},
\end{aligned}
$$

$$
\begin{aligned}
\mathcal{C}^{\rm DVCS}_{T,{\rm TP}-}=\frac{1}{(2-x_{\rm B})^2}\Bigg\{&\left[4(1-x_{\rm B})\mathcal{H}_T-x_{\rm B}^2\mathcal{E}_T+x_{\rm B}(2-x_{\rm B})\widetilde{\mathcal{E}}_T\right]\left(\mathcal{H}^*+\widetilde{\mathcal{H}}^*\right)\\
&-2\widetilde{\mathcal{H}}_T\left(x_{\rm B}^2+(1-x_{\rm B})\frac{\Delta^2}{M^2}\right)(\mathcal{H}^*+\mathcal{E}^*)\\
&-x_{\rm B}\left(x_{\rm B}\mathcal{H}_T-(2-x_{\rm B})\frac{\Delta^2}{4M^2}\widetilde{\mathcal{E}}_T\right)\left(\mathcal{E}^*+\widetilde{\mathcal{E}}^*\right)\\
&-\mathcal{E}_T\left[\left(x_{\rm B}^2+(2-x_{\rm B})^2\frac{\Delta^2}{4M^2}\right)\mathcal{E}^*+x_{\rm B}^2\frac{\Delta^2}{4M^2}\widetilde{\mathcal{E}}^*\right]\Bigg\}.
\end{aligned}
\tag{79}
$$

- Interference of Bethe-Heitler and DVCS amplitudes:

$$
\mathcal{C}^{\mathcal{I}}_{T,{\rm unp}}=-F_2\mathcal{H}_T+2\left(F_1+\frac{\Delta^2}{4M^2}F_2\right)\widetilde{\mathcal{H}}_T+F_1\mathcal{E}_T\,,
\tag{80}
$$

$$
\mathcal{C}^{\mathcal{I}}_{T,{\rm LP}}=F_2\left\{\mathcal{H}_T+\frac{x_{\rm B}}{2}(2\widetilde{\mathcal{H}}_T+\mathcal{E}_T+\widetilde{\mathcal{E}}_T)\right\}+F_1(x_{\rm B}\widetilde{\mathcal{H}}_T+\widetilde{\mathcal{E}}_T)\,,
\tag{81}
$$

$$
\begin{aligned}
\mathcal{C}^{\mathcal{I}}_{T,{\rm TP}+}=&(2F_1+x_{\rm B}F_2)\mathcal{H}_T+x_{\rm B}\left(\frac{x}{2}-\frac{\Delta^2}{4M^2}\right)\left[2(F_1+F_2)\widetilde{\mathcal{H}}_T+F_2\mathcal{E}_T\right]\\
&+\left\{x_{\rm B}F_1+\left(\frac{x_{\rm B}^2}{2}+(2-x_{\rm B})\frac{\Delta^2}{4M^2}\right)F_2\right\}\widetilde{\mathcal{E}}_T\,,
\end{aligned}
\tag{82}
$$

$$
\mathcal{C}^{\mathcal{I}}_{T,{\rm TP}-}=(2F_1+x_{\rm B}F_2)\mathcal{H}_T-(2-x_{\rm B})\frac{\Delta^2}{4M^2}\left[2(F_1+F_2)\widetilde{\mathcal{H}}_T+F_2\mathcal{E}_T\right]+x_{\rm B}\left(F_1+F_2\frac{\Delta^2}{4M^2}\right)\widetilde{\mathcal{E}}_T\,.
\tag{83}
$$

This set of formulae is the complete result for the real-photon leptoproduction cross section in the twist-three approximation. Below, presenting quantitative estimates, we will not discuss the case of transversely polarized target, therefore, the integration with respect to φ gives 2π on the right-hand side of Eq. (22).

4.5 Structure of effective twist-three GPDs

Note that the twist-three GPDs, having generic discontinuities at $|x|=\xi$ [34, 28], enter the CFFs in a singularity-free combination (52). Using the integrals of the type

$$
\int_{-1}^{1}\frac{dx}{|\eta|}\frac{1}{\xi-x-i0}W\left(\frac{x}{\eta},\frac{y}{\eta}\right)=\frac{{\rm sign}(\eta)}{\eta+y}\ln\left(\frac{\eta+\xi}{\xi-y-i0}\right)
$$

in Eq. (52), the convolution of the coefficient functions $C^{(\mp)}_{(0)i}$ and the W-kernels results into an explicit form for the effective twist-three function,

$$\mathcal{F}^{\rm eff}(\xi) = \frac{2}{1+\xi}\mathcal{F}(\xi) + 2\xi\frac{\partial}{\partial\xi}\int_{-1}^{1} dx\, C^{3(\mp)}(\xi,x)F(x,\xi) + \frac{8M^2\xi}{(1-\xi^2)(\Delta^2-\Delta^2_{\rm min})}\mathcal{F}^{\perp}(\xi) \qquad (84)$$
$$-2\xi\int_{-1}^{1} du\int_{-1}^{1} dx\, C^{qGq}(\xi,x,u)\left(S^{+}_{F}(-x,-u,-\xi) - S^{-}_{F}(x,u,-\xi)\right)\Big\},$$

where $\mathcal{F}$ is defined in Eq. (9). The summation over quark flavors is implied, as in Eq. (10), and we have used new notations for the coefficient functions weighted by the quark charge

$$C^{3(\mp)}_{(0)i}(\xi,x) = \frac{Q_i^2}{\xi+x}\ln\frac{2\xi}{\xi-x-i0} \mp \frac{Q_i^2}{\xi-x}\ln\frac{2\xi}{\xi+x-i0}\,, \qquad (85)$$

$$C^{qGq}_{(0)i}(\xi,x,u) = Q_i^2\frac{\partial^2}{\partial x^2}\frac{1+u}{\xi+x}\ln\left(\frac{2\xi}{\xi-x-i0}\right). \qquad (86)$$

The $-$ $(+)$ sign stands here for the vector (axial) sectors, i.e., for $\{\mathcal{H}(\widetilde{\mathcal{H}}),\ \mathcal{E}(\widetilde{\mathcal{E}})\}$. Finally, the functions $\mathcal{F}^{\perp}$ are

$$\mathcal{H}^{\perp}(\xi) = -\frac{\Delta^2}{4M^2}\int_{-1}^{1} dx\left\{\xi\, C^{3(-)}(x,\xi)\,(H+E)\,(x,\xi) - C^{3(+)}(x,\xi)\widetilde{H}(x,\xi)\right\}, \qquad (87)$$

$$\mathcal{E}^{\perp}(\xi) = \int_{-1}^{1} dx\left\{\xi\, C^{3(-)}(x,\xi)\,(H+E)\,(x,\xi) - C^{3(+)}(x,\xi)\widetilde{H}(x,\xi)\right\},$$

$$\widetilde{\mathcal{H}}^{\perp}(\xi) = \int_{-1}^{1} dx\left\{\xi\left(1-\frac{\Delta^2}{4M^2}\right)C^{3(+)}(x,\xi)\widetilde{H}(x,\xi) + \frac{\Delta^2}{4M^2}C^{3(-)}(x,\xi)\,(H+E)\,(x,\xi)\right\},$$

$$\widetilde{\mathcal{E}}^{\perp}(\xi) = \frac{1}{\xi}\int_{-1}^{1} dx\left\{C^{3(+)}(x,\xi)\widetilde{H}(x,\xi) - \xi\, C^{3(-)}(x,\xi)\,(H+E)\,(x,\xi)\right\}.$$

We should note that the kinematical factor $(\Delta^2-\Delta^2_{\rm min})^{-1}$ in Eq. (84) cancels out in the final results for the angular harmonics calculated in sections 4.2 and 4.3. Therefore, it does not lead to a singular behavior of the Fourier coefficients in the cross section (26). For all interference as well as for unpolarized and longitudinally polarized squared DVCS terms this cancellation already appears in the $\mathcal{C}$ functions given in sections 4.4, see Ref. [13] for explicit examples. However, in $c^{\rm DVCS}_{2,\rm TP}$ and $s^{\rm DVCS}_{2,\rm TP}$ this kinematical singularity is annihilated by the prefactor in Eq. (50).

5 Physical observables and access to GPDs

As we have seen, the cross section for leptoproduction of the real photon possesses a quite rich angular structure. The goal of experimental measurements is to pin down the GPDs and this requires a clean disentanglement of different components of the cross section (22). A general strategy, which follows from the analytical results, given above, will be discussed in section 5.1:

sector		harmonics in $\mathcal{I}$				extraction	P of	$\Delta_\perp^l$ behavior	
twist	$\mathcal{C}$'s	unp	LP	TP$_x$	TP$_y$	of CFFs	$\mathcal{Q}^{-P}$	unp, LP	TP
two	$\Re\mathrm{e}\mathcal{C}(\mathcal{F})$, $\Delta\mathcal{C}(\mathcal{F})$	c_1, c_0	c_1, c_0	c_1, c_0	s_1, -	over compl.	1,2	1,0	0,1
	$\Im\mathrm{m}\mathcal{C}(\mathcal{F})$, $\Delta\mathcal{C}(\mathcal{F})$	s_1, -	s_1, -	s_1, -	c_1, c_0	over compl.	1,2	1,0	0,1
three	$\Re\mathrm{e}\mathcal{C}(\mathcal{F}^{\mathrm{eff}})$	c_2	c_2	c_2	s_2	complete	2	2	1
	$\Im\mathrm{m}\mathcal{C}(\mathcal{F}^{\mathrm{eff}})$	s_2	s_2	s_2	c_2	complete	2	2	1
two	$\Re\mathrm{e}\mathcal{C}_T(\mathcal{F}_T)$	c_3	-	-	-	$1\times\Re$e of 4	1	3	2
	$\Im\mathrm{m}\mathcal{C}_T(\mathcal{F}_T)$	-	s_3	s_3	c_3	$3\times\Im$m of 4	1	3	2

Table 1: Fourier coefficients $c_i^{\mathcal{I}}$ and $s_i^{\mathcal{I}}$ of the interference term defined in section 4.3, while the corresponding $\mathcal{C}$ coefficients are given in section 4.4.

separation of twist-two and -three sectors[3], measuring the CFFs, and access to the GPDs. To go along this line, we introduce appropriate asymmetries in section 5.2 and demonstrate how a Fourier transform can distinguish between the interference and squared DVCS contributions.

5.1 Unraveling GPDs

So far we have introduced eight CFFs at the twist-two level, with four of them from the gluonic transversity contribution. Another four new CFFs arise at the twist-three level. These sectors can be separated due to their characteristic azimuthal dependence as summarized in Table 1 for the interference $\mathcal{I}$ and in Table 2 for the squared DVCS amplitude, respectively.

Let us first examine the issue of the dominance of each of the three terms (25-27) in the leptoproduction cross section (22) in different kinematical regions. To do so we have to know the functional dependence of the Fourier coefficients given in Eqs. (25-27) on scaling variables and transferred momenta. For instance, apart from an explicit x_{B}-dependence of multiplicative prefactors there is one hidden in CFFs. It will be argued in section 6 that the latter behave like x_{B}^{-1} in the small-x_{B} region. Thus, for general kinematical settings we expect for the scattering on the unpolarized target from Eqs. (35), (43), and (54) that $c_0^{\mathrm{BH}}\sim x_{\mathrm{B}}^2 c_0^{\mathrm{DVCS}}\sim x_{\mathrm{B}} c_1^{\mathcal{I}}/K$. Taking now the kinematical prefactors in Eqs. (25-27) into account, and the behavior of the BH-propagators (32), we realize that the ratio of the DVCS to BH amplitude behaves like $\sqrt{-(1-y)\Delta^2/y^2\mathcal{Q}^2}$. Obviously, for small (large) y the DVCS (BH) one dominates. As compared to the squared

[3]We talk about the twist-two and twist-three sectors, however, beyond the twist-three approximation each of the associated observables gets corrected by higher-twist, i.e., power-suppressed contributions.

interference of		harmonics in $\lvert\mathcal{T}^{\rm DVCS}\rvert^2$				extraction	P of	$\Delta^l_\perp$ behavior	
twist	$\mathcal{C}$'s	unp	LP	$\rm TP_x$	$\rm TP_y$	of CFFs	$\mathcal{Q}^{-P}$	unp, LP	TP
two & two	$\Re\mathrm{e}\mathcal{C}(\mathcal{F},\mathcal{F}^*)$	c_0	c_0	c_0	-	$3\times\Re\mathrm{e}/\Im\mathrm{m}$	2	0	1
	$\Im\mathrm{m}\mathcal{C}(\mathcal{F},\mathcal{F}^*)$	-	-	-	c_0	$1\times\Im\mathrm{m}/\Re\mathrm{e}$	2	-	1
two & three	$\Re\mathrm{e}\mathcal{C}(\mathcal{F}^{\rm eff},\mathcal{F}^*)$	c_1	c_1	c_1	s_1	$4\times\Re\mathrm{e}/\Im\mathrm{m}$	3	1	1
	$\Im\mathrm{m}\mathcal{C}(\mathcal{F}^{\rm eff},\mathcal{F}^*)$	s_1	s_1	s_1	c_1	$4\times\Im\mathrm{m}/\Re\mathrm{e}$	3	1	1
two & two	$\Re\mathrm{e}\mathcal{C}_T(\mathcal{F}_T,\mathcal{F}^*)$	c_2	-	-	-	$1\times\Re\mathrm{e}/\Im\mathrm{m}$	2	2	-
	$\Im\mathrm{m}\mathcal{C}_T(\mathcal{F}_T,\mathcal{F}^*)$	-	s_2	s_2	c_2	$3\times\Im\mathrm{m}/\Re\mathrm{e}$	2	2	1

Table 2: Fourier coefficients $c_i^{\rm DVCS}$ and $s_i^{\rm DVCS}$ of the squared DVCS amplitude $|\mathcal{T}^{\rm DVCS}|^2$ defined in section 4.2, while the corresponding $\mathcal{C}$ coefficients are given in section 4.4.

amplitudes, the interference term has an additional factor $\sqrt{\Delta^2_\perp/\Delta^2}$. Note that the beam spin-flip contributions provide always an additional damping by the factor y. For the unpolarized or longitudinally polarized target, higher harmonics in any of the three terms are suppressed by powers of K. However, in the case of gluonic transversity, this goes hand in hand with an enhancement by $\mathcal{Q}^2/M^2$. It is important that lower harmonics in the interference term, i.e., $c_0^{\mathcal{I}}$, appear at the twist-three level. Since, they are not proportional to the factor K as compared to c_1, which is, they can be rather important and sizable close to the kinematical boundaries. Fortunately, they only depend on twist-two CFFs, thus, we listed them in Table 1 in the twist-two sector. In the case of transversely polarized target, we observe that both higher and lower twist-three harmonics are suppressed by one power of K.

The analytical structure and simple counting rules, we gave, provide a guideline to separate the three different parts in the leptoproduction cross section. In single spin-flip experiments, which give access to the imaginary part of CFFs, the BH cross section drops out, while in unpolarized or double spin-flip experiments it does not and has to be subtracted. This can certainly be done for not too small values of y. The interference and squared DVCS terms have different azimuthal angular dependencies due to the presence of the BH-propagators in the former. In principle, this fact can be used to separate them by a Fourier analysis. However, this method requires from the experimental side very high-statistics data and from the theoretical side a better understanding of twist-four contributions.

Due to the different charge parity of individual components, it is possible to use the charge asymmetry to separate the interference and squared DVCS terms. The interference term is charge-

odd and can be extracted in facilities that possess both positively and negatively charged leptons [40], i.e.,

$$d\sigma^+ - d\sigma^- \propto \frac{1}{x_{\rm B} y^3 \mathcal{P}_1(\phi)\mathcal{P}_2(\phi)\Delta^2}\left\{c_0^{\mathcal{I}} + \sum_{n=1}^{3}\left[c_n^{\mathcal{I}}\cos(n\phi) + s_n^{\mathcal{I}}\sin(n\phi)\right]\right\}. \tag{88}$$

Its measurement and consequent extraction of separate harmonics provides the real (unpolarized or double spin-flip experiments) and imaginary (single spin-flip experiments) part of linear combinations of twist-two and -three CFFs. An explicit projection procedure of these harmonics will be discussed below in section 5.2.1. Moreover, the charge-even part is given by the sum of the BH and DVCS cross section. The subtraction of the former gives then the Fourier coefficients of the latter:

$$d^+\sigma + d^-\sigma - 2d^{\rm BH}\sigma \propto \frac{1}{y^2\mathcal{Q}^2}\left\{c_0^{\rm DVCS} + \sum_{n=1}^{2}\left[c_n^{\rm DVCS}\cos(n\phi) + s_n^{\rm DVCS}\sin(n\phi)\right]\right\}. \tag{89}$$

In the case of the four CFFs $\mathcal{F} = \{\mathcal{H}, \mathcal{E}, \widetilde{\mathcal{H}}, \widetilde{\mathcal{E}}\}$ we have eight observables given by the first harmonics $\cos(\phi)$ and $\sin(\phi)$ of the interference term, which are accessible away from the kinematical boundaries in polarized beam and target experiments. Thus, experiments with both longitudinally and transversely polarized target can measure all eight Fourier coefficients $c_{1,\Lambda}^{\mathcal{I}}$ and $s_{1,\Lambda}^{\mathcal{I}}$ and, thus, also $\Re{\rm e}/\Im{\rm m}\mathcal{C}_{\Lambda}^{\mathcal{I}}$ with $\Lambda = \{{\rm unp}, {\rm LP}, {\rm TP}_x, {\rm TP}_y\}$. Knowing these $\mathcal{C}$ functions, we can invert them to obtain the CFFs:

$$\begin{aligned}\mathcal{H} = \frac{2-x_{\rm B}}{(1-x_{\rm B})D}\Bigg\{&\left[\left(2 - x_{\rm B} + \frac{4x_{\rm B}^2M^2}{(2-x_{\rm B})\Delta^2}\right)F_1 + \frac{x_{\rm B}^2}{2-x_{\rm B}}F_2\right]\mathcal{C}_{\rm unp}^{\mathcal{I}} \\ &-(F_1+F_2)\left[x_{\rm B}\mathcal{C}_{\rm LP}^{\mathcal{I}} + \frac{2x_{\rm B}^2M^2}{(2-x_{\rm B})\Delta^2}\left(x_{\rm B}\mathcal{C}_{\rm LP}^{\mathcal{I}} - \mathcal{C}_{\rm TP+}^{\mathcal{I}}\right)\right] + F_2\mathcal{C}_{\rm TP-}^{\mathcal{I}}\Bigg\},\end{aligned} \tag{90}$$

$$\begin{aligned}\mathcal{E} = \frac{2-x_{\rm B}}{(1-x_{\rm B})D}\Bigg\{&\left[4\frac{1-x_{\rm B}}{2-x_{\rm B}}F_2 - \frac{4M^2x_{\rm B}^2}{(2-x_{\rm B})\Delta^2}F_1\right]\mathcal{C}_{\rm unp}^{\mathcal{I}} + \frac{4x_{\rm B}M^2}{(2-x_{\rm B})\Delta^2}(F_1+F_2) \\ &\times\left(x_{\rm B}\mathcal{C}_{\rm LP}^{\mathcal{I}} - \mathcal{C}_{\rm TP+}^{\mathcal{I}}\right) + \frac{4M^2}{\Delta^2}F_1\mathcal{C}_{\rm TP-}^{\mathcal{I}}\Bigg\},\end{aligned} \tag{91}$$

$$\begin{aligned}\widetilde{\mathcal{H}} = \frac{2-x_{\rm B}}{(1-x_{\rm B})D}\Bigg\{&(2-x_{\rm B})F_1\mathcal{C}_{\rm LP}^{\mathcal{I}} - x_{\rm B}(F_1+F_2)\mathcal{C}_{\rm unp}^{\mathcal{I}} + \left[\frac{2x_{\rm B}M^2}{\Delta^2}F_1 + F_2\right] \\ &\times\left(x_{\rm B}\mathcal{C}_{\rm LP}^{\mathcal{I}} - \mathcal{C}_{\rm TP+}^{\mathcal{I}}\right)\Bigg\},\end{aligned} \tag{92}$$

$$\begin{aligned}\widetilde{\mathcal{E}} = \frac{2-x_{\rm B}}{(1-x_{\rm B})D}\Bigg\{&\frac{4M^2}{\Delta^2}(F_1+F_2)\left(x_{\rm B}\mathcal{C}_{\rm unp}^{\mathcal{I}} + \mathcal{C}_{\rm TP-}^{\mathcal{I}}\right) + \left[4\frac{1-x_{\rm B}}{x_{\rm B}}F_2 - \frac{4x_{\rm B}M^2}{\Delta^2}F_1\right]\mathcal{C}_{\rm LP}^{\mathcal{I}} \\ &-\frac{4(2-x_{\rm B})M^2}{x_{\rm B}\Delta^2}F_1\mathcal{C}_{\rm TP+}^{\mathcal{I}}\Bigg\},\end{aligned} \tag{93}$$

where

$$D = 4\left(F_1^2 - \frac{\Delta^2}{4M^2}F_2^2\right)\left(1 - \frac{\Delta_{\rm min}^2}{\Delta^2}\right).$$

Consequently, the four Fourier coefficients $c_{0,\Lambda}^{\mathcal{I}}$ as well as the four twist-two DVCS coefficients $c_{0,\Lambda}^{\rm DVCS}$ can serve as experimental consistency checks. Alternatively, they can be used to extract CFFs. Thus, experiments with longitudinally polarized target have the potential to extract the real part of all four CFFs as well as two linear combinations of their imaginary parts from the interference term alone. The missing two imaginary parts could then, in principle, be obtained from the DVCS cross section, i.e., by measuring $c_{0,\rm unp}^{\rm DVCS}$ and $c_{0,\rm LP}^{\rm DVCS}$.

For a polarized beam and target with all polarization options, the real and imaginary part of all four CFFs in the twist-three sector can be extracted from the interference term alone by projection onto the $\cos(2\phi)$ and $\sin(2\phi)$ harmonics and using Eqs. (90-93). Alternatively, knowing the twist-two sector and having only a longitudinally polarized target, one can employ in addition the squared DVCS term, i.e., its $\cos(\phi)$ and $\sin(\phi)$ harmonics, to access the full twist-three sector.

For gluonic transversity, the $\cos(3\phi)$ and $\sin(3\phi)$ harmonics in the interference term can only provide one imaginary and three real parts of certain linear combinations of $\mathcal{F}_T$. Missing information can, in principle, be obtained from the $\cos(2\phi)$ and $\sin(2\phi)$ harmonics of the squared DVCS term. Note that here again a polarized beam and target with all polarizations is necessary. Moreover, the gluonic transversity is suppressed by α_s/π, so one expects a stronger contamination by twist-four effects [44].

As we discussed, a combination of the charge asymmetry with different nucleon/lepton polarizations and projection of the corresponding harmonics provides, at least in principle, a way to explore the real and imaginary part of all CFFs (cf. [3, 42, 43]). This gives maximal access to all GPDs, which enter in a convolution with the real or imaginary part of the coefficient functions, as we have established above in Eqs. (9) and (21). Since these formulae cannot be deconvoluted in practice [45], one has to rely on models with a set of free parameters, which has to be adjusted to experimental data on CFFs. This issue will be discussed below for different available experiments.

5.2 Asymmetries

The measurements of the cross section (22) in different setups, as discussed in the preceding section, would directly lead to determination of the CFFs. However, on the experimental side it is simpler to measure asymmetries since they escape the normalization issue. Thus, we now discuss the separation of twist-two and -three sectors in their terms. The charge and lepton-spin asymmetries used in our previous studies, see, e.g., [43], were restricted to the leading twist approximation for the amplitudes and cannot serve the purpose since they are inevitably contaminated by power-suppressed effects. Due to our poor knowledge of multi-particle correlations inside the nucleon,

this affects the theoretical predictions in an uncontrollable manner[4].

The charge asymmetry

$$A_{\rm C} = \left(\int_{-\pi/2}^{\pi/2} d\phi \frac{d^+\sigma^{\rm unp} - d^-\sigma^{\rm unp}}{d\phi} - \int_{\pi/2}^{3\pi/2} d\phi \frac{d^+\sigma^{\rm unp} - d^-\sigma^{\rm unp}}{d\phi}\right) \Big/ \int_0^{2\pi} d\phi \frac{d^-\sigma^{\rm unp} + d^+\sigma^{\rm unp}}{d\phi}\,, \quad (94)$$

for unpolarized settings contains the contribution of all harmonics due to the presence of the non-negligible ϕ-dependence of BH propagators:

$$A_{\rm C} \propto \sum_{n=0}^{3} I^c_{1,n}(2K/J) c^{\mathcal{I}}_n\,, \quad (95)$$

with

$$I^c_{1,n}(2K/J) \propto \left(\int_{-\pi/2}^{\pi/2} d\phi \frac{\cos(n\phi)}{\mathcal{P}_1(\phi)\mathcal{P}_2(\phi)} - \int_{\pi/2}^{3\pi/2} d\phi \frac{\cos(n\phi)}{\mathcal{P}_1(\phi)\mathcal{P}_2(\phi)}\right)\,, \quad (96)$$

while the normalization is not affected by twist-three corrections. If the final photon is collinear to the incoming (massless) lepton, $\mathcal{P}_1(\phi)$ is peaked at $\phi = \pi$. Thus, the ratio $I^c_{1,n}/I^c_{1,1}$ approaches plus or minus 1 and all harmonics contribute on equal footing. However, since K is then of order $\Delta^2/\mathcal{Q}^2$, only $c^{\mathcal{I}}_0$ and $c^{\mathcal{I}}_1$ give essential contributions at the same order in $\Delta^2/\mathcal{Q}^2$. Thus, for this asymmetry $c^{\mathcal{I}}_0$ may gives an essential effect for large y, since the twist-two part becomes small. For $y \ll y_{\rm col}$, all twist-three harmonics are suppressed in addition by the K-factor. From the expansion of $I^c_{1,n}$ in powers of K we get

$$A_{\rm C} \propto c^{\mathcal{I}}_{1,\rm unp} - \frac{1}{3} c^{\mathcal{I}}_{3,\rm unp} - \frac{2(3-2y)}{2-y}\frac{K}{1-y}\left(c^{\mathcal{I}}_{0,\rm unp} - \frac{1}{3} c^{\mathcal{I}}_{2,\rm unp}\right) + \mathcal{O}\left(K^2, \epsilon\right)\,. \quad (97)$$

If K is not too small, e.g., $K \sim 1/3$ for $-\Delta^2/\mathcal{Q}^2 \sim 1/10$ and $-\Delta^2 \gg -\Delta^2_{\rm min}$, as it is the case in the present fixed target experiments, we realize that $c^{\mathcal{I}}_{0,\rm unp}$ is in fact not numerically suppressed in comparison to $c^{\mathcal{I}}_{1,\rm unp}$. So we would expect a contamination of the leading twist-two prediction by a $\sqrt{-\Delta^2/\mathcal{Q}^2}$ suppressed term, which, however, contains only twist-two CFFs. Even if this $1/\mathcal{Q}$-contamination is small, $A_{\rm C}$ still fails to extracts solely the $c^{\mathcal{I}}_{1,\rm unp}$ coefficient of the interference term and gets additive correction from $c^{\mathcal{I}}_{3,\rm unp}$, which stems from the gluon transversity (and higher, more or equal to four, twist effects). Since the gluon contribution is suppressed by a power of the strong coupling α_s, it may affect the twist-two coefficient $c^{\mathcal{I}}_{1,\rm unp}$ in a modest way, though. Therefore, as a first order approximation the definition (94) can be used for an order of magnitude estimate of the effects.

[4]Note that experimental results from polarized deeply inelastic scattering give only a constraint for the forward limit of the antiquark-gluon-quark content of $\widetilde{\mathcal{H}}^{qGq}$. On the other hand, theoretical arguments that flavor small multi-parton contributions rely on model assumptions [46]. In our opinion, one cannot exclude that these correlations might be important. Thus, one should not rely on the WW-approximation and rather search for their signature in data.

The (definite charge) beam-spin asymmetry on an unpolarized target

$$A_{\rm SL} = \left(\int_0^\pi d\phi \frac{d\sigma^\uparrow - d\sigma^\downarrow}{d\phi} - \int_\pi^{2\pi} d\phi \frac{d\sigma^\uparrow - d\sigma^\downarrow}{d\phi}\right) \Big/ \int_0^{2\pi} d\phi \frac{d\sigma^\uparrow + d\sigma^\downarrow}{d\phi}\,, \tag{98}$$

does not separate the interference term alone. So it does contain contributions from the squared DVCS amplitude:

$$A_{\rm SL} \propto \pm \sum_{n=1}^{2} I^s_{1,n}(2K/J) s^{\mathcal{I}}_{n,\rm unp} - \frac{\Delta^2}{y\mathcal{Q}^2} x_{\rm B} s^{\rm DVCS}_{1,\rm unp}\,, \tag{99}$$

with

$$I^s_{1,n}(2K/J) = -\frac{1}{y^2}\left(\int_0^\pi d\phi \frac{\sin(n\phi)}{\mathcal{P}_1(\phi)\mathcal{P}_2(\phi)} - \int_\pi^{2\pi} d\phi \frac{\sin(n\phi)}{\mathcal{P}_1(\phi)\mathcal{P}_2(\phi)}\right). \tag{100}$$

In the collinear limit, the asymmetry vanishes. While for $y \to 0$, it is determined by the twist-three coefficient $s^{\rm DVCS}_{1,\rm unp}$. The expansion with respect to K reads:

$$A_{\rm SL} \propto s^{\mathcal{I}}_{1,\rm unp} - \frac{2(3-2y)}{3(2-y)} \frac{K}{1-y} s^{\mathcal{I}}_{2,\rm unp} - \frac{(1-y)(2-y)\Delta^2}{y\mathcal{Q}^2} x_{\rm B} s^{\rm DVCS}_{1,\rm unp} + \mathcal{O}\left(K^2, \epsilon\right). \tag{101}$$

The $1/\mathcal{Q}$-suppressed effect stemming from the BH propagators induces a contamination by the second harmonic suppressed by $K/(1-y)$. Depending on the kinematics and the size of multi-particle contributions, this contamination together with $s^{\rm DVCS}_{1,\rm unp}$ may not allow clean access to the twist-two GPDs even from high-precision measurements of this asymmetry. Note that for general reasons, $s^{\mathcal{I}}_{3,\rm unp}$ ($s^{\rm DVCS}_{2,\rm unp}$) is absent in the unpolarized interference (squared DVCS) term. The normalization of $A_{\rm SL}$ is affected by $1/\mathcal{Q}$-effects in the interference term, however, mainly due to the coefficient $c^{\mathcal{I}}_{0,\rm unp}$.

5.2.1 Facilities with positively and negatively charged lepton beams

As we have already mentioned, when lepton beams of both charges are available, this provides a clean separation of twist-two and -three GPDs. In these settings one can discuss charge-odd and -even parts of the cross section (22), which extract the interference, and squared DVCS and BH amplitudes, respectively. The integrated charge-even part of the cross section does not contain any twist-three contributions — the interference term cancels there, while after azimuthal averaging the c_0 coefficient of the squared DVCS and all harmonics of squared BH amplitudes survive. So we will use it as a unique normalization of the asymmetries discussed below. Namely, independent from the target polarization we introduce

$$\mathcal{N}^{-1}_{+-} \equiv \int_0^{2\pi} d\phi \frac{d^+\sigma^{\rm unp} + d^-\sigma^{\rm unp}}{d\phi} = 2\int_0^{2\pi} d\phi \frac{d^{\rm BH}\sigma^{\rm unp} + d^{\rm DVCS}\sigma^{\rm unp}}{d\phi}\,. \tag{102}$$

- Charge-odd part:

In this case, we end up with the interference term alone. However, because of the ϕ-dependence of the BH propagators we have to include an additional weight factor and use the measure

$$dw = 2\pi \frac{\mathcal{P}_1(\phi)\mathcal{P}_2(\phi)d\phi}{\int_0^{2\pi} \mathcal{P}_1(\phi')\mathcal{P}_2(\phi')d\phi'}\,, \tag{103}$$

for the azimuthal integration in order to compensate for the strong ϕ-dependence of the product of lepton propagators. The measure dw has the properties

$$\int_0^{2\pi} dw = 2\pi\,, \qquad dw(\phi) = dw(-\phi) = dw(\phi + 2\pi)\,.$$

Now we can exactly separate the Fourier coefficients in Eq. (27). Note that dw has its minimum at $\phi = \pi$, when the outgoing photon lies in the lepton scattering plane. In the case when its momentum is collinear to the lepton beam, this minimum approaches zero in the massless limit.

To project out different harmonics, on can either (i) do the azimuthal averaging with appropriate weights, namely,

$$\cos(n\phi)dw\,, \qquad\qquad \sin(n\phi)dw\,, \tag{104}$$

where $n = 0, \ldots, 3$, or, (ii) use the fact that there is only a finite number of terms in the Fourier sum of the cross section and integrate over different partitions of the azimuthal sphere. For $n > 0$ this has an advantage of having a numerical enhancement by the factor of $4/\pi$ with respect to the first method. Let us present the charge odd asymmetries (CoA), which distinguish the cosine, $\cos(n\phi)$, and sine, $\sin(n\phi)$, harmonics.

The cos-harmonics, i.e., $c_n^{\mathcal{I}}$ coefficients, are projected out by means of the integrals

$$\mathrm{CoA}^{\Lambda}_{c(0)} = \mathcal{N}_{+-} \int_0^{2\pi} dw \frac{d^+\sigma^{\Lambda} - d^-\sigma^{\Lambda}}{d\phi}\,, \tag{105}$$

$$\mathrm{CoA}^{\Lambda}_{c(1)} = \mathcal{N}_{+-} \left(\int_{-\pi/2}^{\pi/2} dw \frac{d^+\sigma^{\Lambda} - d^-\sigma^{\Lambda}}{d\phi} - \int_{\pi/2}^{3\pi/2} dw \frac{d^+\sigma^{\Lambda} - d^-\sigma^{\Lambda}}{d\phi} \right) + \frac{1}{3}\mathrm{CoA}^{\Lambda}_{c(3)}\,, \tag{106}$$

$$\mathrm{CoA}^{\Lambda}_{c(n)} = \mathcal{N}_{+-} \sum_{k=1}^{2n} (-1)^{k+1} \int_{(2k-3)\pi/(2n)}^{(2k-1)\pi/(2n)} dw \frac{d^+\sigma^{\Lambda} - d^-\sigma^{\Lambda}}{d\phi}\,, \tag{107}$$

with n running over $n = 2, 3$ in the last equation. Here we adopt the analogous decomposition of asymmetries as for the cross section in Eq. (34) so that $\Lambda = \{\mathrm{unp}, \mathrm{LP}, \mathrm{TP}\}$. The projection can be achieved by an appropriate flip of the target polarization vector. For a transversely polarized target, asymmetries are given in terms of two different combinations of CFFs. They are separable by the projection of the first odd and even harmonics in φ, while the average $\int_0^{2\pi} d\varphi\, \mathrm{CoA}^{\mathrm{TP}} = 0$ vanishes.

Next, the sin-harmonics, $s_n^{\mathcal{I}}$, can analogously be separated with the help of the formulae

$$\mathrm{CoA}^{\Lambda}_{s(1)} = \mathcal{N}_{+-} \left(\int_0^{\pi} dw \frac{d^+\sigma^{\Lambda} - d^-\sigma^{\Lambda}}{d\phi} - \int_{\pi}^{2\pi} dw \frac{d^+\sigma^{\Lambda} - d^-\sigma^{\Lambda}}{d\phi} \right) - \frac{1}{3}\mathrm{CoA}^{\Lambda}_{s(3)}\,, \tag{108}$$

$$\mathrm{CoA}^{\Lambda}_{s(n)} = \mathcal{N}_{+-} \sum_{k=1}^{2n} (-1)^{k+1} \int_{(k-1)\pi/n}^{k\pi/n} dw \frac{d^{+}\sigma^{\Lambda} - d^{-}\sigma^{\Lambda}}{d\phi}\,, \tag{109}$$

where $n = 2, 3$.

- Charge-even part:

Furthermore, we define the azimuthal asymmetries of the charge-even part. To do this in the cleanest way, we subtract at first the BH term. This might be possible in practice in the analysis of experimental data since the BH cross section is known exactly (up to electromagnetic radiative corrections), see section 4.1, with the nucleon form factors measured elsewhere. This gives us the squared DVCS amplitude

$$2d^{\mathrm{DVCS}}\sigma = d^{+}\sigma + d^{-}\sigma - 2d^{\mathrm{BH}}\sigma\,.$$

Then an appropriate azimuthal averaging, now with the conventional measure $d\phi$, separates the cos-harmonics, c_n^{DVCS}, via

$$\mathrm{CeA}^{\Lambda}_{c(0)} = 2\mathcal{N}_{+-} \int_{0}^{2\pi} d\phi \frac{d^{\mathrm{DVCS}}\sigma^{\Lambda}}{d\phi}\,, \tag{110}$$

$$\mathrm{CeA}^{\Lambda}_{c(n)} = 2\mathcal{N}_{+-} \sum_{k=1}^{2n} (-1)^{k+1} \int_{(2k-3)\pi/(2n)}^{(2k-1)\pi/(2n)} d\phi \frac{d^{\mathrm{DVCS}}\sigma^{\Lambda}}{d\phi}\,, \tag{111}$$

with $n = 1, 2$, and sin-dependent coefficients by means of

$$\mathrm{CeA}^{\Lambda}_{s(n)} = 2\mathcal{N}_{+-} \sum_{k=1}^{2n} (-1)^{k+1} \int_{(k-1)\pi/n}^{k\pi/n} d\phi \frac{d^{\mathrm{DVCS}}\sigma^{\Lambda}}{d\phi}\,, \tag{112}$$

with $n = 1, 2$.

To conclude, an experimental facility having electron and positron beams is an ideal place to study GPDs and, thus, to extract the fundamental information about the spin structure of the nucleon.

5.2.2 Facilities with single-charge lepton beam

Now let us come to the situation when only one kind of the lepton beam is available. Here the study of single (lepton or nucleon) spin asymmetries allows to remove the background BH cross section. Note, however, that when both the beam and target are polarized, and one studies double-spin asymmetries, one gets the contamination from the BH harmonics too. In the single (lepton or hadron) spin experiments, still the twist-two coefficient $s_1^{\mathcal{I}}$ is contaminated by power-suppressed effects, since both the interference and squared DVCS terms contribute. The best one can do in

these circumstances is to cancel completely the twist-three part of the interference term in the numerator. However, still one will have the presence of the power-suppressed DVCS cross section. For instance, for the single lepton-spin experiment one enables to probe $s^{\mathcal{I}}_{1,\mathrm{unp}}$ plus $(1-y)\Delta^2/y\mathcal{Q}^2$ corrections from $|\mathcal{T}_{\mathrm{DVCS}}|^2$ and this can be done with the formula

$$\mathrm{SSA}_1 = \left(\int_0^{\pi} dw \frac{d\sigma^{\uparrow} - d\sigma^{\downarrow}}{d\phi} - \int_{\pi}^{2\pi} dw \frac{d\sigma^{\uparrow} - d\sigma^{\downarrow}}{d\phi} \right. \\ \left. -\frac{1}{3}\sum_{k=1}^{6}(-1)^{k+1} \int_{(k-1)\pi/6}^{k\pi/6} dw \frac{d\sigma^{\uparrow} - d\sigma^{\downarrow}}{d\phi} \right) \Big/ \int_0^{2\pi} d\phi \frac{d\sigma^{\uparrow} + d\sigma^{\downarrow}}{d\phi} \,. \tag{113}$$

Analogous extraction of the twist-two coefficient $s^{\mathcal{I}}_{1,\mathrm{LP}}$ is available for the nucleon-spin asymmetry (with the unpolarized lepton beam). The projection of the same components can be achieved by weighting the integral with $\sin(\phi)dw$.

For smaller value of y the contamination from the squared DVCS term may be large. Let us demonstrate that a separation of the interference and squared DVCS terms can be achieved by a Fourier transform. The multiplication of the cross section with $dw/d\phi$ induces new harmonics in the squared DVCS term. Projection of all three harmonics, i.e., measuring also

$$\mathrm{SSA}_n = \left(\sum_{k=1}^{2n}(-1)^{k+1} \int_{(k-1)\pi/n}^{k\pi/n} dw \frac{d^+\sigma^{\uparrow} - d^-\sigma^{\downarrow}}{d\phi} \right) \Big/ \int_0^{2\pi} d\phi \frac{d\sigma^{\uparrow} + d\sigma^{\downarrow}}{d\phi} \,, \tag{114}$$

(where $n = 2, 3$) provides the desired Fourier coefficients:

$$s^{\mathcal{I}}_{1,\mathrm{unp}} \propto \left(\mathrm{SSA}_1 - \frac{w_{s,11}}{w_{s,13}} \mathrm{SSA}_3 \right), \quad s^{\mathcal{I}}_{2,\mathrm{unp}} \propto \left(\mathrm{SSA}_2 - \frac{w_{s,12}}{w_{s,13}} \mathrm{SSA}_3 \right), \quad s^{\mathrm{DVCS}}_{1,\mathrm{unp}} \propto \mathrm{SSA}_3, \tag{115}$$

with $w_{s,km} = \int_0^{2\pi} dw \sin(k\phi)\sin(m\phi)$. Thus the extraction of twist-three harmonics is, in principle, possible, however, it requires high precision data.

Such a modified Fourier analysis might be employed to separate the coefficients of the interference and squared DVCS term also in unpolarized and double spin-flip experiments. One has to be aware that the weighted cross section contains now four odd and five even harmonics and that the BH cross section must be removed.

6 Properties of Compton form factors

To compare twist-two and -three contributions quantitatively, we use essentially the same ansatz for the GPDs as in [43]. GPDs are constrained by sum rules and reduction formulae to the forward kinematics, which give us a guideline on how to model them. One may hope that these constraints, once implemented into a parametrization, provide a realistic order of magnitude estimate for cross

sections and asymmetries. However, we should emphasize that our evaluations (as well as by other authors) are strongly affected by the model ambiguities involved. Experimental data will necessarily constrain GPDs via theoretical formulae. Therefore, it is important to understand the (i) theoretical uncertainties and (ii) influence of the model parameters on predictions. While the first issue is relatively straightforward to handle, provided one has enough knowledge on higher-order and -twist corrections, the second issue relies, more or less, on the experience that has to be collected by applying different GPD models.

6.1 Ansatz for GPDs

To give a quantitative estimate of the CFFs we have to model, or parametrize, GPDs. Let us discuss this issue for the twist-two sector, where we set $\eta = -\xi$. Note that the time-reversal invariance and hermiticity imply that the twist-two GPDs are real valued functions symmetric in η.

6.1.1 General remarks

For the reader's convenience let us remind the definition of the twist-two GPDs in terms of light-ray operators and their reduction to the conventional parton densities. We will use this information for the modeling of the former. The twist-two quark GPDs are given by

$$\langle P_2|\bar\psi(-\kappa n)\gamma\cdot n\,\psi(\kappa n)|P_1\rangle = \int_{-1}^{1} dx \mathrm{e}^{-ix\kappa(P\cdot n)}\left\{h\cdot n\,H(x,\xi,\Delta^2)+e\cdot n\,E(x,\xi,\Delta^2)\right\}, \quad (116)$$

$$\langle P_2|\bar\psi(-\kappa n)\gamma\cdot n\,\gamma_5\psi(\kappa n)|P_1\rangle = \int_{-1}^{1} dx \mathrm{e}^{-ix\kappa(P\cdot n)}\left\{\tilde h\cdot n\,\widetilde H(x,\xi,\Delta^2)+\tilde e\cdot n\,\widetilde E(x,\xi,\Delta^2)\right\}, \quad (117)$$

for the vector and axial channels, respectively. The Dirac bilinears are introduced in Eq. (8). We have contracted the free Lorentz index with the light-like vector n_μ in order to render the operators twist-two. For brevity we dropped the path ordered exponential between the quark fields, which makes the nonlocal operators gauge invariant, and did not indicate their scale dependence. This dependence arise from the renormalization procedure of the light-ray operators and is governed by a renormalization group equation [47, 30].

On the other hand unpolarized and polarized quark $(f, \Delta f)$ and antiquark $(\bar f, \Delta\bar f)$ densities are defined similarly by equations

$$\langle p|\bar\psi(0)\gamma\cdot n\psi(\kappa n)|p\rangle = 2p\cdot n\int_0^1 dx\left\{f(x)\mathrm{e}^{-ix\kappa(p\cdot n)}-\bar f(x)\mathrm{e}^{ix\kappa(p\cdot n)}\right\}, \quad (118)$$

$$\langle p|\bar\psi(0)\gamma\cdot n\,\gamma_5\psi(\kappa n)|p\rangle = 2s\cdot n\int_0^1 dx\left\{\Delta f(x)\mathrm{e}^{-ix\kappa(p\cdot n)}+\Delta\bar f(x)\mathrm{e}^{ix\kappa(p\cdot n)}\right\}, \quad (119)$$

with the nucleon polarization vector $s_\mu = \frac{1}{2}\bar{U}(p)\gamma_\mu\gamma_5 U(p)$. Here, the limiting procedure from the off-forward kinematics is defined as $\Delta \to 0$, so that $P_1 = P_2 \equiv p$, and one gets a restriction on the GPDs H and $\widetilde{H}$:

$$H(x,0,0) = f(x)\theta(x) - \bar{f}(-x)\theta(-x)\,, \qquad \widetilde{H}(x,0,0) = \Delta f(x)\theta(x) + \Delta\bar{f}(-x)\theta(-x)\,. \tag{120}$$

The first moments of the twist-two GPDs are equal to the corresponding parton form factors in the nucleon

$$\begin{aligned} \int_{-1}^{1} dx\, H(x,\xi,\Delta^2) &= F_1(\Delta^2)\,, \qquad \int_{-1}^{1} dx\, E(x,\xi,\Delta^2) = F_2(\Delta^2)\,, \\ \int_{-1}^{1} dx\, \widetilde{H}(x,\xi,\Delta^2) &= G_1(\Delta^2)\,, \qquad \int_{-1}^{1} dx\, \widetilde{E}(x,\xi,\Delta^2) = G_P(\Delta^2)\,, \end{aligned} \tag{121}$$

i.e., Dirac, Pauli, axial, and pseudoscalar form factors, respectively.

For the gluonic GPDs we have the parametrization

$$\begin{aligned} \langle P_2|n_\alpha G_{\alpha\mu}(-\kappa n) G_{\mu\beta}(\kappa n) n_\beta|P_1\rangle &= \frac{1}{4}\,(P\cdot n)\int_{-1}^{1} dx\; \mathrm{e}^{-ix\kappa(P\cdot n)} \\ &\quad \times \Big\{ h\cdot n\, H_G(x,\xi,\Delta^2) + e\cdot n\, E_G(x,\xi,\Delta^2)\Big\}\,, \end{aligned} \tag{122}$$

$$\begin{aligned} \langle P_2|n_\alpha G_{\alpha\mu}(-\kappa n) i\widetilde{G}_{\mu\beta}(\kappa n) n_\beta|P_1\rangle &= \frac{1}{4}\,(P\cdot n)\int_{-1}^{1} dx\; \mathrm{e}^{-ix\kappa(P\cdot n)} \\ &\quad \times \Big\{ \tilde{h}\cdot n\, \widetilde{H}_G(x,\xi,\Delta^2) + \tilde{e}\cdot n\, \widetilde{E}_G(x,\xi,\Delta^2)\Big\}\,, \end{aligned} \tag{123}$$

for the even- and odd-parity sectors, respectively. To make the contact with the forward parton densities, let us recall the definitions of the gluonic distributions,

$$\langle p|n_\alpha G_{\alpha\mu}(0) G_{\mu\beta}(\kappa n) n_\beta|p\rangle = (p\cdot n)^2 \int_0^1 dx\; x g(x)\left\{\mathrm{e}^{-ix\kappa p_+} + \mathrm{e}^{ix\kappa p_+}\right\}\,, \tag{124}$$

$$\langle p|n_\alpha G_{\alpha\mu}(0) i\widetilde{G}_{\mu\beta}(\kappa n) n_\beta|p\rangle = (s\cdot n)\,(p\cdot n)\int_0^1 dx\; x\Delta g(x)\left\{\mathrm{e}^{-ix\kappa p_+} - \mathrm{e}^{ix\kappa p_+}\right\}\,. \tag{125}$$

Therefore, we must have

$$H_G(x,0,0) = xg(x)\theta(x) - xg(-x)\theta(-x)\,, \qquad \widetilde{H}_G(x,0,0) = x\Delta g(x)\theta(x) + x\Delta g(-x)\theta(-x)\,. \tag{126}$$

The first moment of these GPDs is related to gluonic form factors. The vector form factor is measurable in diffractive meson production [48] and was theoretically estimated in Ref. [49].

In different regions of the phase space GPDs share common properties with conventional inclusive parton densities for $|x| > \xi$, and exclusive distribution amplitudes for $|x| < \xi$. Moreover, their experimental exploration will resolve the target from different perspectives and will enable to obtain its real-space image [50, 51].

To model the GPDs we will use the representation in terms of the so-called double distributions (DDs) [1, 4]. In this representation one treats both s- and t-channel momentum flows independently with the corresponding fractions y and z, respectively. For the matrix element of the composite operator constructed out of scalar field operators, ϕ, we would have

$$\begin{aligned}\langle P_2|\phi(-\kappa n)\phi(\kappa n)|P_1\rangle &= \int_{-1}^{1} dy \int_{-1+|y|}^{1-|y|} dz \mathrm{e}^{-iy\kappa(P\cdot n)-iz\kappa(\Delta\cdot n)} f(y,z,\Delta^2) \\ &= \int_{-1}^{1} dx \mathrm{e}^{-ix\kappa(P\cdot n)} q(x,\xi,\Delta^2)\,. \end{aligned} \tag{127}$$

The function introduced on the first line of Eq. (127) is the aforementioned double distribution $f(y,z,\Delta^2)$, and $q(x,\xi,\Delta^2)$ is the corresponding GPD. The expression of $q(x,\xi,\Delta^2)$ in terms of $f(y,z,\Delta^2)$ is given via

$$q(x,\xi,\Delta^2) = \int_{-1}^{1} dy \int_{-1+|y|}^{1-|y|} dz\, \delta(y+\xi z - x) f(y,z,\Delta^2)\,, \tag{128}$$

and the inversion is known as the Radon transformation [33, 52].

However, in the case of spin-1/2 quarks there is an additional vector index associated with the Dirac matrix inserted in between the field operators. This leads to the appearance of extra Lorentz structures in the decomposition of the matrix element, which once discarded, lead to a violation of the polynomiality condition for the GPDs. In the historically first definition, the relevant structure was erroneously neglected and one used the same Eq. (128) even for the nucleon matrix elements of QCD operators. This problem has been resolved by taking into account an extra term, the so-called D-term [53]. It is only concentrated in the exclusive region, i.e., $|x/\xi| \leq 1$. Such contributions arise from isolated mesonic-like states[5]. However, there is yet another possibility to resolve the polynomiality problem [33]. Unfortunately, in this case one has to deal with a more singular double distribution at $y = 0$, which requires, in general, a regularization that is invisible in the forward case. We will accept for the time being the former solution, which allows us to have a comparison with numerical results of Ref. [15].

6.1.2 Models

As we have said above, we assume a two-component form for the GPDs. Namely, for the unpolarized case one has for each i-type quark

$$H_i(x,\xi,\Delta^2) = q_i(x,\xi,\Delta^2) + \frac{1}{N_f}\theta(1-|x/\xi|)D(x/\xi,\Delta^2)\,, \tag{129}$$

[5]From the partonic interpretation of GPDs, it is clear that the exclusive region is always governed by mesonic-like states. In general, there is a cross talk between the exclusive and inclusive regions, e.g., this ensures the polynomiality condition for moments [54]. If this is not the case, we call them isolated mesonic-like states.

$$E_i(x,\xi,\Delta^2) = r_i(x,\xi,\Delta^2) - \frac{1}{N_f}\theta(1-|x/\xi|)D(x/\xi,\Delta^2)\,, \tag{130}$$

with the D-term contributing equally to all N_f active quark species. Similar equations hold for the gluonic GPDs with $i = G$ and a gluonic D-term, $N_f^{-1}D(x/\xi) \to D_G(x/\xi)$. Note that the D-term drops out in the sum $H + E$ and, thus, has to be an antisymmetric function of x/ξ. For three active quark flavors we set $N_f = 3$. In the following we take an oversimplified factorized ansatz of the Δ^2-dependence from the other two scaling variables x and ξ for all functions. Note that due to the antisymmetry of the D-term it does not enter into the sum rule (121) and, therefore, its Δ^2-dependence is not constrained by it. As a model we take

$$D(z,\Delta^2) = \left(1 - \frac{\Delta^2}{m_{\rm D}^2}\right)^{-3} D(x/\xi)\,, \tag{131}$$

where the Δ^2-dependence is characterized by the cutoff mass $m_{\rm D}$, considered as a free parameter.

Obviously, q^i is a sum of valence- and sea-quark contributions. According to this we make a decomposition in these components and extract the momentum transfer dependence into valence and sea form factors, namely,

$$q_i(x,\xi,\Delta^2) = F_1^{i,\rm val}(\Delta^2)\, q_i^{\rm val}(x,\xi) + F_1^{\rm sea}(\Delta^2)\, q_i^{\rm sea}(x,\xi)\,, \tag{132}$$

for $i = u, d, s$, and $q_s^{\rm val}(x,\xi) = 0$ for the s-quarks.

At this point let us say that the (x,ξ)-dependence of the function $r(x,\xi,\Delta^2)$ is not constrained at all. However, since its first moment is given by the Pauli form factor, we extract it from $r(x,\xi,\Delta^2)$ and naively set the remainder of r equal to $q(x,\xi)$, i.e.,

$$r_i(x,\xi,\Delta^2) = F_2^{i,\rm val}(\Delta^2)\, q_i^{\rm val}(x,\xi) + F_2^{\rm sea}(\Delta^2)\, q_i^{\rm sea}(x,\xi)\,. \tag{133}$$

The valence u- and d-quark form factors can be extracted from the proton and neutron form factors via the formulae

$$2F_{1,2}^{u,\rm val}(\Delta^2) = 2F_{1,2}^{p}(\Delta^2) + F_{1,2}^{n}(\Delta^2)\,, \qquad F_{1,2}^{d,\rm val}(\Delta^2) = F_{1,2}^{p}(\Delta^2) + 2F_{1,2}^{n}(\Delta^2)\,. \tag{134}$$

The latter are known fairly well from experimental measurements and can be parametrized by dipole formulae in the small-Δ^2 region

$$G_E^p(\Delta^2) = \frac{1}{1+\kappa_p}G_M^p(\Delta^2) = \frac{1}{\kappa_n}G_M^n(\Delta^2) = \left(1 - \frac{\Delta^2}{m_V^2}\right)^{-2}, \qquad G_E^n(\Delta^2) = 0\,. \tag{135}$$

Note that we have set the neutron electric form factor equal to zero since at small momentum transfer it vanishes as a first power of Δ^2 with $-1/6$ times the neutron charge radius r_n^2 as a

coefficient, which is quite small, $r_n^2 \approx -0.113\,\mathrm{fm}^2$. Here the proton and neutron magnetic moments are $\kappa_p = 1.793$ and $\kappa_n = -1.913$, respectively. We have used Sachs electric and magnetic form factors related to Dirac and Pauli ones by

$$G_E^i(\Delta^2) = F_1^i(\Delta^2) + \frac{\Delta^2}{4M^2} F_2^i(\Delta^2)\,, \tag{136}$$

$$G_M^i(\Delta^2) = F_1^i(\Delta^2) + F_2^i(\Delta^2)\,, \tag{137}$$

respectively. They are characterized by the cutoff mass $m_V = 0.84\,\mathrm{GeV}$, see, e.g., [62]. The sea-quark form factors are guided by the counting rules and read in terms of Sachs form factors

$$G_E^{\rm sea}(\Delta^2) = \frac{1}{1+\kappa_{\rm sea}} G_M^{\rm sea}(\Delta^2) = \left(1 - \frac{\Delta^2}{m_{\rm sea}^2}\right)^{-3}, \tag{138}$$

with yet another mass cutoff $m_{\rm sea}$. The slope of $F_1^{\rm sea}$ is given by $B_{\rm sea} = \partial F_1^{\rm sea}/\partial\Delta^2|_{\Delta^2=0} = 3/m_{\rm sea}^2 - \kappa_{\rm sea}/4M^2$. The two free parameters $B_{\rm sea}$ and $\kappa_{\rm sea}$ will be specified below. Note that $\kappa_{\rm sea}$ enters in the sum rule that gives the fraction of the orbital angular momentum carried by quarks [2]. With our ad hoc assumption $r^i = q^i$ this sum rule reads

$$\begin{aligned} J^q &= \lim_{\Delta\to 0} \sum_{i=u,d,s} \frac{1}{2} \int_{-1}^{1} dx\, x \Big\{ H^i(x,\xi,\Delta^2,\mathcal{Q}^2) + E^i(x,\xi,\Delta^2,\mathcal{Q}^2) \Big\} \\ &= \frac{1}{2} \Big\{ (1+\kappa_p+\kappa_n/2)\, P^{u_{\rm val}} + (1+\kappa_p+2\kappa_n)\, P^{d_{\rm val}} + (1+\kappa_{\rm sea})\, P^{\rm sea} \Big\}\,, \end{aligned} \tag{139}$$

where the momentum fractions P^i carried by quarks can be deduced from deeply inelastic data alone.

The D-term does not affect the forward limit of GPDs. Therefore, we use Eq. (128) and model the quark $f_i(y,z)$ according to Ref. [55] as a product of a profile function π with the conventional type-i quark $f_i(y)$ and antiquark $\bar{f}_i$ densities. Namely, for valence and sea contributions we have

$$f_i^{\rm val}(y,z) = f_i^{\rm val}(y)\theta(y)\pi(|y|,z;b_{\rm val})\,, \tag{140}$$

$$f_i^{\rm sea}(y,z) = \Big\{ \bar{f}_i(y)\theta(y) - \bar{f}_i(-y)\theta(-y) \Big\} \pi(|y|,z;b_{\rm sea})\,, \tag{141}$$

with the usual definition for the valence density $f_i^{\rm val}(y) \equiv f_i(y) - \bar{f}_i(y)$. Here the profile is assumed to be universal for all valence- and sea-quark species and reads

$$\pi(y,z;b) = \frac{\Gamma\left(b+\frac{3}{2}\right)}{\sqrt{\pi}\Gamma(b+1)} \frac{[(1-y)^2 - z^2]^b}{(1-y)^{2b+1}}\,. \tag{142}$$

This ansatz ensures that the reduction formula (120) holds true. The parameter b encodes the skewedness effect, i.e., a larger value of b suppresses the ξ-dependence, and $q^i(x,\xi,\mathcal{Q}^2)$ reduces to the parton density $f^i(x,\mathcal{Q}^2)$ in the limit $b\to\infty$. This limit will be called the forward parton

distribution (FPD) model [56]. The idea driving the form of the ansatz (142) is that the profile function $\pi^i(y=0,z)$ mimics a mesonic-like two-parton state characterized by the longitudinal momentum fraction z. In the case of valence quarks one may choose the asymptotic distribution amplitude, which implies $b_{\rm val}=1$. In the case of sea quarks we consider $b_{\rm sea}$ as a free parameter, which will be discussed below. It will be adjusted by the comparison of our predictions to the H1 small-$x_{\rm B}$ data.

We similarly assume a factorized ansatz for the gluonic DD

$$f_G(y,z,\Delta^2)=F_G(\Delta^2)f_G(y,z)\,, \tag{143}$$

where

$$f_G(y,z)=y\left\{g(y)\theta(y)-g(-y)\theta(-y)\right\}\pi(|y|,z;b_G)\,. \tag{144}$$

The quark D-term was given in [15], making use of the results of the chiral quark soliton model [57] at the very low normalization point $\mu^2\approx 0.36$ GeV^2, in the form of an expansion in terms of Gegenbauer polynomials, $D(z)\approx -4.0\,C_1^{3/2}(z)-1.2\,C_3^{3/2}(z)-0.4\,C_5^{3/2}(z)$. The expansion coefficients have been fixed under the assumption that the polynomiality can only be restored with the help of the D-term and fit to the chiral soliton model evaluation. Compared to Ref. [16], we can adjust its fall-off with Δ^2 in Eq. (131) by the cutoff mass $m_{\rm D}$. Note that the evolution upwards to our input scale $\mathcal{Q}_0^2=4$ GeV^2 from $\mu^2\approx 0.36$ GeV^2 reduces the absolute value of the Gegenbauer polynomial coefficients by about 25% or even more, provided that the gluonic D-term is neglected. This reduction is larger (smaller) for positive (negative) expansion coefficients of the gluonic D-term. However, to study the significance of such a term for DVCS observables, we ignore any evolution effects.

The twist-two CFF $\mathcal{H}(\xi,\Delta^2)$ at LO in the QCD coupling constant reads in terms of the model (128) with the D-term included, i.e., Eq. (129),

$$\begin{aligned}\mathcal{H}(\xi,\Delta^2)=\frac{1}{\xi}\int_{-1}^{1}\frac{dx}{1-x/\xi-i0}\Bigg\{&\frac{2}{N_f}\sum_{i=u,d,s}Q_i^2\left(1-\frac{\Delta^2}{m_{\rm D}^2}\right)^{-3}\theta(1-|x/\xi|)D(x/\xi)\\
&+\int_{-1}^{1}dy\int_{-1+|y|}^{1-|y|}dz\,\delta(y+\xi z-x)\sum_{i=u,d,s}Q_i^2\Bigg\{F_1^{i,{\rm val}}(\Delta^2)\left(f_i^{\rm val}(y)\theta(y)-f_i^{\rm val}(-y)\theta(-y)\right)\pi(|y|,z;b_{\rm val})\\
&+2\,F_1^{\rm sea}(\Delta^2)\left(\bar f_i(y)\theta(y)-\bar f_i(-y)\theta(-y)\right)\pi(|y|,z;b_{\rm sea})\Bigg\}\Bigg\}\,,\end{aligned} \tag{145}$$

where $N_f=3$. Obviously, the replacements $D(x/\xi)\to -D(x/\xi)$ and $F_1\to F_2$ lead to the definition of $\mathcal{E}$.

In the following we take the MRS A' [58] parametrizations at $\mathcal{Q}_0^2=4$ GeV^2. This input scale ensures that evolution effects are small and are, therefore, not considered. We will neglect SU(2)

breaking in the sea and its charm component, i.e., $\bar{u} = \bar{d} = \bar{s}/2$. We use these forward parton densities in our LO analysis of DVCS and we are aware that this may result in a deviation of our predictions from the forward structure functions, measured experimentally in deeply inelastic scattering,

$$F_2(x_{\rm B}, \mathcal{Q}^2) \approx 2x_{\rm B}F_1(x_{\rm B}, \mathcal{Q}^2) = \frac{x_{\rm B}}{\pi}\Im{\rm m}\mathcal{H}^{\rm LO}(\xi = x_{\rm B}, \eta = 0, \Delta^2 = 0, \mathcal{Q}^2)\,, \tag{146}$$

up to 20%. Here we employed the Callan-Gross relation, valid in LO of perturbation theory. Recall that for a general two-photon process in the light-cone dominated region with a virtual outgoing γ-quantum, the CFF is given by $\mathcal{H}(\xi, \eta, \Delta^2, \mathcal{Q}^2)$. We will demonstrate below that the error involved in this approximation is small in comparison to the uncertainties induced by other sources.

Note that the fraction of the orbital angular momentum, given by the sum rule (139) with the assumed MRS parametrization, results into

$$J^q \approx 0.3 + 0.09\kappa_{\rm sea}\,, \qquad \text{for} \qquad \mathcal{Q}^2 = 4\ {\rm GeV}^2. \tag{147}$$

Estimates based on lattice calculations [59] and QCD sum rules [60] provide $J^q = 0.3 \pm 0.14$ and $J^q = 0.15 \pm 0.13$ at $\mu^2 \approx 1\ {\rm GeV}^2$, respectively. So we conclude that for consistency of these predictions, $\kappa_{\rm sea}$ may vary in a wide range $-3 < \kappa_{\rm sea} < 2$.

By the same token as above, the polarized quark GPD $\widetilde{H}$ is modeled according to

$$\widetilde{H}_i(x, \xi, \Delta^2) = G_1^{i,{\rm val}}(\Delta^2)\,\Delta q_i^{\rm val}(x, \xi) + G_1^{\rm sea}(\Delta^2)\,\Delta q_i^{\rm sea}(x, \xi)\,, \tag{148}$$

for $i = u, d, s$, and $\Delta q_s^{\rm val}(x, \xi) = 0$ for the s-quarks. Note that there is no D-term in this function [17]. The polarized valence- and sea-quark contributions are

$$\Delta f_i^{\rm val}(y, z) = \Delta f_i^{\rm val}(y)\theta(y)\pi(|y|, z; b_{\rm val})\,, \tag{149}$$

$$\Delta f_i^{\rm sea}(y, z) = \left\{\Delta \bar{f}_i(y)\theta(y) + \Delta \bar{f}_i(-y)\theta(-y)\right\}\pi(|y|, z; b_{\rm sea})\,, \tag{150}$$

with the usual definition for the polarized valence-quark density $\Delta f_i^{\rm val}(y) \equiv \Delta f_i(y) - \Delta \bar{f}_i(y)$. Obviously, $\Delta f_s^{\rm val} = 0$. In the forward limit this formula leads to Eq. (120). For the forward densities we use the GS A [61] parametrization with an SU(3) symmetric sea, again at the input scale $\mathcal{Q}^2 = 4\ {\rm GeV}^2$.

The axial form factors are

$$G_1^{i,{\rm val}}(\Delta^2) = \left(1 - \frac{\Delta^2}{m_A^2}\right)^{-2}, \qquad G_1^{\rm sea}(\Delta^2) = \left(1 - \frac{B_A}{3}\Delta^2\right)^{-3}, \tag{151}$$

where i runs over u- and d-quark species and the scale is $m_A = 0.9\,\mathrm{GeV}$ [62]. The slope B_A is considered as a free parameter, which should be fixed from experimental data.

The polarized CFF $\widetilde{\mathcal{H}}(\xi,\Delta^2)$ in terms of the model (128) has the form

$$\widetilde{\mathcal{H}}(\xi,\Delta^2) = \frac{1}{\xi}\int_{-1}^{1}\frac{dx}{1-x/\xi-i0}\int_{-1}^{1}dy\int_{-1+|y|}^{1-|y|}dz\,\delta(y+\xi z-x) \tag{152}$$
$$\times\sum_{i=u,d,s}Q_i^2\Big\{G_1^{i,\mathrm{val}}(\Delta^2)\left(\Delta f_i^{\mathrm{val}}(y)\theta(y)+\Delta f_i^{\mathrm{val}}(-y)\theta(-y)\right)\pi(|y|,z;b_{\mathrm{val}})$$
$$+2\,G_1^{\mathrm{sea}}(\Delta^2)\left(\Delta\bar{f}_i(y)\theta(y)+\Delta\bar{f}_i(-y)\theta(-y)\right)\pi(|y|,z;b_{\mathrm{sea}})\Big\}\Big\}.$$

For $\widetilde{E}$ we accept the pion pole-dominated ansatz of Ref. [63]

$$\widetilde{E}^u(x,\xi,\Delta^2) = -\widetilde{E}^d(x,\xi,\Delta^2) = \frac{1}{2}F_\pi(\Delta^2)\frac{\theta\,(\xi>|x|)}{2\xi}\phi_\pi\!\left(\frac{x+\xi}{2\xi}\right), \tag{153}$$

with $F_\pi(\Delta^2)$ taken in our estimates in the form given in Eq. (39) of Ref. [63],

$$F_\pi(\Delta^2) \approx \frac{4g_A^{(3)}M^2}{m_\pi^2-\Delta^2}\left(1+\frac{1.7\,\mathrm{GeV}^2(\Delta^2-m_\pi^2)}{(1-\Delta^2/2\,\mathrm{GeV}^2)^2}\right), \tag{154}$$

valid for $|\Delta^2| \ll M^2$. The pion mass is $m_\pi \approx 0.14$ GeV. For the pion distribution amplitude ϕ_π we take for simplicity its asymptotic form $\phi_\pi(u) = \phi^{\mathrm{asy}}(u) \equiv 6u(1-u)$, $0 \le u \le 1$.

Finally, the parity-odd gluonic GPD, $\widetilde{H}_G$, is modeled via the reduction to DD, and the latter taken in the form

$$\Delta f_G(y,z) = y\,\{\Delta g(y)\theta(y)+\Delta g(-y)\theta(-y)\}\,\pi(|y|,z;b_G)\,. \tag{155}$$

6.2 Features of Compton form factors

Now, before we come in section 7 to numerical estimates for the cross sections and asymmetries, it is worthwhile to study the properties of CFFs in the twist-two and -three approximations: the magnitude and shape of CFFs, the ratio of their real to imaginary part, the relation between twist-two and -three CFFs in the WW-approximation, and the effect of NLO corrections. Within our approximation it is consistent to take $\xi = x_{\mathrm{B}}/(2-x_{\mathrm{B}})$. Since we use a factorized form of GPDs with Δ^2-dependence separated from the scaling variables, we can safely set $\Delta^2 = 0$ in the most of estimates made in this section. These calculations are done with $\mathcal{Q}^2 = \mathcal{Q}_0^2 = 4$ GeV^2.

6.2.1 Twist-three versus twist-two effects

As observed above, the real and imaginary parts of the partonic CFFs are convex or concave functions of ξ (see the archive version of [33]). In Fig. 2 we show the CFFs for the valence

up-quarks (a,b) and up-antiquarks (c,d) based on the MRS A' parametrization without the D-term and with $b_{\rm val} = b_{\rm sea} = 1$. Here we rescaled the CFFs with ξ^{α_i}, and used $\alpha_u^{\rm val} = 0.441$ and $\alpha_u^{\rm sea} = 1.17$, which determine the small momentum fraction behavior of the corresponding forward parton densities [58]. The D-term affects only the real part of the CFFs by a shift, e.g., $\mathcal{H}_u^{\rm sea}$ and $C_u^{3(-)} \otimes H_u^{\rm sea}$ are shifted by a constant value of ≈ -1.66 and ≈ -0.22, respectively. Then, the entire CFF $\mathcal{H}(\xi) = \sum_{i=u,d,s} \mathcal{H}_i(\xi)$ will have a significant change: it starts now with a negative value at large ξ and turns over to a positive one at $x_{\rm B} \approx 0.2$. Obviously, the sign of $\Re{\rm e}\mathcal{H}$ in the valence-quark region[6] is determined by the cancellation between the positive sea-quark and negative valence-quark effects, both for double distribution ansatz alone and with the addition of the D-term. We will demonstrate below that a clear signature for the D-term can be washed away at $\Delta^2 \neq 0$ since the Δ^2-dependence of the sea quarks and the D-term is not constrained by the sum rules (121) as we have discussed in section 6.1.2 after Eq. (130).

The shapes of the CFFs can be understood in the following way. The phases $\phi_i(\xi) = {\rm Arg}\, \mathcal{H}_i(\xi)$ and the absolute values $|\mathcal{H}_i(\xi)|$ are monotonically increasing functions of the scaling variable ξ. It is interesting to note that in the WW-approximation the phase difference $\Delta\phi_i = \phi_i(\xi) - \phi_i^{\rm eff-WW}(\xi)$ is not very large. Neglecting the D-term and $\mathcal{H}_i^{\perp}$, we find that $|\Delta\phi_u^{\rm val}| < 0.4$ and $|\Delta\phi_u^{\rm sea}| < 0.16$ for all values of ξ. Moreover, these differences will vanish in the limit $\xi \to 0$. This property is obviously significant for observables that arise from the interference of twist-two and twist-three CFFs. Note also that the absolute value of the effective twist-three CFFs in the WW-approximation is of the same order as the twist-two ones. Thus, there is no numerical enhancement of the twist-three effects in this approximation. The relative size of twist-three contributions as compared to the twist-two harmonics is governed solely by kinematical factors appearing in the Fourier coefficients computed in section 4.

6.2.2 Small-$x_{\rm B}$ behavior

Let us now study the properties of the CFFs for small $x_{\rm B}$ in LO approximation. At intermediate momentum transfer this kinematics was discussed within the BFKL approach in Ref. [64]. In Fig. 2 we observe a scaling power-law behavior of the CFFs for small ξ, which has been already established in Refs. [65, 66] and the archive version of [33] for the FPD model. The small-ξ behavior of the CFFs is governed by the small momentum fraction asymptotics of the parton densities. If the latter behave like $x^{-\alpha}$ with $\alpha > 0$, then the real and imaginary part of $\mathcal{H}$ goes like $\xi^{-\alpha}$, and the ratio of the real to imaginary part is given by $\tan((\alpha-1)\pi/2) = -\cot(\alpha\pi/2)$. The small x-behavior of polarized parton densities, i.e., $y^{-\widetilde{\alpha}}$, induces an analogous growth of $\widetilde{\mathcal{H}}$,

[6] It implies that $x_{\rm B} \approx 1/3$, which we understand in the following as the region $0.1 < x_{\rm B} < 0.6$.

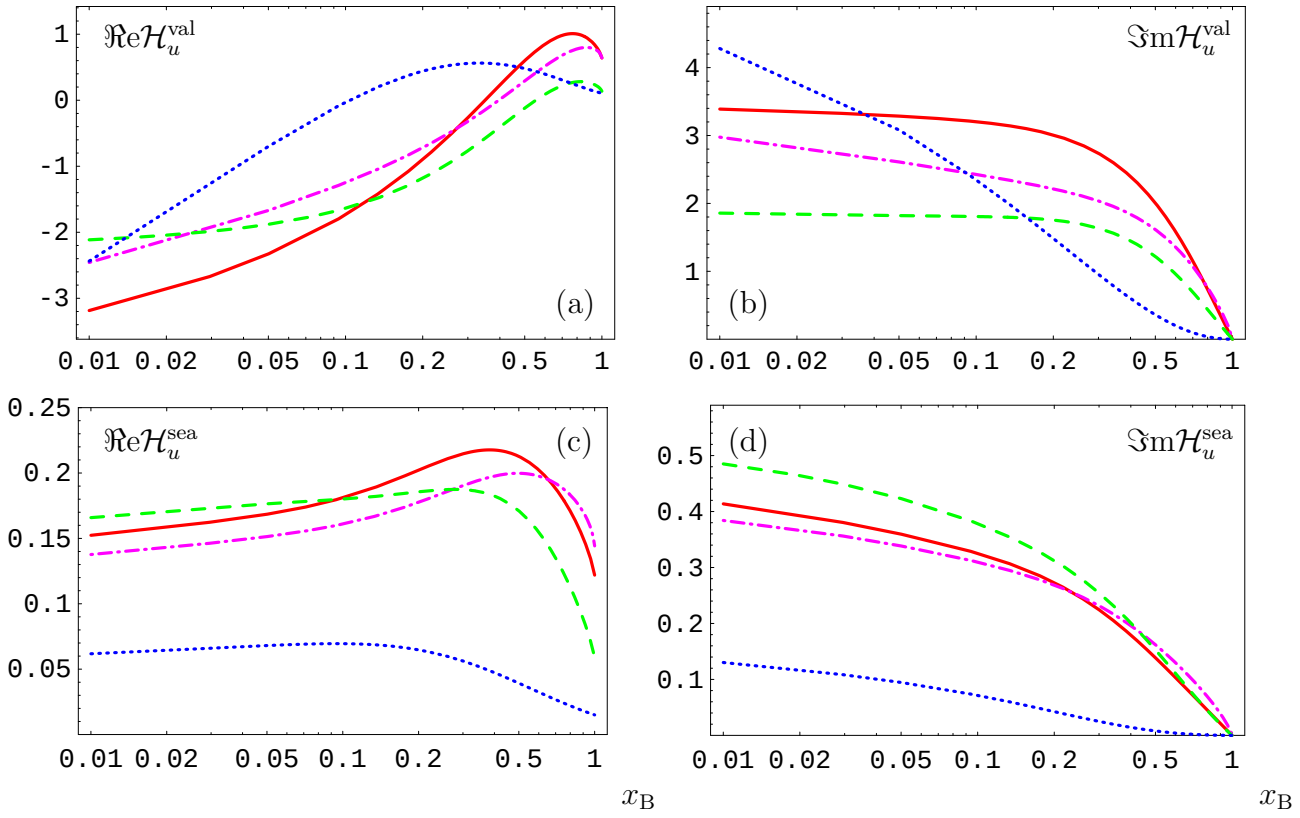

Figure 2: The real (a,c) and imaginary (b,d) part of the u-quark CFFs $\xi^\alpha\mathcal{H}$ in LO (solid) and NLO (dash-dotted). It displays also the twist-three functions in the WW approximation $\xi^\alpha\mathcal{H}^{\mathrm{eff-WW}}$ with $\mathcal{H}^\perp = 0$ (dashed), and the additive contribution $\xi^\alpha C^{3(-)} \otimes H$ (dotted), which enter the CFF $\mathcal{H}^{\mathrm{eff}}$ multiplied by a kinematical factor singular at $\Delta^2 = \Delta^2_{\mathrm{min}}$. The valence and sea u-quark contributions are shown in (a,b) and (c,d), respectively, as a function of x_{B} with $x_{\mathrm{B}} \geq 0.05$. The GPDs are taken at $\Delta^2 = 0$ and $\mathcal{Q}^2 = 4$ GeV^2 with $b_{\mathrm{val}} = b_{\mathrm{sea}} = 1$.

however, the ratio of the real to imaginary part is now $\tan(\tilde{\alpha}\pi/2)$.

Such a behavior can be understood in a model-independent way. The essential assumption is that the double distributions, which belong to the class of mathematical distributions, develop an expansion in the vicinity of the point $y = 0$ of the form

$$f_i(y,z) = y^{-\alpha_i}\left\{d_i(0,z) + \ldots\right\}. \tag{156}$$

Note that a δ-like singularity at $y = 0$ gives a contribution that is entirely concentrated in the exclusive region. We refer to it as an isolated mesonic-like state. In the forward limit of GPDs, such a contribution appears as a δ-like singularity and, thus, it will affect sum rules for parton

densities. So we may conclude that such singularities are absent in the spin non-flip GPDs[7] H and $\widetilde{H}$, however, they may be present in the spin-flip ones. Furthermore, we assume that $f(y,z)$ and, consequently, also $d(0,z)$ vanish fast enough when they approach the boundary of their support. By 'fast enough' we mean that $|d(0,z)| < |1 \mp z|^{\mathrm{Max}(0,\alpha-1)+\varepsilon}$ with $\varepsilon > 0$ for $z \to \pm 1$. We only discuss the region $0 \leq y$ in the following. The results of antiquark contributions for negative y can be easily deduced from the sea quarks at $y > 0$ employing the (anti)symmetry property of corresponding GPDs. We also assume that $\alpha_i < 2$ in the vector and $\widetilde{\alpha}_i < 1$ in the axial-vector sector to ensure the existence of certain integrals.

Since GPDs are reduced to the parton densities $f_i(y)$ according to Eqs. (120), we see that at small momentum fraction y, the parton densities are given by $y^{-\alpha_i} \int_{-1}^{1} dz\, d_i(0,z)$ with the exponential α_i, which determines their small-y behavior. Furthermore, a straightforward calculation shows that the imaginary and real parts of the twist-two CFFs at LO behave like:

$$\begin{aligned} \Im\mathrm{m}\mathcal{H}_i(\xi,\Delta^2,\mathcal{Q}^2) &= Q_i^2 \pi \xi^{-\alpha_i} \int_{-1}^{1} dz\, \frac{d_i(0,z,\Delta^2,\mathcal{Q}^2)}{(1-z)^{\alpha_i}}\,, \\ \Re\mathrm{e}\mathcal{H}_i(\xi,\Delta^2,\mathcal{Q}^2) &= \tan\left((\alpha_i-1)\frac{\pi}{2}\right) \Im\mathrm{m}\mathcal{H}_i(\xi,\Delta^2,\mathcal{Q}^2)\,, \end{aligned} \tag{157}$$

where the parameter α_i may depend on Δ^2 and $\mathcal{Q}^2$. The first equation agrees with the earlier considerations in Ref. [65] and the second one was discussed in Ref. [66]. An analogous formula holds true for the spin-flip contributions $\mathcal{E}_i$. Note that the D-term is not important in this limit, however, the small-ξ behavior can, in principle, be altered by other terms concentrated at $y = 0$, i.e., $\frac{d^n}{dy^n}\delta(y)$. So far such a behavior is not excluded by sum rules.

Let us also give the ratio of the imaginary part of the CFFs to parton densities,

$$\frac{\Im\mathrm{m}\mathcal{H}_i(\xi,\Delta^2,\mathcal{Q}^2)}{q_i(\xi,\mathcal{Q}^2)} = Q_i^2 \xi^{-\alpha_i^0/\alpha_i} \frac{\pi \int_{-1}^{1} dz\, (1-z)^{-\alpha_i} d_i(0,z,\Delta^2,\mathcal{Q}^2)}{\int_{-1}^{1} dz\, d_i(0,z,0,\mathcal{Q}^2)}\,, \tag{158}$$

where $\alpha_i^0 \equiv \alpha_i(\Delta^2 = 0)$. For the GPD ansatz, we are using with $b_{\mathrm{sea}} = 1$, the leading behavior comes from the sea quarks with $\alpha_{\mathrm{sea}} = 1.17$, which provides their ratio (158) of order $\approx 1.75\pi Q_i^2 F_1^{\mathrm{sea}}(\Delta^2)$ for each sea quark species.

For the axial-vector channel, analogous relations can be derived, however, with a difference that the ratio of the real to imaginary part is now tangent rather than minus cotangent,

$$\begin{aligned} \Im\mathrm{m}\widetilde{\mathcal{H}}_i(\xi,\Delta^2,\mathcal{Q}^2) &= Q_i^2 \pi \xi^{-\widetilde{\alpha}_i} \int_{-1}^{1} dz\, \frac{\widetilde{d}_i(0,z,\Delta^2,\mathcal{Q}^2)}{(1-z)^{\widetilde{\alpha}_i}}\,, \\ \Re\mathrm{e}\widetilde{\mathcal{H}}_i(\xi,\Delta^2,\mathcal{Q}^2) &= \tan\left(\widetilde{\alpha}_i\frac{\pi}{2}\right) \Im\mathrm{m}\widetilde{\mathcal{H}}_i(\xi,\Delta^2,\mathcal{Q}^2)\,. \end{aligned} \tag{159}$$

[7] Unfortunately, this is not necessarily true since they can vanish in the forward limit with Δ^2, too.

The ratio of the imaginary part of $\widetilde{\mathcal{H}}_i$ to the polarized parton density Δq_i is determined by

$$\frac{\Im\mathrm{m}\widetilde{\mathcal{H}}_i(\xi,\Delta^2,\mathcal{Q}^2)}{\Delta q_i(\xi,\mathcal{Q}^2)} = Q_i^2\xi^{-\widetilde{\alpha}_i^0/\widetilde{\alpha}_i}\,\frac{\pi\int_{-1}^1 dz\,(1-z)^{-\widetilde{\alpha}_i}\widetilde{d}_i(0,z,\Delta^2,\mathcal{Q}^2)}{\int_{-1}^1 dz\,\widetilde{d}_i(0,z,0,\mathcal{Q}^2)}\,, \tag{160}$$

with $\widetilde{\alpha}_i^0 = \widetilde{\alpha}_i(\Delta^2=0)$. However, in contrast to the vector channel, the small-$x_{\rm B}$ behavior of the polarized parton distributions has not been explored in experiments. Usually, one assumes a similar behavior of the polarized valence- and sea-quark distributions with $\widetilde{\alpha}_i \approx 0.5$. Thus, the leading behavior of $\widetilde{\mathcal{H}}$ is determined by all parton species and in the forward limit it is suppressed with respect to $\mathcal{H}$ by an extra $\sqrt{\xi}$ or similar.

In the case of twist-three contributions, the power behavior remains the same, however, the normalization of the real and imaginary part will be changed. It is sufficient to discuss the convolution with the $C_{(0)}^{3(\pm)}$-kernels. The behavior of the effective twist-three contribution in the WW-approximation of Eq. (84), can then be simply predicted. For the imaginary part we find a modification of the integrand by the hypergeometric function:

$$\Im\mathrm{m}\left\{C_{(0)i}^{3(\mp)}\otimes F_i\right\} = Q_i^2\frac{\pi}{\alpha_i}\xi^{-\alpha_i}\int_{-1}^1 dz\,\frac{d_i(0,z,\Delta^2,\mathcal{Q}^2)}{(1-z)^{\alpha_i}}\,{}_2F_1\left(\begin{matrix}1,\alpha_i\\1+\alpha_i\end{matrix}\middle|-\frac{1+z}{1-z}\right). \tag{161}$$

The ratio of the real to imaginary part remains the same as in the twist-two case, i.e., $-\cot(\pi\alpha/2)$ and $\tan(\pi\widetilde{\alpha}/2)$ for the convolution with $C^{3(-)}$ and $C^{3(+)}$ kernels [see Eqs. (157) and (159)], respectively.

From Fig. 3 we observe that the relative deviation of the dominant partonic CFFs $\mathcal{H}_u^{\rm sea}$ and $\widetilde{\mathcal{H}}_u^{\rm val}$ from their asymptotic values given in Eqs. (157) and (159), respectively, is of order of 20% for $x_{\rm B}=10^{-2}$ and decreases to 10% level, and even further at $x_{\rm B}\le 10^{-3}$. Note, however, that a faster convergence of the effective twist-three CFFs to its asymptotic form (161) in comparison to the twist-two sector is caused by an essential cancellation occurred in the WW-approximation. For instance, the convolution $\left\{C_i^{3(\mp)}\otimes F_i\right\}$ alone has a large deviation of order of 40% for $x_{\rm B}=10^{-2}$.

Finally, let us add a word on the isolated mesonic-like states, which we mentioned at the beginning of this section. It is easy to show that these δ-like singularities, i.e., $\frac{d^n}{dy^n}\delta(y)$, convoluted with the hard scattering part yield contributions proportional to ξ^{-n-1}. Since the hard scattering part possesses definite symmetry properties, the exponent n is odd (even) for $\mathcal{E}$ ($\widetilde{\mathcal{E}}$).

6.2.3 Radiative corrections

Now we address the theoretical uncertainties due to radiative corrections, which have been analytically worked out in a number of papers for the twist-two sector at NLO [18, 19, 20, 21, 22], and numerical studies have been performed in Refs. [23, 24, 25]. For the quark sector alone the

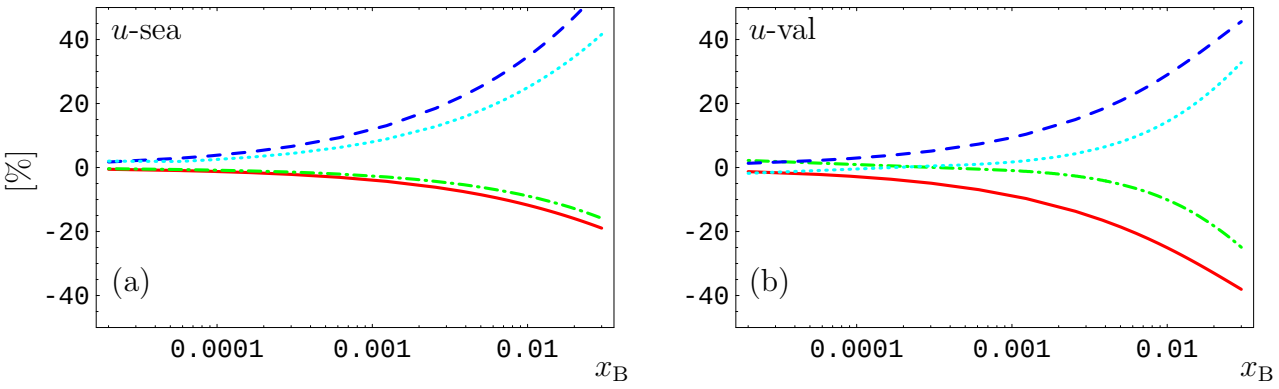

Figure 3: The relative deviation of the sea u-quark CFF from its asymptotic value is displayed for $\Im\mathrm{m}\mathcal{H}$ and $\Re\mathrm{e}\mathcal{H}/\Im\mathrm{m}\mathcal{H}$ as the solid and dashed line, respectively, in (a). The same quantities are plotted for $\mathcal{H}^{\mathrm{eff-WW}}$ with $\mathcal{H}^{\perp}=0$ as dash-dotted and dotted lines, respectively. The right panel (b) shows the same as in (a) but for the valence u-quark CFF $\widetilde{\mathcal{H}}$. The GPD-parameters are the same as in Fig. 2.

NLO amplitudes are shown as dash-dotted curves in Fig. 2. The one-loop corrections turn out to be moderate for each quark specie. However, model-dependent considerations that involve gluonic contributions showed that NLO effects can be quite sizable both in the valence [23, 25] and small-x_{B} [25] region. In the following we have a closer look to this issue and propose a solution to the problem of large NLO effects.

The NLO corrections are evaluated with the same set of GPDs as earlier. We disregard the evolution of the coupling and set it equal to $\alpha_s/\pi=0.1$. The D-term and pion-pole contributions will separately be considered below. If the real part of a CFF is close to zero at some ξ, e.g., due to cancellations between different quark species, the relative radiative corrections are blowing up. Thus, it is more convenient to discuss their magnitude in terms of the absolute values $|\mathcal{F}|=\sqrt{(\Re\mathrm{e}\mathcal{F})^2+(\Im\mathrm{m}\mathcal{F})^2}$ and phases $\mathrm{Arg}\,\mathcal{F}$.

Let us study at first the naive scale setting condition $\mu_F=\mathcal{Q}$. In this case the radiative corrections to the absolute value of the CFFs, i.e.,

$$\mathcal{R}_b^{\mathrm{abs}}=|\mathcal{H}^{\mathrm{NLO}}|/|\mathcal{H}^{\mathrm{LO}}|-1\,, \tag{162}$$

are rather moderate provided gluon contributions are totally neglected. Then for the choice of the DD-model b-parameter $b_{\mathrm{sea}}=1$, one observes that $\mathcal{R}_1^{\mathrm{abs}}$ is of order -10% in both valence and small-x_{B} region, as shown in Fig. 4 (a) by the dashed line. For the FPD case when $b_{\mathrm{sea}}\to\infty$, the $\mathcal{R}_\infty^{\mathrm{abs}}$ is a factor of 2 larger as compared to $\mathcal{R}_1^{\mathrm{abs}}$, i.e., $\mathcal{R}_\infty^{\mathrm{abs}}\sim-20\%$. The radiative corrections

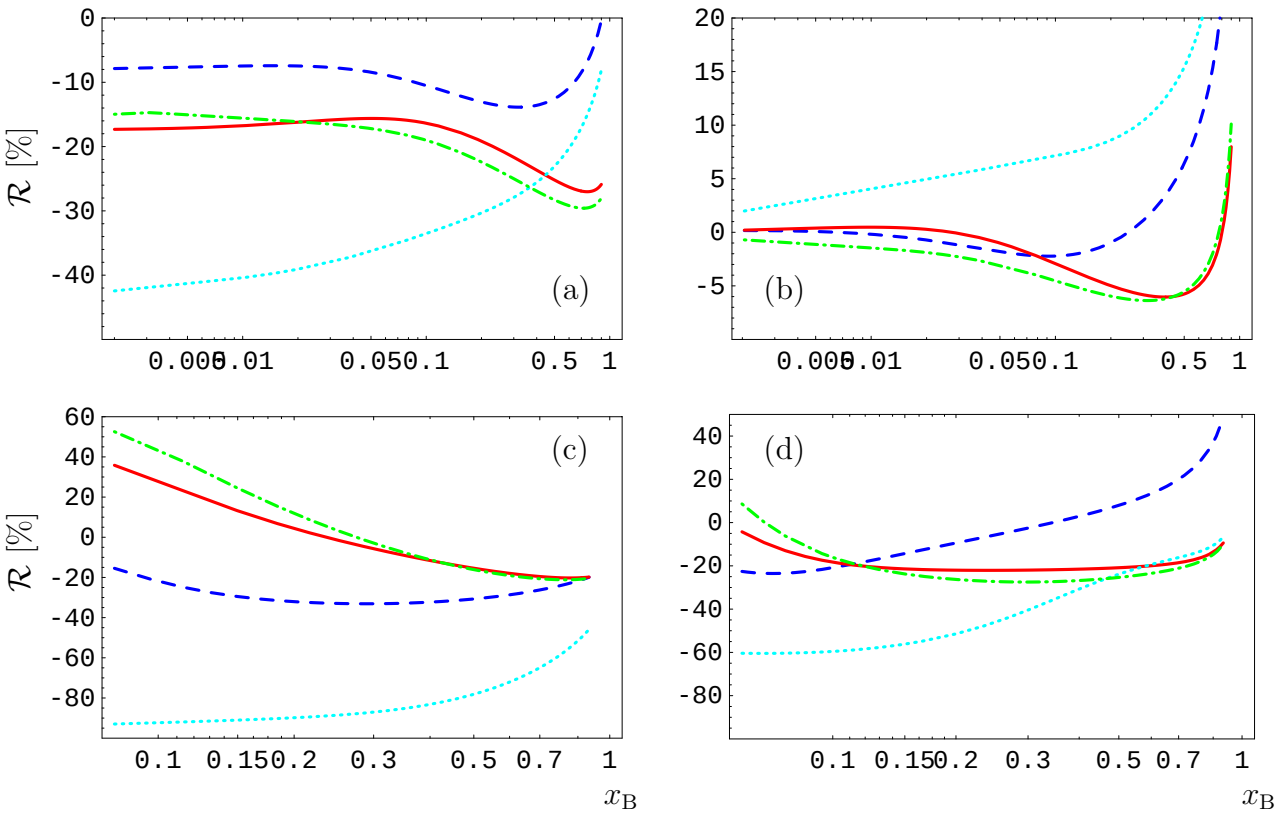

Figure 4: The relative NLO corrections $\mathcal{R}$ (see Eq. 162) to the absolute value (a,c) and the phase (b,d) of the CFFs $\mathcal{H}$ (a,b) and $\widetilde{\mathcal{H}}$ (c,d). The magnitude of radiative corrections with neglected gluon GPD contributions are displayed as dashed and solid curves for the factorization scale setting $\mu_F = \mathcal{Q}$ and $\mu_F \approx \mu_F^{\rm DVCS}$, respectively. The complete (quark + gluon) NLO result is given for these both scale settings by dotted and dash-dotted lines, respectively. The coupling is set to $\alpha_s/\pi = 0.1$, the quark GPD-parameters are the same as in Fig. 2, and $b_G = 2$.

stemming from the quark sector alone to the phase of CFFs are defined as in Eq. (162) but with the obvious replacements of $\mathcal{R}^{\rm abs}$ by $\mathcal{R}^{\rm ph}$, and $\mathcal{H}$ by $\mathrm{Arg}\,\mathcal{H}$. They are smaller than 20% in the valence quark region, and are on a percent level at small $x_{\rm B}$, see the dashed line in Fig. 4 (b). Qualitatively, the same features hold for $\widetilde{\mathcal{H}}$. However, quantitatively we find here a slightly larger effect in the valence-quark region where relative corrections are of order of -30% and $\pm 20\%$ for the absolute value and phase, respectively, see the dashed curves in Fig. 4 (c) and (d).

To have a feeling on the magnitude of CFFs we give a few numbers. For $\mathcal{H}$ we have

$$\mathcal{H}^{\rm LO}(\xi = 5\cdot 10^{-5}, \Delta^2 = 0, \mathcal{Q}^2 = 4\ \mathrm{GeV}^2) \approx (0.39 + 1.37i)\cdot 10^5\,,$$

which is considerably larger than its polarized counterpart,

$$\widetilde{\mathcal{H}}^{\rm LO}(\xi = 5 \cdot 10^{-5}, \Delta^2 = 0, \mathcal{Q}^2 = 4 \text{ GeV}^2) \approx 200 + 163i\,,$$

mainly reflecting the fact that $\widetilde{\alpha}_i < \alpha_{\rm sea}$.

So far, at the level of amplitudes the NLO radiative corrections in the quark sector were moderate within the model with $b_{\rm sea} = 1$. This gives us some confidence in the applicability of the perturbative approach to the DVCS process. Now we come to the gluonic contributions, which enter for the first time at order $\mathcal{O}(\alpha_s)$. For $\mu_F = \mathcal{Q}$ they are displayed as dotted curves in Fig. 4. As we see, with our model for gluonic GPDs their effects in the amplitudes are large. However, the size of the product $\alpha_s/2\pi\times$ gluonic CFF, compared to the LO result, is not a measure for the quality of perturbation theory, it rather gives the ratio of 'leading' gluonic to quark CFFs. Of course, one cannot exclude that these large α_s-contributions are merely generated by an unrealistically oversized ansatz for the gluonic GPDs.

To understand the physical meaning of these large contributions, it is instructive to study the evolution of the gluonic GPD. We use throughout $b_G = 2$ in the profile function (142). Taking the GRV parametrization at its intrinsic low scale $\mathcal{Q}_0^2 = 0.49$ GeV^2, it has been observed that the gluon GPD changes under evolution much stronger than their non-singlet quark counterparts [67]. This is of course also true in the forward case. However, if we take the MRS A' parametrization at the input scale $\mathcal{Q}_0^2 = 4$ GeV^2, we observe a strong scale dependence of the NLO result, which is in line of observations made in Refs. [24, 25]. Since the NLO coefficient functions can be expressed in terms of evolution kernels [18], thus, a strong change under evolution implies a large gluonic contribution in the one-loop approximation. Analogous to deeply inelastic scattering one can study the scale dependence by taking the logarithmic derivative of the CFFs, i.e.,

$$\mathcal{Q}^2 \frac{d}{d\mathcal{Q}^2} \ln \mathcal{H}(\xi) = \frac{\alpha_s(\mathcal{Q}^2)}{2\pi} \frac{\sum_{i=u,d,s} C_i^{(-)} \otimes \left[V^{qq} \otimes H_i + \frac{1}{\xi} V^{qG} \otimes H_G\right](\xi)}{\mathcal{H}(\xi)}\,, \tag{163}$$

where V^{qq} and V^{qG} are the LO evolution kernels. This quantity is demonstrated in Fig. 5 for two quite different factorization scale settings at $x_{\rm B} \leq 0.1$, where the gluonic term produces, indeed, a dominant contribution.

Of course, it would be delightful if gluon contributions would be also moderate. Then DVCS observables can be estimated relying solely on LO approximation, and the phenomenology of DVCS can in the first stage be restricted to the quark sector alone. However, even in the opposite situation we can minimize the size of large radiative corrections, originated by strong evolution effects. The restriction to the quark sector can be achieved by an appropriate factorization scale setting, namely, in such a way that the gluonic contribution does not enter the amplitude, e.g., at

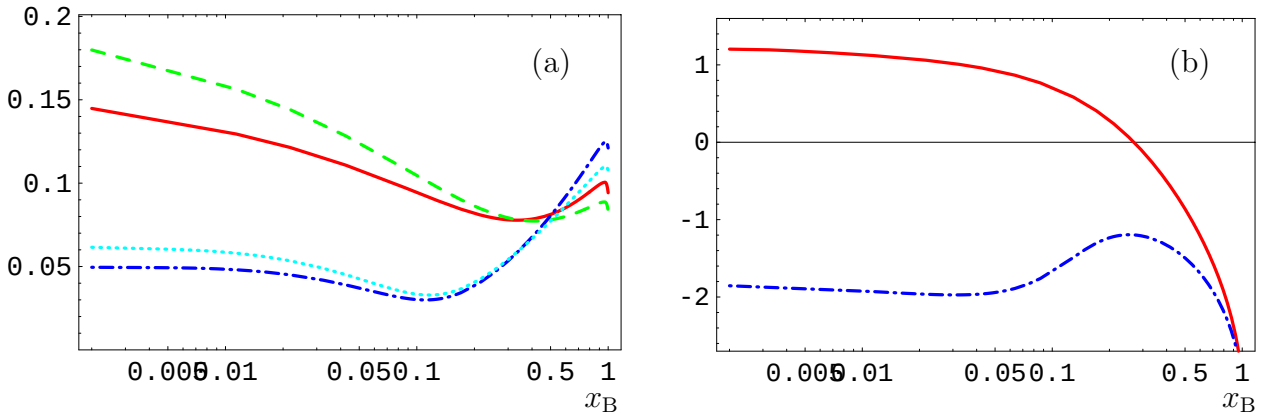

Figure 5: The real (a) and imaginary (b) part of $\mathcal{Q}^2 \frac{d}{d\mathcal{Q}^2} \ln \mathcal{H}$ for MRS A' parametrization with $b_{\rm val} = b_{\rm sea} = 1$ at $\Delta^2 = 0$. The dash-dotted (dotted) line shows the scale violation due to the evolution of quarks, while the solid (dashed) one includes also the evolution of gluons for the scale setting $\mu_F = 3.8\mathcal{Q}$ ($\mu_F = \mathcal{Q}$). The parameters are set as in Fig. 4.

NLO

$$\mathcal{H}_G(\xi, \mathcal{Q}^2) = \frac{\alpha_s}{2\pi} \sum_{i=u,d,s} Q_i^2 \int_{-1}^{1} dx\, C_G(x/\xi, \mathcal{Q}^2/\mu_F^2) H_G(x, \xi, \mu_F^2)_{\mu_F = \mu_F^{\rm DVCS}} = 0\,. \tag{164}$$

This scale setting procedure will go under the name of the DVCS scheme. It requires two (x, ξ)-dependent factorization scales μ_F inside the convolution, i.e., one for parity even and odd CFFs, respectively. Consequently, this procedure provides two (one for real and one for imaginary part) real-valued effective scales $\mu_F^{\rm eff}(\xi)$, that depend on ξ, for each CFF.

An inspection of the imaginary part of the NLO coefficient in the vector case tells us that the desired factorization scale is almost ξ-independent. For our model it is given by $\mu_F^{\rm DVCS} \approx \sqrt{2}{\rm e}\mathcal{Q} \approx 3.8\mathcal{Q}$. Since the real part is expressed in term of the imaginary part by means of a dispersion relation, we expect that also the absolute value of $\mathcal{H}_G$ is minimized in this way. This is demonstrated in Fig. 4, where we display the relative NLO corrections, see Eq. (162) for the definition, coming from quarks (dashed, solid) and from all partons, including gluons, (dotted, dash-dotted). We also employ the scale found for $\mathcal{H}$ in the evaluation of $\widetilde{\mathcal{H}}$ in the valence quark region. Here we should mention that with our models, the CFF $\widetilde{\mathcal{H}}$ can be safely neglected in $\mathcal{C}_{\rm unp}^{\rm DVCS}$ and $\mathcal{C}_{\rm unp}^{\mathcal{I}}$ for an unpolarized target. In the vector (a,b) and axial-vector (c,d) cases the gluonic contributions drastically reduce the LO quark contributions for the naive $\mu = \mathcal{Q}$ scale setting (dotted line). For $\mu_F = 3.8\mathcal{Q}$, the radiative gluonic NLO corrections are small (cf. dash-dotted and solid curves). The displayed change of the quark radiative corrections (for the absolute value from -10% to -20%) should be considered as a bound, since we did not include evolution

effects. Doing so, they will compensate the change we have displayed. Let us emphasize again, that our quantitative considerations are model-dependent. Taking, for instance, the FPD model, at $\mu_F = \mathcal{Q}$ we observe the value of $\mathcal{R}^{\rm abs}$ is twice larger in both sectors. For the choice $\mu_F = 3.8\mathcal{Q}$, the gluonic NLO contribution is now about 10%, while the quark and the whole NLO corrections are even smaller as demonstrated in Fig. 4 (a).

Let us now come to contributions that show up only in the exclusive region. For the D-term we find to NLO accuracy

$$\mathcal{H}_{\rm D-term} = -4.98 \left\{ 1 + \frac{\alpha_s}{2\pi} \left(1.83 - 2.34 \ln \frac{\mathcal{Q}^2}{\mu_F^2} \right) + \cdots \right\} . \tag{165}$$

If we set the factorization scale $\mu_F = \mathcal{Q}$, the relative correction is positive and of order of 10%. If the gluon model is realistic, we should better employ the DVCS scheme, in which the D-term is reduced by about 20%.

For the pion-pole contribution the scale dependence drops out in the hard scattering part since we have chosen the asymptotic form of the pion distribution amplitude. We get at NLO

$$\mathcal{E}(\xi, \Delta^2) = \frac{1}{2\xi} F_\pi(\Delta^2) \left\{ 1 - \frac{10}{3} \frac{\alpha_s}{2\pi} \right\} , \tag{166}$$

which acquires the correction of order 15%.

6.3 Summary

Let us summarize the results of this section. We introduced a simple model with several free parameters based on the factorization of Δ^2 and $(x, \xi, \mathcal{Q}^2)$ dependence. The latter is modeled according to the DD ansatz with MRS A' and GS A parametrization for the parton densities at the input scale $\mathcal{Q}_0^2 = 4$ GeV^2. This oversimplification is only justified by the fact that there is no model-independent knowledge available about the functional dependence of GPDs on their arguments.

In this model the NLO corrections to the partonic quark CFFs are moderate. The theoretical uncertainties entering at NLO mainly arise from the lack of information on the form of gluonic GPDs. Also in the case when a realistic gluon GPD provides NLO corrections of the same order as the quark contributions at LO (in $\mathcal{H}^G$ we observed a different overall sign with respect to the unpolarized sea-quark contribution within our model), we can exclude them from the NLO analysis by choosing the DVCS scheme. Although this favors a rather large factorization scale, the NLO corrections in the quark sector remain moderate. However, note that the results for the FPD model of $\mathcal{H}$ is a factor of 2 larger than the corresponding estimate with $b_{\rm sea} = 1$. Therefore, NLO effects can be quite sizable, especially, in the squared DVCS term. In this product of DVCS

amplitudes they are twice larger than in the interference term, which is linear in the them. For a rough estimate of observables, which are affected in an uncontrollable manner by the models accepted for quantitative estimates, it is enough to work in the quark sector at LO. However, for extraction of model parameters from experimental data with high accuracy, a NLO analysis will be inevitable.

Moreover, we found from general assumptions, that the parametrization of the CFFs $\mathcal{F} = \sum_{i=u,d,s} \mathcal{F}_i$ in the small-$x_{\rm B}$ region is rather unique, and is in fact governed by the small y-behavior of the DDs. The skewedness effect is included in the normalization of the CFFs. Our analysis suggests that we can take the following general parametrization, derived in the DVCS-scheme at a given input scale $\mathcal{Q}_0^2 > 1{\rm GeV}^2$, at small $x_{\rm B}$:

$$\begin{aligned}
\left\{ \begin{matrix} \Re{\rm e} \\ \Im{\rm m} \end{matrix} \right\} \mathcal{H}(\xi,\Delta^2) &= \left\{ \begin{matrix} -\cot(\alpha\,\pi/2) \\ 1 \end{matrix} \right\} N_{\mathcal{H}}(\Delta^2)\,\xi^{-\alpha(\Delta^2)}\,, \qquad (167)\\
\left\{ \begin{matrix} \Re{\rm e} \\ \Im{\rm m} \end{matrix} \right\} \mathcal{E}(\xi,\Delta^2) &= \left\{ \begin{matrix} -\cot(\beta\,\pi/2) \\ 1 \end{matrix} \right\} N_{\mathcal{E}}(\Delta^2)\,\xi^{-\beta(\Delta^2)} + \left\{ \begin{matrix} 1 \\ 0 \end{matrix} \right\} M_{\mathcal{E}}(\Delta^2)\,\xi^{-2p}\,,\\
\left\{ \begin{matrix} \Re{\rm e} \\ \Im{\rm m} \end{matrix} \right\} \widetilde{\mathcal{H}}(\xi,\Delta^2) &= \left\{ \begin{matrix} \tan(\widetilde{\alpha}\,\pi/2) \\ 1 \end{matrix} \right\} N_{\widetilde{\mathcal{H}}}(\Delta^2)\xi^{-\widetilde{\alpha}(\Delta^2)}\,,\\
\left\{ \begin{matrix} \Re{\rm e} \\ \Im{\rm m} \end{matrix} \right\} \widetilde{\mathcal{E}}(\xi,\Delta^2) &= \left\{ \begin{matrix} \tan\left(\widetilde{\beta}\,\pi/2\right) \\ 1 \end{matrix} \right\} N_{\widetilde{\mathcal{E}}}(\Delta^2)\xi^{-\widetilde{\beta}(\Delta^2)} + \left\{ \begin{matrix} 1 \\ 0 \end{matrix} \right\} \frac{F_\pi(\Delta^2)}{2\xi} + \left\{ \begin{matrix} 1 \\ 0 \end{matrix} \right\} M_{\widetilde{\mathcal{E}}}(\Delta^2)\,\xi^{-2\widetilde{p}-1}\,,
\end{aligned}$$

where we have $\alpha(\Delta^2=0) \sim 1.2$ and $\widetilde{\alpha}(\Delta^2=0) \sim 0.5$ and $p, \widetilde{p} \geq 1$ are positive integers that reflect the appearance of isolated mesonic-like states. So they provide the dominant contributions in the spin-flip CFFs and could overwhelm the small-$x_{\rm B}$ behavior of the spin non-flip CFFs. Note also that because of the small- and large-ξ behavior, and the simple shape of the (partonic) CFFs, it is obvious that one can extend the parametrization in the whole kinematical region by allowing a weak ξ-dependence in the N-factors and additionally in the phase, while the M-factors remain ξ-independent.

7 Quantitative estimates for DVCS observables

In this section we give numerical estimates for DVCS observables in the twist-two and -three approximation at LO of perturbation theory for several choices of kinematical invariants and compare them, whenever possible, with available experimental data. To this end, we use exact expressions for the BH propagators and K-factor, when the latter appears as a prefactor in the Fourier coefficients. In section 7.1 we use the DVCS data by H1 collaboration to adjust free parameters in the sea-quark sector of our model. Then we consider asymmetries for unpolarized

fixed target experiments in section 7.2. We compare our model expectations with the beam-spin asymmetry measurements of HERMES and CLAS collaborations and give then predictions for the E-01-113 experiment at Jefferson Lab [10]. We deliver a general discussion about the magnitude of twist-three versus twist-two effects in these kinematical situations. Furthermore, we present a detailed numerical analysis of the size of twist-three effects for an unpolarized target and derive constraints for certain charge azimuthal asymmetries. Finally, we give in section 7.3 a few estimates for longitudinally polarized fixed target experiments[8].

The reference frame used in the analyses by these experimental collaborations differs from the one we employ in our considerations, see Fig. 1, by the direction of the z-axis. Both, HERMES and CLAS use the third direction pointing along the virtual photon's three-momentum. Thus, their frame (distinguished below by the prime on symbols) is deduced from ours by the rotation around the x-axis on the angle π. Therefore, the proton azimuthal angles in our frame ϕ and their frame ϕ'_N are related by $\phi + \phi'_N = 2\pi$. The same relation holds for the real photon angles $\phi_\gamma + \phi'_\gamma = 2\pi$. The proton and photon angles are related to each other by the equations $\phi_\gamma = \phi + \pi$ and $\phi'_N = \phi'_\gamma + \pi$ in our and their frames, respectively. Therefore, the proton and real photon azimuth is given in terms of the angle ϕ by

$$\phi'_N = 2\pi - \phi\,, \qquad \phi'_\gamma = \pi - \phi\,.$$

7.1 Small-$x_{\rm B}$ estimates

In this paragraph we address two questions: (i) What can we learn from DVCS in the small-$x_{\rm B}$ region? (ii) Is there a kinematical window left to measure twist-three effects? Thanks to the small-$x_{\rm B}$ parametrization devised in Eq. (167) and the analytical expressions for the Fourier coefficients, computed in section 4, both of these questions can be answered in a straightforward manner. Although we only consider an unpolarized proton, the analysis is rather complex and we cannot cover all possible scenarios, which are allowed by the residual degrees of freedom left in the parametrizations (167).

Let us address the first question. We will now see how one can test the structure of CFFs and measure its small-$x_{\rm B}$ behavior in a model-independent manner. This includes a test of the absence of isolated mesonic-like states, the measurement of $\mathcal{H}$, and, perhaps, access to the spin-

[8] We refer to the longitudinal polarization in our frame. In the laboratory frame with the z-direction defined with respect to the lepton beam it implies that the target has a transverse polarization either. The reverse is also true, if in the lab-frame the target is longitudinally polarized, in the frame Fig. 1 we will have both longitudinal as well as transverse components of the nucleon polarization vector. The projection on the first one is easily done by integrating over the whole range of the angle φ.

flip CFF $\mathcal{E}$. The strategy is to rely first on the hypothesis of the sea-quark dominance in $\mathcal{H}$ and then to derive relations between different observables. A violation observed in such constraints will then be regarded as a signature of other contributions involved and not accounted for in the approximation adopted here.

Employing Eqs. (167), we can now drastically simplify the twist-two Fourier coefficients. For an unpolarized target the squared DVCS term [see Eqs. (43) and (69)] reads

$$c_{0,\mathrm{unp}}^{\mathrm{DVCS}} = 2(2-2y+y^2)\left\{\frac{1}{\sin^2(\alpha\,\pi/2)}\frac{N_{\mathcal{H}}^2}{\xi^{2\alpha}} - \frac{\Delta^2}{4M^2}\left(\frac{1}{\sin^2(\beta\,\pi/2)}\frac{N_{\mathcal{E}}^2}{\xi^{2\beta}} + \frac{F_\pi^2}{4}\right)\right\}_{|\xi=x_{\mathrm{B}}/2}, \quad (168)$$

where the term $F_\pi^2/4$ arises from the pion-pole contribution[9] in $\widetilde{\mathcal{E}}$. The latter is absent in the interference term, which is given by [see Eqs. (54) and (69)]

$$\begin{aligned}\begin{Bmatrix} c_{1,\mathrm{unp}}^{\mathcal{I}} \\ s_{1,\mathrm{unp}}^{\mathcal{I}} \end{Bmatrix} &= 8K \begin{Bmatrix} -(2-2y+y^2) \\ \lambda y(2-y) \end{Bmatrix} \\ &\times \left[F_1\begin{Bmatrix} -\cot(\alpha\,\pi/2) \\ 1 \end{Bmatrix}\frac{N_{\mathcal{H}}}{\xi^\alpha} - \frac{\Delta^2}{4M^2}F_2\begin{Bmatrix} -\cot(\beta\,\pi/2) \\ 1 \end{Bmatrix}\frac{N_{\mathcal{E}}}{\xi^\beta}\right]_{|\xi=x_{\mathrm{B}}/2}.\end{aligned} \quad (169)$$

Note that the D-term can be safely neglected as emphasized above and $\widetilde{\mathcal{H}}$ does not contribute if we assume that $\widetilde{\alpha} \ll \alpha$. The last assumption is expected to hold for parton densities in view of current experimental data. The normalization factors can be expressed in terms of model-dependent parameters. In our case they are determined by the partonic form factors, skewedness effects, and normalization of parton densities. Relying on the sea-quark dominance we find

$$N_{\mathcal{H}}(\Delta^2) = \sum_{i=u,d,s} Q_i^2 \frac{n_{\mathrm{sea}}(1+\gamma_{\mathrm{sea}})}{3}\, F_1^{\mathrm{sea}}(\Delta^2) \frac{\pi\Gamma(1+b_{\mathrm{sea}}-\alpha_{\mathrm{sea}})\Gamma(2+2b_{\mathrm{sea}})}{2^{\alpha_{\mathrm{sea}}}\Gamma(1+b_{\mathrm{sea}})\Gamma(2+2b_{\mathrm{sea}}-\alpha_{\mathrm{sea}})}, \quad (170)$$

and analogous equation for $N_{\mathcal{E}}(\Delta^2)$ with F_1^{sea} being replaced by F_2^{sea}. Here γ_{sea} contains the SU(3) flavor-breaking effect and for the MRS parametrization it is $\gamma_{\mathrm{sea}} = 1/10$. Note that the SU(2) flavor breaking, i.e., the non-zero difference $\bar{d}-\bar{u}$ behaves as a valence-quark density and, thus, can be neglected in the small-x_{B} region. In the MRS A' parametrization the normalization factor for the sea-quark contribution is $n_{\mathrm{sea}} = 0.956$ and $\alpha \equiv \alpha_{\mathrm{sea}} = 1.17$. We should emphasize that at LO of perturbation theory,

$$N_{F_1} \equiv \lim_{b_{\mathrm{sea}}\to\infty}\frac{1}{2\pi}N_{\mathcal{H}}(\Delta^2=0) = \sum_{i=u,d,s} Q_i^2\,\frac{n_{\mathrm{sea}}(1+\gamma_{\mathrm{sea}})}{6}$$

is given in terms of the normalization of the structure function $F_1(x_{\mathrm{B}},\mathcal{Q}^2)$ of deeply inelastic scattering, see Eq. (146),

$$F_1(x_{\mathrm{B}},\mathcal{Q}^2) \approx N_{F_1}(\mathcal{Q}^2)\, x_{\mathrm{B}}^{-\alpha_{\mathrm{sea}}(\Delta^2=0,\mathcal{Q}^2)}.$$

[9]Since we assume $\widetilde{\beta} > -1$, we can safely set $N_{\widetilde{\mathcal{E}}} = 0$.

Of course, this relation is spoiled by both radiative corrections to the Wilson–coefficients and evolution effects.

In the coefficient $c_{0,\mathrm{unp}}^{\mathrm{DVCS}}$ of the squared DVCS amplitude the pion-pole contribution induces an x_{B}-independent term. As we see from Eq. (168), it can be neglected with respect to the $\mathcal{H}$ contribution, if the condition $\xi^{\alpha}\sqrt{-\Delta^2/4M^2} \ll 2N_{\mathcal{H}}/\left(F_{\pi}\sin\left(\frac{\alpha\pi}{2}\right)\right)$ is fulfilled. Indeed, it is obeyed in the allowed region of the parameter space for B_{sea} and κ_{sea}, provided $x_{\mathrm{B}} \leq 0.01$ and $-\Delta^2 \leq 0.5$ GeV^2. It is interesting that the spin-flip contributions $\mathcal{E}$ could already be significant at low momentum transfer, if $\beta > \alpha$. Note that further isolated mesonic-like states contribute to the small-x_{B} behavior of $c_{0,\mathrm{unp}}^{\mathrm{DVCS}}$. For instance, if there would be such a term in $\mathcal{E}$ with $p = 1$, we will have an additional contribution proportional to $\left(\xi^2 + \frac{\Delta^2}{4M^2}\right) M_{\mathcal{E}}^2 \xi^{-4}$. The effect is even more significant in the case of $\widetilde{\mathcal{E}}$, where it would overwhelm the pion-pole contribution and induce an interference term with $\widetilde{\mathcal{H}}$ that gives a dominant effect.

Now let us discuss the extraction of free parameters of our model making use of experimental results from HERA. To do this, we narrow down the number of unknowns by assuming the absence of isolated mesonic states and consider the small momentum transfer kinematics. Thus, $\mathcal{E}$ can be neglected in the Fourier coefficients (168) and (169). Then the absolute value of $\mathcal{H}$ can be extracted from the unpolarized cross section as it has been measured by H1 collaboration [8]. The parameter α can be obtained from the x_{B}-dependence of the measured DVCS cross section. More directly it can be gotten from a measurement of the unpolarized azimuthal asymmetries, which are proportional to the real part of $\mathcal{H}$:

$$\cos^2\left(\alpha\frac{\pi}{2}\right) = \frac{\left(c_{1,\mathrm{unp}}^{\mathcal{I}}\right)^2}{32K^2(2-2y+y^2)c_{0,\mathrm{unp}}^{\mathrm{DVCS}}} \propto \frac{\left(\mathrm{CoA}_{c(1)}^{\mathrm{unp}}\right)^2}{\mathrm{CeA}_{c(0)}^{\mathrm{unp}}}\,. \tag{171}$$

Note that for small values of the lepton energy loss y the squared DVCS term is enhanced by $1/y^2$ compared to the squared BH term. Thus, a cleaner separation of the interference and squared DVCS term can be done by means of the charge asymmetry. Obviously, the consistency of such measurements tests the dominance of both $\mathcal{H}$ and its sea-quark component, since the measured value α should be consistent with deeply inelastic scattering data. However, we cannot exclude that a possible Δ^2-dependence of α alters this relation.

If the polarized lepton beam will be available, one would probe the imaginary part of $\mathcal{H}$ and have so the possibility to measure α directly as a ratio of the real to imaginary part of the amplitudes,

$$\cot\left(\alpha\frac{\pi}{2}\right) = \frac{y(2-y)c_{1,\mathrm{unp}}^{\mathcal{I}}}{(2-2y+y^2)s_{1,\mathrm{unp}}^{\mathcal{I}}} = \frac{y(2-y)\mathrm{CoA}_{c(1)}^{\mathrm{unp}}}{(2-2y+y^2)\mathrm{CoA}_{s(1)}^{\mathrm{unp}}}\,. \tag{172}$$

Knowing the parameter α, one has an opportunity to access the normalization in any of these experiments and, thus, to study the effects of skewedness, which is parametrized by $b_{\rm sea}$ in our model. Unfortunately, also the slope $B_{\rm sea}$ of the form factor $F_1^{\rm sea}$ is unknown, so that the skewedness effect cannot be measured in integrated asymmetries. However, due to the extrapolation $\lim_{\Delta^2\to 0} N_{\mathcal{H}}(\Delta^2)/N_{F_1}$, so far it is possible.

Perhaps, the most interesting quantity is the CFF $\mathcal{E}$ since it contains information about the orbital angular momentum fraction carried by partons. In our simplistic model the relevant parameter is the anomalous magnetic moment $\kappa_{\rm sea}$ of sea quarks. Unfortunately, we cannot say if $\mathcal{E}$ is accessible from unpolarized proton beam experiments at HERA. (A discussion about the potential of a polarized proton beam can be found in Ref. [43].) From the formulae for the twist-two Fourier coefficients (168) and (169) one expects that $\mathcal{E}$ can be accessed at larger momentum transfer, where, however, the statistics is low. The absence of isolated mesonic states and negligible contribution of the spin-flip CFF $\mathcal{E}$ allows us to derive a relation between the Fourier coefficients,

$$\frac{c_{0,\rm unp}^{\rm DVCS}}{2-2y+y^2} = \frac{y^2(2-y)^2\left(c_{1,\rm unp}^{\mathcal{I}}\right)^2 + (2-2y+y^2)^2\left(s_{1,\rm unp}^{\mathcal{I}}\right)^2}{32F_1^2K^2y^2(2-y)^2(2-2y+y^2)^2}\,, \tag{173}$$

which can serve as a test of our considerations. If the spin-flip contribution $\mathcal{E}$ is larger than the pion-pole term and compatible with $\mathcal{H}$, the deviation from this relation is a measure of $N_{\mathcal{E}}$. Without any further assumptions or theoretical predictions, we cannot directly invert the three Fourier coefficients $c_1^{\mathcal{I}}$, $s_1^{\mathcal{I}}$, and $c_0^{\rm DVCS}$ for an unpolarized target to get the four parameters α, $N_{\mathcal{H}}$, β, and $N_{\mathcal{E}}$. Fortunately, if the quality of data is good enough, one can measure the α,β-parameters by fitting the slope of the $x_{\rm B}$-dependence. Then again, one has an over-constrained set of observables, which can be used to exclude contributions from isolated mesonic-like states.

Let us now demonstrate how the model parameters can be adjusted by using the H1 data [8] for unpolarized Compton scattering with the positron beam off the proton, where the hard momentum transfer $\mathcal{Q}$ and the invariant energy W,

$$W = \sqrt{M^2 + \mathcal{Q}^2\frac{1-x_{\rm B}}{x_{\rm B}}}\,, \tag{174}$$

varied in the range

$$2\ {\rm GeV}^2 < \mathcal{Q}^2 < 20\ {\rm GeV}^2\,, \qquad 30\ {\rm GeV} < W < 120\ {\rm GeV}\,.$$

In this kinematical window the lepton energy loss y is not large, i.e., $0.01 \le y \le 0.16$. The cross section (22) is integrated over the momentum transfer squared with the restriction $|\Delta^2| < 1\ {\rm GeV}^2$, $\mathcal{Q}^2$ or W, as specified, and the azimuthal angle is integrated out entirely, $0 \le \phi \le 2\pi$. For simplicity we choose α to be independent on Δ^2, and neglect the evolution and radiative corrections

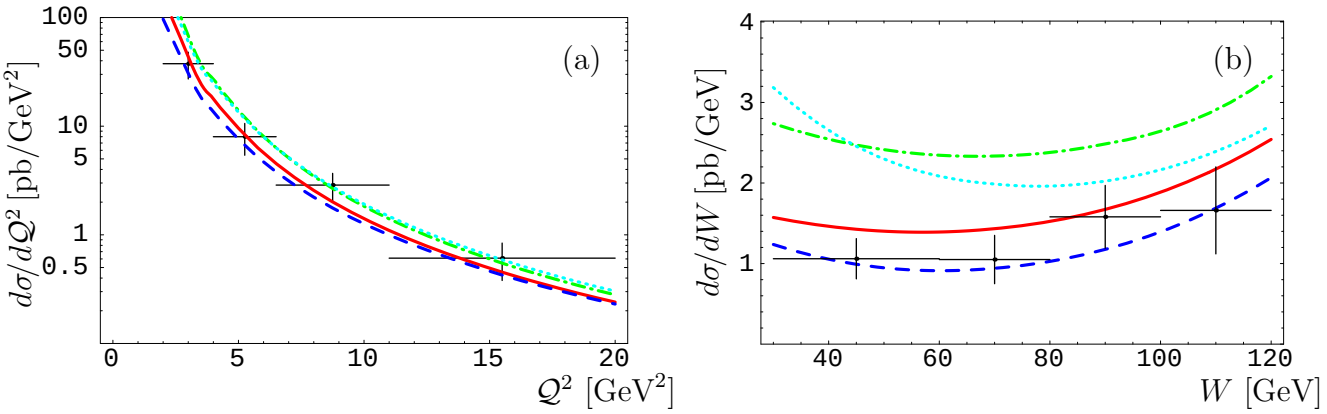

Figure 6: Differential cross sections $\frac{d\sigma}{d\mathcal{Q}^2}$ (a) and $\frac{d\sigma}{dW}$ (b) for $e^+p \to e^+p\gamma$ measured by H1 collaboration [8]. The data are compared with the LO predictions for different parametrizations: MRS A' with $b_{\rm sea} \to \infty$ and $B_{\rm sea} = 9$ GeV^{-2} (solid line) as well as $B_{\rm sea} = 5$ GeV^{-2} (dash-dotted); MRS G with $B_{\rm sea} = 9$ GeV^{-2} and $b_{\rm sea} \to \infty$ (dashed) as well as $b_{\rm sea} = 1$ (dotted).

as well as we set $\kappa_{\rm sea} = 0$. The integration over the azimuthal angle projects on the constant terms in the squared DVCS and interference term. In the first case this procedure is exact, while for the latter, due to the lepton propagators involved, we only approximately pick out the power-suppressed Fourier coefficient $c_0^{\mathcal{I}}$. Fortunately, for the H1 kinematics and within the WW-approximation adopted in the estimate, a cancellation occurs between contributions in the interference term, and the latter gives a negligible effect (on a percent level) in the total differential cross section. The ratio of BH and DVCS cross sections is proportional to $(1-y)|\Delta^2|/y^2\mathcal{Q}^2$ and, therefore, the BH contribution is much smaller than the DVCS one. In Fig. 6 (a) and (b) we show the measured cross sections $\frac{d\sigma}{d\mathcal{Q}^2}$ and $\frac{d\sigma}{dW}$, respectively, versus model predictions for different values of adjustable parameters in our ansatz. Here we take all CFFs into account, however, as was explained above, only the sea-quark component of $\mathcal{H}$ is dominant.

The measured normalization of the cross section $\frac{d\sigma}{dW}$, see Fig. 6 (b), can be achieved by tuning to a larger value of the slope $B_{\rm sea}$, a smaller skewedness effect, or a smaller value of $\alpha_{\rm sea}$. The best agreement we obtain with the MRS G set of forward parton distributions with $\alpha_{\rm sea} = 1.067$ [68], $B_{\rm sea} = 9$ GeV^{-2}, and $b_{\rm sea} \to \infty$ (dashed line in Fig. (6)). Taking the MRS A' value $\alpha_{\rm sea} = 1.17$ we slightly overshoot the data (solid line). The (integrated) DVCS cross section is roughly proportional to $1/B_{\rm sea}$, thus, for a lower value $B_{\rm sea} = 5$ GeV^{-1} we increase the theoretical estimate by almost the factor of 2 for small W (or small y) (dash-dotted). The skewedness effect for the MRS G parametrization can be read off from the normalization (170) and provides an enhancement of the DVCS cross section by the factor of $(1.588)^2 \approx 2.5$ (dotted line). All of these parametrizations

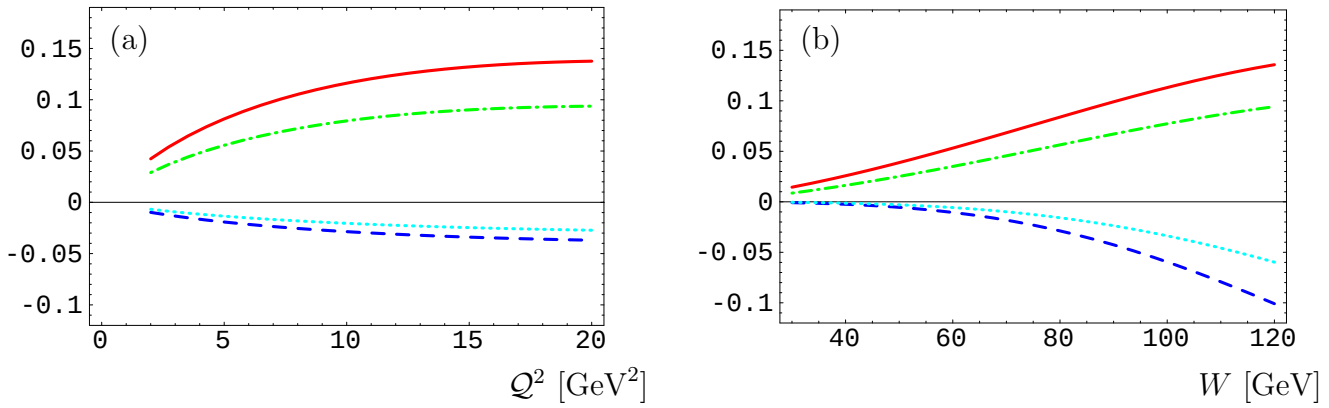

Figure 7: Twist-two azimuthal charge asymmetries for $\vec{e}^{\pm}p \to e^{\pm}p\gamma$ as functions of $\mathcal{Q}^2$ for $W = 75$ GeV and $\Delta^2 = -0.1$ GeV^2 (a) as well as functions of W for $\mathcal{Q}^2 = 4.5$ GeV^2 and $\Delta^2 = -0.1$ GeV^2 (b) for the model of GPDs based on the MRS A' parametrization with $b_{\rm sea} \to \infty$ and $B_{\rm sea} = 9$ GeV^{-2}. For $\kappa_{\rm sea} = 2$ ($\kappa_{\rm sea} = -3$) the asymmetries $\mathrm{CoA}^{\rm unp}_{c(1)}$ and $\mathrm{CoA}^{\rm unp}_{s(1)}$ are plotted as solid (dash-dotted) and dashed (dotted) lines, respectively.

are consistent with the measured differential cross section $\frac{d\sigma}{d\mathcal{Q}^2}$, Fig. (6) (a). The evolution flow with $\mathcal{Q}^2$, which we presently neglect, will give a moderate logarithmic change of $\mathcal{H}$ with increasing $\mathcal{Q}^2$. Note that according to Ref. [8] the data can also be fit in the aligned jet model [69] and by adopting the reggeon and soft pomeron exchange mechanism [70].

Since the DVCS amplitudes enter the DVCS cross section in square, the size of NLO corrections there is twice of what we have found for the CFF $\mathcal{H}$ in section 6.2.3. They are of order -40% even in the DVCS scheme. This requires a NLO analysis in order to extract the NLO parameters of the GPD models. However, since our ultimate goal is to compare twist-two and -three approximation, with the latter available only in LO of perturbation theory, a consistent approach is to use the LO parameters we have extracted. We will stick in the following to the MRS A' set with $b_{\rm sea} \to \infty$ and $B_{\rm sea} = 9$ GeV^{-2}. Note that the dependence of predictions on the $\kappa_{\rm sea}$ parameter is weak and was previously neglected. However, in the following we can use it also as a free fitting parameter.

As in the case of cross sections, the size of asymmetries can easily be estimated from the analytical formulae we have presented. The advantage is obvious: (i) one gets an understanding of the size of asymmetries depending on kinematical changes and modification of model parameters, (ii) one can easily scan the parameter space quantitatively.

The magnitudes of the twist-two azimuthal charge asymmetries $\mathrm{CoA}^{\rm unp}_{c(1)}$ and $\mathrm{CoA}^{\rm unp}_{s(1)}$ are displayed in Fig. 7 for $\Delta^2 = -0.1$ GeV^2. The absolute values of the asymmetries arising from the $\cos(\phi)$- and $\sin(\phi)$-dependence in the interference term can reach almost 15% and 10%, respec-

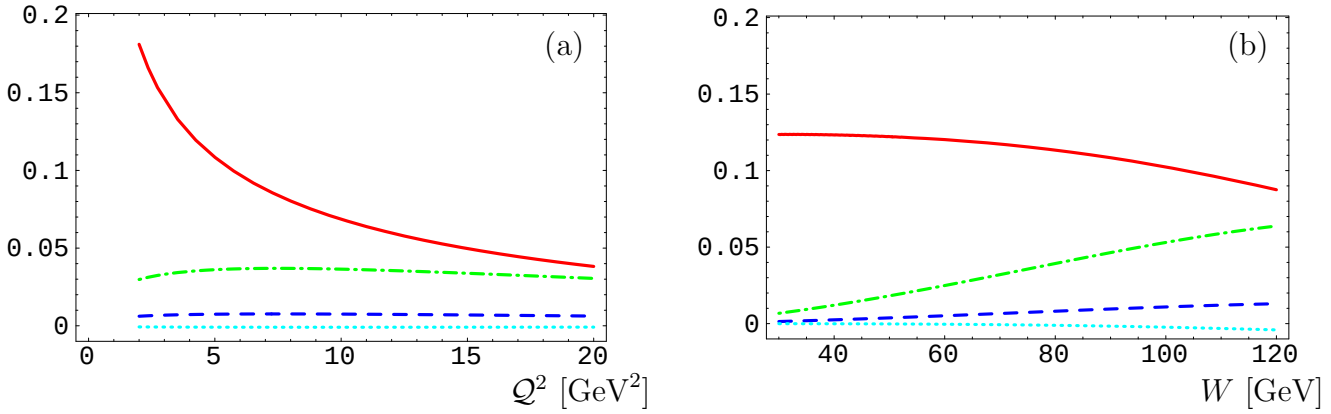

Figure 8: Twist-three azimuthal charge asymmetries for the same settings as in Fig. 7 (a) and (b), respectively, are plotted for $\mathrm{CeA}^{\mathrm{unp}}_{c(1)}$ (solid), $\mathrm{CoA}^{\mathrm{unp}}_{c(0)}$ (dash-dotted), $\mathrm{CoA}^{\mathrm{unp}}_{c(2)}$ (dashed), and $\mathrm{CoA}^{\mathrm{unp}}_{s(2)}$ (dotted).

tively. It is interesting that the asymmetries are reduced by about 30% if we vary the parameter κ_{sea} from 2 to -3. This dependence arises mainly from the interference term, where the $\mathcal{E}$-contribution is enhanced by the normalization of F_2, i.e., by the anomalous magnetic moment of the proton [cf. Eqs. (169)]. Consequently, even with a low mean value of the momentum transfer, e.g., $\Delta^2 \approx -0.1$ GeV^2, the $\mathcal{E}$-contribution can be significant for charge and lepton single-spin asymmetries. Note that for $\kappa_{\mathrm{sea}} = -3$ in our ansatz, $\mathcal{E}$ contributes already for $\Delta^2 \approx -0.6$ GeV^2 with the same magnitude as $-\mathcal{H}$. Asymmetries, averaged over the momentum transfer with the restriction $|\Delta^2| < 1$ GeV^2, have almost the same size as the ones displayed in Fig. 7, e.g.,

$$\mathrm{CoA}^{\mathrm{unp}}_{c(1)}(W = 75\ \mathrm{GeV}, \mathcal{Q}^2 = 4.5\ \mathrm{GeV}^2) \approx 8\%\,,$$
$$\mathrm{CoA}^{\mathrm{unp}}_{s(1)}(W = 75\ \mathrm{GeV}, \mathcal{Q}^2 = 4.5\ \mathrm{GeV}^2) \approx -2\%\,,$$

however, with a weak κ_{sea}-dependence.

Now we want to answer the second question we raised at the beginning of this section about the size of twist-three effects. In the WW-approximation for our model only the sea-quark part of $\mathcal{H}$ is dominant. Moreover, from Eqs. (84) and (87) we see that $\mathcal{H}^{\perp}(\xi, \Delta^2)$ drops out for small x_{B}. Thus, in the limit $b_{\mathrm{sea}} \to \infty$ we discover from the WW-approximation of Eq. (84) with the help of Eqs. (157) and (161),

$$\mathcal{H}^{\mathrm{eff-WW}}(\xi, \Delta^2) \;=\; \left\{2 - \alpha_{\mathrm{sea}}\left[\psi\left(\frac{1+\alpha_{\mathrm{sea}}}{2}\right) - \psi\left(\frac{\alpha_{\mathrm{sea}}}{2}\right)\right]\right\}\mathcal{H}(\xi, \Delta^2)\,, \tag{175}$$

a known relation, which was derived in the archive version of Ref. [33]. For $\alpha_{\mathrm{sea}} = 1.17$ the ratio $\mathcal{H}^{\mathrm{eff-WW}}/\mathcal{H}$ is ≈ 0.65, while for $b_{\mathrm{sea}} = 1$ we find ≈ 0.48. Apparently, the size of the twist-three effects is entirely given by the kinematical factors in front of the 'universal' $\mathcal{C}$ functions in

model	$b_{\rm val}$	$b_{\rm sea}$	$B_{\rm sea}$ [GeV^{-2}]	$\kappa_{\rm sea}$
A	1	∞	9	0
B	∞	∞	9	-3
C	1	1	5	0

Table 3: Parameter sets for models of H- and E-type GPDs.

the definition of Fourier coefficients (44), (53), and (55). Thus, we realize that the twist-three harmonics are relatively suppressed by the factor $\sqrt{-(1-y)\Delta_\perp^2/\mathcal{Q}^2}$. For instance, the suppression is already about the factor of 4 for $\Delta^2 = -0.1$ GeV^2 and $\mathcal{Q}^2 = 2$ GeV^2. In Fig. 8 we demonstrate that this counting is not justified however for the asymmetry $\mathrm{CoA}^{\rm unp}_{c(0)}$ as one can easily realize from Eq. (53). For $\Delta^2 = -0.1$ GeV^2 we find a contribution (dash-dotted line) that is of order of a few percent. Fortunately, it is expressed in terms of twist-two CFFs and so this twist-three azimuthal asymmetry can be employed to pin down twist-two CFFs. Within our model we expect that the addendum (72) does not contribute in Eq. (53) and, thus, we have the ratio

$$\frac{\mathrm{CoA}^{\rm unp}_{c(0)}}{\mathrm{CoA}^{\rm unp}_{c(1)}} = \frac{\pi}{2}\frac{(2-y)^3}{(2-2y+y^2)}\frac{-\Delta^2}{\mathcal{Q}^2 K}\left\{\left(1-\frac{\Delta^2_{\rm min}}{\Delta^2}\right) - \frac{2(1-y)}{(2-y)^2}\right\}.$$

The largest size among the twist-three azimuthal asymmetries has $\mathrm{CeA}^{\rm unp}_{c(1)}$ (solid line), which arises from the $\cos(\phi)$ term of the squared DVCS term. Its twist-two counterpart $\mathrm{CeA}^{\rm unp}_{c(0)}$ approaches the value 1 for small W (small y), which reflects the fact that the DVCS process dominates over BH one. If we average over the momentum transfer squared, we still find a few percent effect for the twist-three azimuthal charge asymmetries that is comparable with the twist-two ones,

$$\mathrm{CeA}^{\rm unp}_{c(1)}(W = 75\ \mathrm{GeV}, \mathcal{Q}^2 = 4.5\ \mathrm{GeV}^2) \approx 7\%\,,$$
$$\mathrm{CoA}^{\rm unp}_{c(0)}(W = 75\ \mathrm{GeV}, \mathcal{Q}^2 = 4.5\ \mathrm{GeV}^2) \approx 2\%\,,$$

for $-\Delta^2_{\rm min} \leq |\Delta^2| < 1$ GeV^2.

7.2 Asymmetries in unpolarized fixed target experiments

After fixing the parameters in the sea-quark sector from the H1 data, we could hope to give better numerical estimates also for unpolarized fixed target experiments. To have a comprehensive understanding of this issue, we define three parameter sets for $\mathcal{H}$ and $\mathcal{E}$ based on the MRS A' parametrization. They are summarized in Table 3. The slope parameter $B_{\rm D} = 3/m_{\rm D}^2$ of the

D-term will be fixed later. In $\widetilde{\mathcal{H}}$ we use the parameters

$$b_{\rm val} = b_{\rm sea} = 1\,, \qquad B_A = 3/m_A^2 \approx 3.7\ {\rm GeV}^{-2}\,.$$

Obviously, in the models A and B, which are compatible with the H1 measurements, the sea-quark contributions are relatively small. For the model C this is not the case and our predictions overshoot the H1 data. If our oversimplified model has some realistic features, the model C will hardly describe the beam-spin asymmetries measured at HERMES and Jefferson Lab. The philosophy would be then again to employ experiments to fix the model parameters left in the valence-quark sector or to discriminate between the model A and B, or any other.

In the following section 7.2.1 we compare these models, used for estimates of the DVCS amplitudes calculated in the twist-three approximation, with the experimental measurements and discuss theoretical uncertainties in the extraction of model-dependent parameters. Then we have in section 7.2.2 a closer look to the twist-three effects. Especially, we show that asymmetries, usually discussed in the literature, are not quite suitable to access GPDs. In the third section 7.3 we estimate the size and parameter dependence of nucleon-spin asymmetries for the CLAS kinematics.

7.2.1 Beam-spin asymmetry measured with HERMES and CLAS

The azimuthal angular dependence of the beam-spin asymmetry, i.e.,

$$A_{\rm LU}(\phi) = \frac{d\sigma^{\uparrow}(\phi) - d\sigma^{\downarrow}(\phi)}{d\sigma^{\uparrow}(\phi) + d\sigma^{\downarrow}(\phi)}\,, \tag{176}$$

has been recently measured in two different fixed target experiments, namely, by HERMES [6] and CLAS [9] collaborations with the positron and electron beam of 27.6 GeV and 4.25 GeV, respectively, scattered on hydrogen targets. At HERMES the average values of kinematical variables are $\langle \mathcal{Q}^2\rangle = 2.6$ GeV^2, $\langle x_{\rm B}\rangle = 0.11$ and $\langle -\Delta^2\rangle = 0.27$ GeV^2 [6]. The results at CLAS are integrated over the regions 1 GeV$^2 < \mathcal{Q}^2 < 1.75$ GeV^2, $0.13 < x_{\rm B} < 0.35$, and 0.1 GeV$^2 < -\Delta^2 < 0.3$ GeV^2 with the condition that $W > 2$ GeV [9].

In both experiments we have a large average value of $\langle y\rangle$, i.e., ~ 0.5 and ~ 0.85 for the HERMES and CLAS measurements, respectively. Thus, we expect that the BH part of the total cross section dominates over the DVCS one [like $(1-y)\Delta^2/y^2\mathcal{Q}^2$ as indicated by Eqs. (25-27)], which is indeed the case. So the denominator, $d\sigma^{\uparrow} + d\sigma^{\downarrow}$, of the beam-spin asymmetry (176) is prevailed by the BH contribution with $c_{0,\rm unp}^{\rm BH}$-coefficient being the dominant one and higher harmonics suppressed by one or two powers of K. The BH part provides a much stronger contribution for the CLAS than the for HERMES experiment. Thus, we realize that the ϕ-dependence of the BH propagators in $A_{\rm LU}(\phi)$ almost cancels. From this qualitative discussion

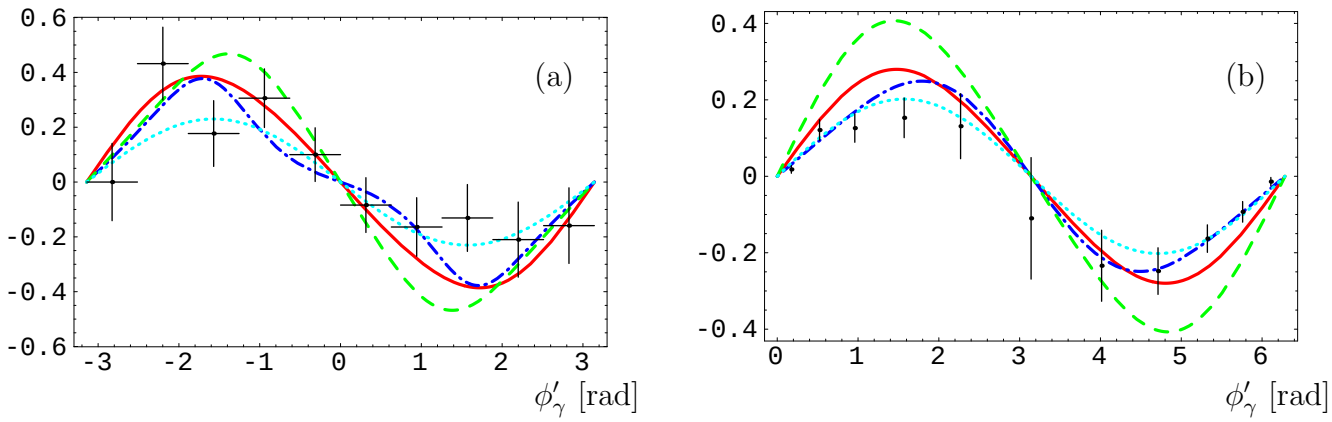

Figure 9: The beam-spin asymmetry as function of the azimuthal angle measured in $e^+p \to e^+p\gamma$ with $E = 27.6$ GeV from HERMES (a) and $e^-p \to e^-p\gamma$ with $E = 4.25$ GeV from CLAS (b) collaborations. The dotted lines show the $\sin(\phi)$ function with the amplitude 0.23 and 0.202 for HERMES and CLAS, respectively. The other curves are predicted by the model A (solid) and C (dashed) in the WW approximation as well as the model B beyond this approximation (dash-dotted), as specified in the text, for $\mathcal{Q}^2 = 2.6$ GeV^2, $x_{\rm B} = 0.11$, and $-\Delta^2 = 0.27$ GeV^2 in (a) as well as for $\mathcal{Q}^2 = 1.31$ GeV^2, $x_{\rm B} = 0.19$, and $-\Delta^2 = 0.15$ GeV^2 in (b).

we expect that in the kinematics, we are considering, the azimuthal dependence is approximately given by the $\sin(\phi)$ function:

$$A_{\rm LU}(\phi) \sim \pm\frac{x_{\rm B}}{y}\frac{s^{\mathcal{I}}_{1,\rm unp}}{c^{\rm BH}_{0,\rm unp}}\sin(\phi) \propto \Im{\rm m}\left\{F_1\mathcal{H} + \frac{x_{\rm B}}{2-x_{\rm B}}(F_1+F_2)\widetilde{\mathcal{H}} - \frac{\Delta^2}{4M^2}F_2\mathcal{E}\right\}\sin(\phi)\,, \qquad (177)$$

where higher harmonics are suppressed by $\Delta/\mathcal{Q}$. Moreover, $A_{\rm LU}(\phi)$ in this approximation is linear in CFFs, and in the kinematics, we are discussing, the dominant contribution arises from $\Im{\rm m}\mathcal{H}$ within our model. In LO the imaginary part is directly given by the GPDs on the diagonal $x = \pm\xi$. Thus, uncertainties due to our poor knowledge of GPDs are minimized for the beam-spin asymmetry. Moreover, after fixing the parameters for $\mathcal{H}_{\rm sea}$ from the H1 data, we can confront our predictions with the data. Obviously, the D-term can only slightly affect the beam-spin asymmetry. Nevertheless, we include it and set the sea- and D-slope parameters equal $B_{\rm D} = B_{\rm sea}$.

Now let us compare our expectations at the twist-three level for LO CFFs with the results from the two experiments shown in Fig. 9.

The model predictions for the CLAS experiment, plotted in Fig. 9 (b), possess a much smaller deviation from the $\sin(\phi)$-like shape than the HERMES one shown on the panel (a). For this kinematics a stronger contamination by higher harmonics, due to the higher average $\langle y\rangle$, can be induced by the squared DVCS term in $d\sigma^{\uparrow} + d\sigma^{\downarrow}$ as well as twist-three effects. The model A is

compatible with the HERMES data (solid curve). For the integrated asymmetry

$$A_{\rm LU} = 2\int_0^{2\pi} d\phi'_\gamma \sin(\phi'_\gamma)\frac{d\sigma^\uparrow - d\sigma^\downarrow}{d\phi'_\gamma}\Bigg/\int_0^{2\pi} d\phi'_\gamma \frac{d\sigma^\uparrow + d\sigma^\downarrow}{d\phi'_\gamma} \tag{178}$$

the experimental result from HERMES

$$A_{\rm LU} = -0.23 \pm 0.04({\rm stat}) \pm 0.03({\rm syst})\,,$$

is in agreement with the model-A prediction

$$A_{\rm LU} = -0.27\,.$$

If we take a smaller slope parameter $B_{\rm sea}$ or a smaller $b_{\rm sea}$ parameter, the absolute value of the asymmetry will increase. For instance, the model C leads to

$$A_{\rm LU} = -0.37$$

with an obvious deviation from a simple $\sin(\phi)$-shape (dashed), which is mainly caused by purely kinematical effects. This parameter set yields a prediction that is close to the result of Ref. [15]. On the other hand we can also decrease the absolute value of $A_{\rm LU}$ if we take a larger value of $b_{\rm val}$, a smaller $\kappa_{\rm sea}$, or if we go beyond the WW-approximation. To demonstrate possible effects due to the antiquark-gluon-quark correlations, we assume a rather large contribution proportional to the twist-two one, however, with a unique phase difference[10] ϕ^{qGq},

$$\mathcal{F}^{qGq} = \frac{1}{\xi}|\mathcal{F}|\exp\left\{i\ \arg(\mathcal{F}) + i\phi^{qGq}\right\}\,, \quad \text{for} \quad \mathcal{F} = \left\{\mathcal{H}, \mathcal{E}, \widetilde{\mathcal{H}}\right\}\,. \tag{179}$$

Here we also included an extra factor $1/\xi$ since the convolution given in Eq. (84) looks rather singular. Now the model B with $\phi^{qGq} = -\pi/3$ results in a smaller asymmetry,

$$A_{\rm LU} = -0.16\,,$$

which is also compatible with the data (dash-dotted curve). In this case, we observe the appearance of $\sin(2\phi)$ and $\sin(3\phi)$ harmonics, which arise from the interplay of twist-three effects in the interference term and purely kinematical effects. Note that the amplitude of the $\sin(\phi)$-harmonic in $A_{\rm LU}(\phi)$ is insensitive to the twist-three sector[11]. However, for the azimuthal beam-spin asymmetry (178) this does not necessarily hold true.

[10] We have to emphasize that this is only a toy model in which possible constraints due to sum rules and reduction to the forward kinematics for antiquark-gluon-quark GPDs were not implemented.

[11] Such dependence arises mainly from twist-three effects in the denominator on the right-hand side of Eq. (176), which is, however, dominated by the BH cross section.

Now we come to the measurements of CLAS collaboration, which can be fit by

$$A_{\rm LU}(\phi'_\gamma) = \alpha \sin(\phi'_\gamma) + \beta \sin(2\phi'_\gamma)\,,$$

with[12] [9]

$$\alpha = 0.202 \pm 0.028(\text{stat}) \pm 0.013(\text{syst})\,,$$
$$\beta = -0.024 \pm 0.021(\text{stat}) \pm 0.009(\text{syst})\,.$$

The β-parameter is obviously compatible with zero. In the case of the model C (dashed curve) and now also for the model A (solid curve) one fails to describe the data since one gets

$$\alpha = 0.4\,, \qquad \beta = 0.028\,,$$

and

$$\alpha = 0.28\,, \qquad \beta = 0.014\,,$$

respectively. Taking now the model B and going beyond the WW-approximation by inclusion of antiquark-gluon-quark effects with the phase difference $\phi^{qGq} = \pi$, we find a result compatible with the data (dash-dotted curve), namely,

$$\alpha = 0.24\,, \qquad \beta = -0.03\,.$$

As we mentioned before, the value of α is almost insensitive to the antiquark-gluon-quark contribution. Indeed, in the WW-approximation we have for the model B the same value of α but quite different β, i.e.,

$$\alpha = 0.24\,, \qquad \beta = 0.014\,,$$

which is slightly out of the experimental range. Our model-dependent analysis shows that the CLAS measurement of the beam-spin asymmetry is sensitive to antiquark-gluon-quark contributions. However, due to the large experimental uncertainties, this statement might be premature. On the theoretical side, the legitimacy of this assertion depends on the answers to the following two crucial questions: (i) Can we be sure that our equations are valid at low $\mathcal{Q}^2$ as of order of 1 GeV^2? (ii) If yes, is the sign of β model-independent in the WW-approximation?

To address the first question, we give now a more qualitative discussion about our present understanding of corrections, which are expected to modify our predictions. We provide here

[12]Do not mix α and β in this parametrization with y and ξ exponents of parton densities and GPDs, respectively, discussed in the preceding sections.

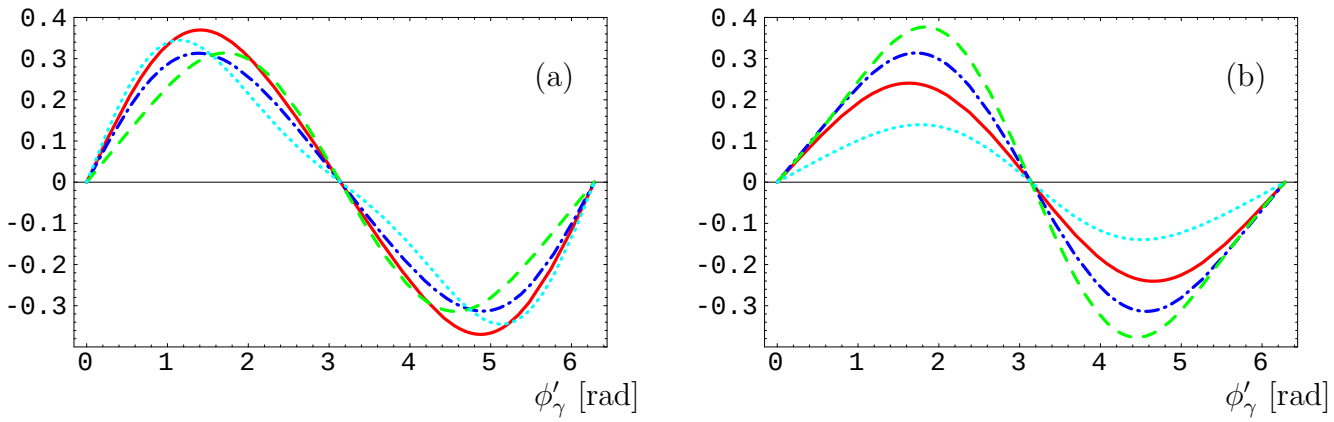

Figure 10: Estimates of the beam spin asymmetry $A_{\rm LU}(\phi)$ for the E-01-113 experiment at Jefferson Lab [10] with the $E = 6$ GeV electron beam scattered on a proton target. Predictions for the model A (solid) in the WW-approximation and B (dash-dotted) in the same approximation as well as with the antiquark-gluon-quark contribution with $\phi^{qGq} = \pi$ (dashed) and $\phi^{qGq} = 0$ (dotted) are plotted in (a) for $x_{\rm B} = 0.3$, $\Delta^2 = -0.25$, and $\mathcal{Q} = 2.5$ GeV^2. Here the D-term has been taken into account with $B_{\rm D} = B_{\rm sea}$. In (b) we show the model B estimates with $\phi^{qGq} = \pi$ for $x_{\rm B} = 0.35$, $\mathcal{Q}^2 = 3$ GeV^2 (solid), $x_{\rm B} = 0.3$, $\mathcal{Q}^2 = 2.5$ GeV^2 (dash-dotted), $x_{\rm B} = 0.25$, $\mathcal{Q}^2 = 2$ GeV^2 (dashed), and $x_{\rm B} = 0.19$, $\mathcal{Q}^2 = 2$ GeV^2 (dotted), where in all cases $\Delta^2 = -0.25$ GeV^2.

some hints rather than answers. In both experiments the perturbative NLO effects in the DVCS scheme may be of order of -20% or so (cf. Fig. 4). Furthermore, we expect that the evolution effects can alter predictions on a few percent level at most. The power corrections involved in the analysis are of two kinds $-\Delta^2/\mathcal{Q}^2$ and $M^2/\mathcal{Q}^2$. While the first correction in our model is naively expected to be of $\pm 10\%$ or so in both experiments, the latter is certainly larger for the CLAS settings and, therefore, their quantitative estimate is desirable. To this end, one can adopt the partial result of Ref. [17]. In contrast to the forward case, where each power of the target mass M^2 is accompanied by a suppression factor $x_{\rm B}^2$, the situation in the DVCS kinematics is not so obvious and requires detailed numerical studies. So far it is likely that besides radiative corrections also power-suppressed contributions are important for the interpretation of the CLAS experiment. This is especially crucial for the interpretation of the $\sin(2\phi)$ harmonic.

Keeping these reservations in mind, we finally estimate the beam-spin asymmetry $A_{\rm LU}(\phi)$ that we expect from future measurements at Jefferson Lab with the electron beam energy $E = 6$ GeV in E-01-113 experiment with CLAS. Our expectations are shown in Fig. 10 (a) and (b) for the models A and B in different approximations as well as for different average values of the kinematical variables. They are chosen so, that $0.7 < y < 0.76$ and, thus, the DVCS amplitude is kinematically

suppressed. We have a similar situation as discussed above, however, for larger $\mathcal{Q}^2$. This may offer a possibility to investigate a deviation from the predicted asymmetries, expected in the WW-approximation, in more detail. To clarify the issue whether this deviation is caused by the antiquark-gluon-quark or the mass corrections, it is necessary to fix $x_{\rm B}$ and vary $\mathcal{Q}^2$. For instance, our expectation for the average value of $x_{\rm B} = 0.19$ (as in Fig. 9 (b)), are shown as the dotted line in Fig. 10 (b) for $\mathcal{Q}^2 = 2$ GeV^2. For this kinematics, we have only a tiny deviation from the $\sin(\phi)$-shape in the WW-approximation, i.e.,

$$A_{\rm LU}(\phi'_\gamma) = 0.136\sin(\phi'_\gamma) + 0.005\sin(2\phi'_\gamma)\,.$$

A shape closer to a $\sin(\phi)$-like form in the E-01-113 measurement would indicate that the source of higher harmonics in the CLAS experiment at lower beam energy is caused by mass corrections, since they are now relatively suppressed by the factor of ≈ 0.65. Obviously, a definite statement requires higher statistics in order to decrease the error on β.

7.2.2 A closer inspection of twist-three effects

The essential feature of the twist-three contributions is the appearance of new coefficients including a ϕ-independent harmonic in the interference term. It can be seen from the equations given in sections 4.2 and 4.3 that higher Fourier coefficients in the squared DVCS as well as interference term are relatively suppressed by the factor $K \propto \sqrt{(1-y)}\Delta_\perp/\mathcal{Q}$ with an additional multiplicative y-dependence. Thus, higher harmonics vanish faster at the kinematical boundaries $\Delta_\perp \to 0$ and $y \to 1$ than the twist-two ones. The nonperturbative dependence of the twist-three CFFs is given by the universal $\mathcal{C}$ coefficients. In the WW-approximation these CFFs have a magnitude similar to the twist-two ones (see Fig. 2). Although for the longitudinally polarized target the constant interference terms $c_0^{\mathcal{I}}$, defined in Eqs. (53) and (57), are suppressed by $1/\mathcal{Q}$, they do not vanish at the kinematical boundaries. Therefore, we expect the existence of phase space regions where the interference term is strongly contaminated by this purely kinematical twist-three effect. Note that this is not the case for $c_{0,\rm TP}^{\mathcal{I}}$, see Eq. (61).

Let us study the twist-three effects for the longitudinally polarized fixed target experiment in more detail. For $\Delta^2 = -0.25$ GeV^2 and $\mathcal{Q}^2 = 4$ GeV^2, we expect a suppression of the higher harmonics, arising beyond the twist-two approximation, roughly by the factor of 4. Note that $\Delta^2/\mathcal{Q}^2 \sim 0.06$ and the target mass effects, i.e., $M^2/\mathcal{Q}^2$ could be suppressed by a similar factor since they are combined with an extra multiplicative ξ-dependence. So in the future precise DVCS measurements there will hopefully be a kinematical window left, where twist-three effects are accessible and $1/\mathcal{Q}^2$-power corrections are quantitatively not important. We set for the following numerical estimates $E_{\rm beam} = 27.6$ GeV, and take the model A with the pion pole and D-term,

having equal slopes $B_{\rm D} = B_{\rm sea}$. For the squared DVCS term we find, indeed, the anticipated suppression in the WW-approximation. For the longitudinally polarized target and polarized lepton beam, the Fourier series for $x_{\rm B} = 0.1$ ($y \approx 0.77$) reads

$$\frac{d\sigma^{\rm DVCS}}{dx_{\rm B}d|\Delta^2|d\mathcal{Q}^2d\phi} \approx \Big\{0.0023\,[1 + 0.19\cos(\phi) - 0.09\lambda\sin(\phi)] \\ +0.0004\Lambda\,[\lambda + 0.16\lambda\cos(\phi) - 0.04\sin(\phi)]\Big\}\frac{\rm nb}{\rm GeV^4}. \tag{180}$$

Let us comment on these numbers. The normalization of the cross section strongly depends on the parameter set we have chosen. For instance, for the model C we find an enhancement in the normalization almost by the factor of 3. However, it depends only weakly on the pion-pole and D-term contributions. The suppression of terms involving target polarization arises rather from the destructive interference of $\mathcal{H}$ and $\widetilde{\mathcal{H}}$ and should be considered as a reflection of the model taken for the estimate. For the $\cos(\phi)$ harmonics we have the expected damping, while the strong suppression of the $\sin(\phi)$ terms arises from the adopted WW-approximation. The main ingredient of the latter leading to this feature is the fact that the twist-three CFFs have a phase similar to the twist-two ones. Thus, the imaginary part of their interference is roughly zero. A strong deviation from such a small value would indicate an antiquark-gluon-quark contribution having quite a different phase structure as compared to the twist-two CFFs.

The interference term for the positron scattering reads

$$\frac{d\sigma^{\mathcal{I}}}{dx_{\rm B}d|\Delta^2|d\mathcal{Q}^2d\phi} \approx \frac{1}{1 + 0.93\cos(\phi) + 0.08\cos(2\phi)} \\ \times\Big\{-0.007\,[0.56 + \cos(\phi) + 0.17\cos(2\phi)] - 0.02\lambda\,[\sin(\phi) + 0.06\sin(2\phi)] \\ +0.002\lambda\Lambda\,[0.52 + \cos(\phi) + 0.03\cos(2\phi)] - 0.006\Lambda\,[\sin(\phi) + 0.09\sin(2\phi)]\Big\}\frac{\rm nb}{\rm GeV^4}\,, \tag{181}$$

with the same kinematical settings as above. Again, the overall normalization strongly depends on the GPD models. The suppression of higher harmonics is of the magnitude we have expected or even larger, by the same token as before. The constant term is rather large. As already mentioned, this is a purely kinematical twist-three term, i.e., it is completely determined by the twist-two CFFs. So we see that such a term can alter the cross section in a much stronger manner than the others. However, it will not spoil the separation of the dynamical twist-two and -three sectors. Thus, it is helpful for both experimental consistency checks and access to the real part of CFFs. Let us also note that the ϕ-dependence arising from the BH-propagators is rather strong for the kinematics, we have chosen.

It is instructive to compare our results in the WW-approximation with the one given in [15]. The sets of GPDs used there presently differ by the choice of the forward parton densities and

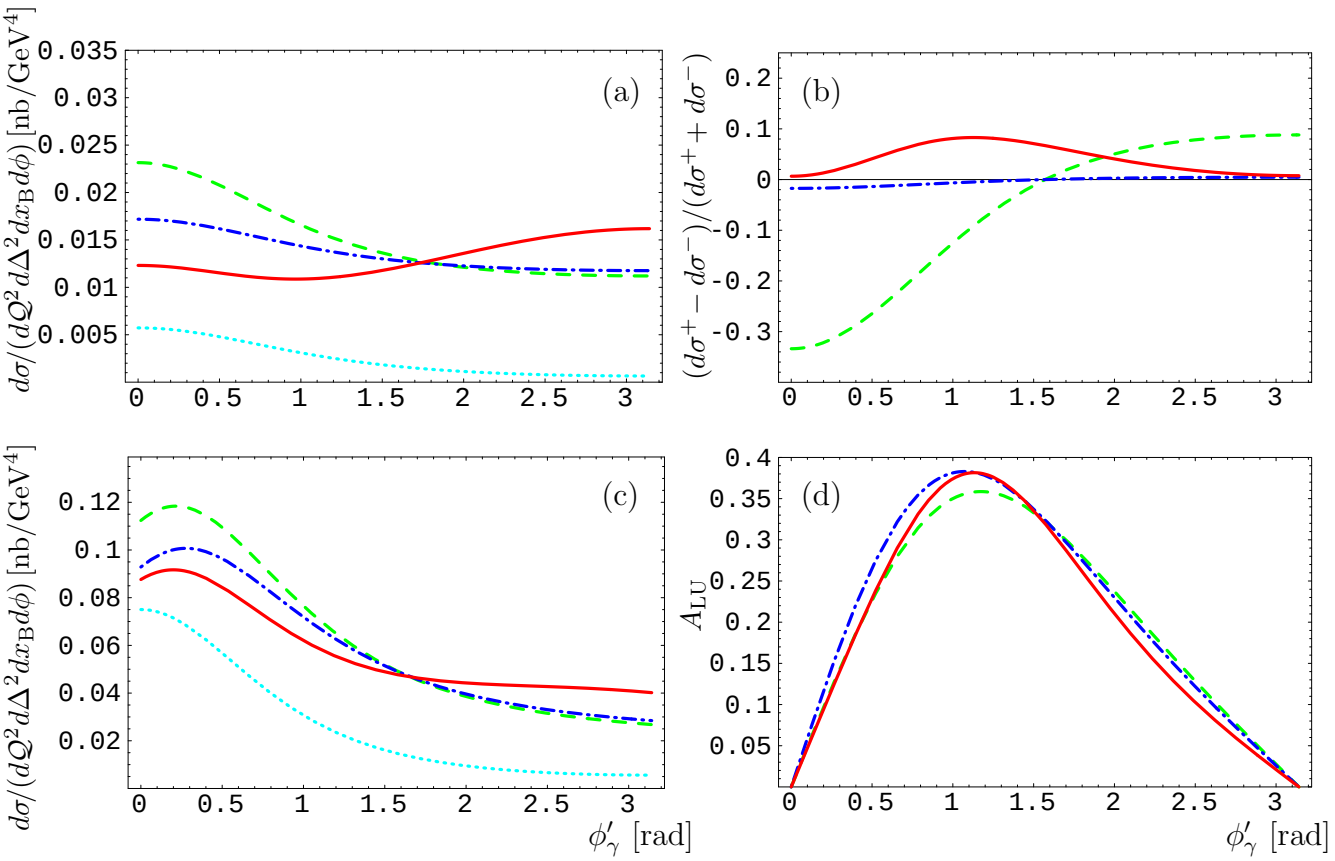

Figure 11: The unpolarized $e^- p \to e^- p\gamma$ cross section (a), the charge asymmetry (b) for $\mathcal{Q}^2 = 2.5$ GeV^2, $\Delta^2 = -0.25$ GeV^2 and $x_B = 0.3$ as well as the polarized electron-beam cross section (c), and the single-spin asymmetry (d) for $\mathcal{Q}^2 = 2.5$ GeV^2, $\Delta^2 = -0.25$ GeV^2 and $x_B = 0.15$ are shown for the BH term (dotted), the twist-two without the D-term (dashed), twist-two (dash-dotted) and -three (solid) with the D-term for electron beam within the model C.

partonic form factors. To be close to the settings of Ref. [15], we take the model C with $B_D = B_{sea} = 5$ GeV^{-2}. Note that our H_{sea} increases less rapidly at small ξ than in the parametrization from Ref. [68], and we choose a stronger fall-off with Δ^2 of the D-term. In Fig. 11, we show the same predictions for the ϕ-dependence of the cross section as given in Figs. 2 and 4 of Ref. [15]. Our estimates for the unpolarized cross section (a) and the polarized beam ($\lambda = 1$) cross section (b) for electron scattering on the unpolarized proton target with $\mathcal{Q}^2 = 2.5$ GeV^2 and $\Delta^2 = -0.25$ GeV^2 look quite similar to [15]. We can clearly observe large differences of the cross sections and charge asymmetry, i.e., $\{d\sigma^+(\phi) - d\sigma^-(\phi)\}/\{d\sigma^+(\phi) + d\sigma^-(\phi)\}$, between twist-two (dash-dotted curve) and -three (solid curve) contributions. As we have shown previously in Eq. (181), the main effect comes here from the interplay of the constant interference term with the ϕ-dependence of the BH propagators.

The most significant differences of both results are prominent in the charge azimuthal asymmetry, displayed in Fig. 11 (b). Since in our parametrization the positive sea-quark contribution is larger, we find without the D-term a large negative value of this asymmetry at $\phi'_\gamma = 0$ in the twist-two approximation (dashed curve). Adding the D-term contribution we get the asymmetry, which is compatible with zero in the same approximation (dash-dotted curve), while the parametrization of [15] yields a large positive value at $\phi'_\gamma = 0$. So we conclude that due to many parameters involved in the modeling of GPDs there is no unequivocal experimental signature of the D-term. Moreover, at the twist-three level without the D-term we have a similar magnitude of the asymmetry as displayed by the solid curve in Fig. 11 (b), which includes the D-term. This tells us that there is a large cancellation between the twist-two and -three effects induced by the D-term. Consequently, to access the twist-two GPDs one has to separate the twist-two and -three sectors. Note that the cancellation between sea- and valence-quarks as well as the D-term contributions induces a rather strong dependence on the parametrization for the unpolarized beam-charge asymmetry, and, thus, may also induce a stronger contamination by radiative corrections as was observed for separate contributions.

The beam-spin asymmetry in Fig. 11 (d) is only slightly modified by the twist-three contributions in the WW-approximation. These corrections enter mainly in the denominator of this asymmetry, while the contamination of the numerator by new harmonics remains small as we have discussed above in Eqs. (180) and (181). Again, for this asymmetry we expect only moderate changes due to radiative corrections within our ansatz of order of 20% or so.

7.2.3 Estimates and parameter dependence of charge asymmetries

As we have demonstrated in the previous two paragraphs for the beam-spin and charge asymmetries, an important phenomenological issue is the separation of the twist-two and -three sectors. This problem is completely resolved by the introduction of charge asymmetries via Eqs. (105-109) and partially for the single-spin asymmetry defined by Eq. (113). We emphasize again that the charge asymmetries allow also to access the imaginary part of the interference term in a clean manner, which is hardly possible for the beam-spin asymmetries. Differences encountered due to various definitions of the charge and beam-spin asymmetries in the twist-two and -three approximations are shown in Fig. 12. The asymmetries $A_{\rm C}$ (a), $A_{\rm SL}$ and SSA_1 (b) are normalized to the unpolarized cross section that does not or only weakly does depend on the dynamical twist-three contributions. However, as was pointed out above, the constant term in the interference may generate an important effect. From the differences of the twist-three (dotted) and twist-two (dash-dotted) approximation one observes in the panel (b) that the twist-three contamination is

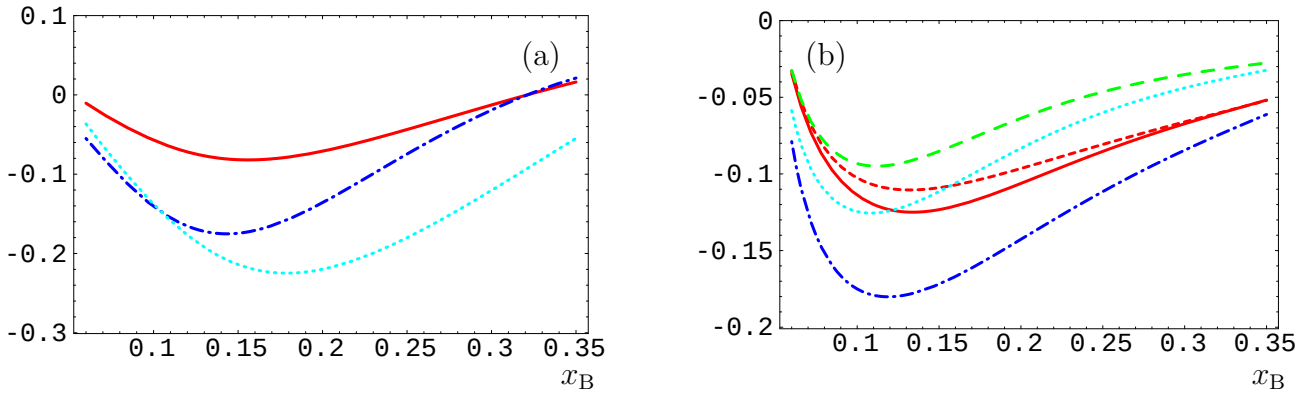

Figure 12: The azimuthal charge asymmetry A_C (a) and the beam-spin asymmetry A_{SL} (b) are plotted in twist-two (dash-dotted) and twist-three (dotted) for the HERMES kinematics with $\mathcal{Q}^2 = 2.5$ GeV^2 and $\Delta^2 = -0.25$. The solid curves show the predictions of the improved charge asymmetries $\mathrm{CoA}^{\mathrm{unp}}_{c(1)}$ and $\mathrm{CoA}^{\mathrm{unp}}_{s(1)}$. In (b) the short-dashed and dashed curves display SSA_1 in twist-two and -three approximation, respectively. All curves are given for model A with $B_D = 9$ GeV^2 and includes an antiquark-gluon-quark correlation with $\phi^{qGq} = -\pi/3$.

quite essential for smaller values of x_B, i.e., larger value of y, where the BH propagator $\mathcal{P}_1(\phi)$ induces a rather strong ϕ-dependence. In the case of the beam-spin asymmetry an improvement is necessary if considerable antiquark-gluon-quark correlations are present. As it can be seen by comparison of the twist-two (short-dashed) and -three (dashed) approximation for SSA_1, a clean separation is only achieved when the DVCS amplitude is suppressed with respect to the BH one, i.e., $\sqrt{-(1-y)\Delta^2}/y\mathcal{Q} \ll 1$. Note also that the twist-two approximation of SSA_1 is close to the charge asymmetry $\mathrm{CoA}^{\mathrm{unp}}_{s(1)}$. The deviation of $\mathrm{CoA}^{\mathrm{unp}}_{s(1)}$ from SSA_1 arises only from the interference term in the denominator.

Unfortunately, the improved definitions reduce the size of asymmetries. This disadvantage is unavoidable provided one is willing to extract in a clean way information on the twist-two and -three GPDs.

Now let us discuss in more detail the magnitude of the improved charge azimuthal asymmetries, defined in Eqs. (105-112) for the charge-odd and -even parts of the cross section, in dependence on the twist-two parametrizations and antiquark-gluon-quark correlations. For the twist-two sector, we present our estimates in Fig. 13 with the models A and C. As was mentioned above in section 7.2.2, in contrast to the $\sin(\phi)$ harmonic the size and the sign of the $\cos(\phi)$ term crucially depends on the parametrization of the valence- and sea-quark densities as well as the D-term contribution. According to our model, the sea quarks give a positive real part of $\mathcal{H}$, while the valence quarks

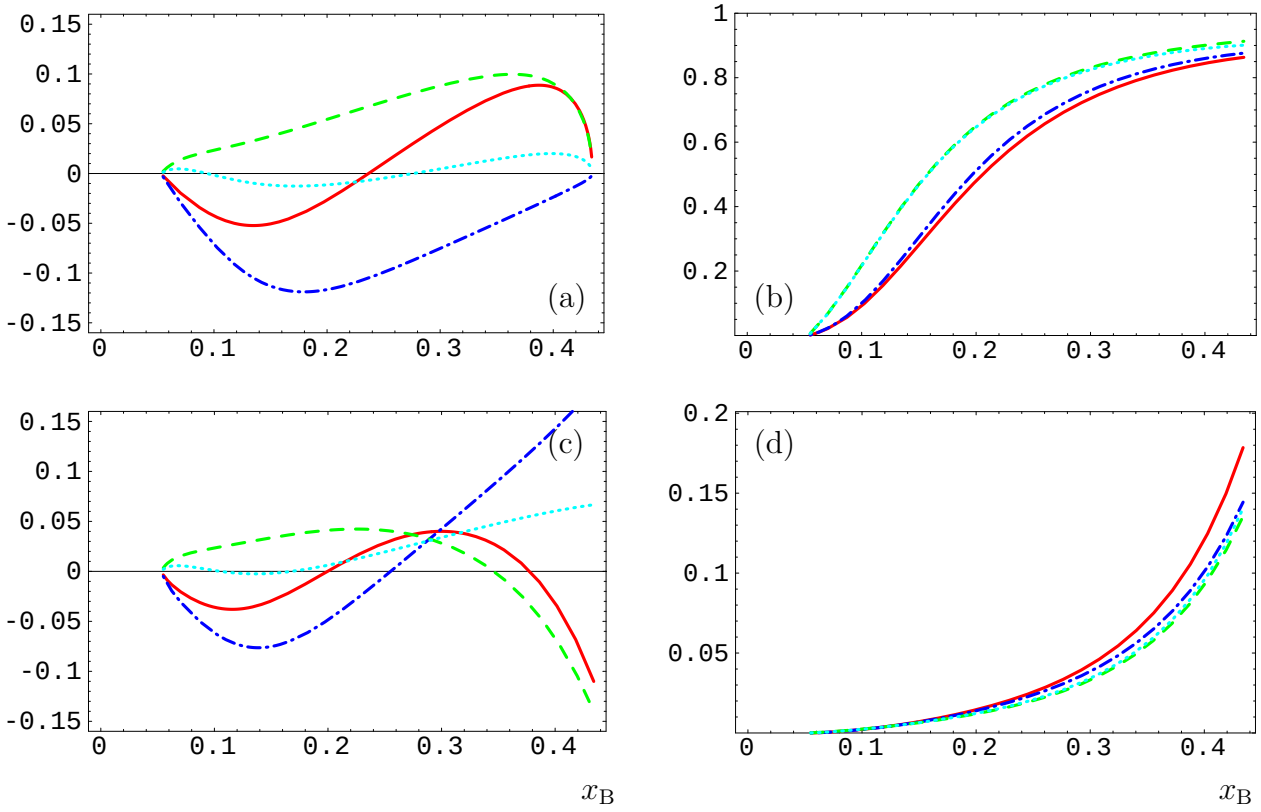

Figure 13: Azimuthal charge asymmetries of cos-harmonics $\mathrm{CoA}^{\mathrm{unp}}_{c(1)}$ (a), $\mathrm{CeA}^{\mathrm{unp}}_{c(0)}$ (b), $\mathrm{CoA}^{\mathrm{unp}}_{c(0)}$ (c), and $\mathrm{CoA}^{\mathrm{unp}}_{\Delta}$ (d) are plotted for $E_{\mathrm{beam}} = 27.6$ GeV, $\Delta^2 = -0.25$, and $\mathcal{Q}^2 = 2.5$ GeV^2. The model A (C) with the D-term, $B_{\mathrm{D}} = 5$ GeV^{-2}, and neglected one are displayed as dash-dotted (dotted) and solid (dashed) curves, respectively.

and D-term provide a negative effect. The $\mathrm{CA}^{\mathrm{odd}}_{c(1),\mathrm{unp}}$, plotted in panel (a), is now positive if it is dominated by the sea quarks, like in the model C without the D-term (dashed), contrary to all other cases. There is also a possibility that those contributions may compensate each other and this will lead to the almost vanishing asymmetry. Since the model C (dashed) is ruled out by the beam-spin measurement, we rather expect a sign alternating asymmetry [the model A without the D-term (solid)] or a negative one [the model A with $B_{\mathrm{D}} = 5$ GeV^{-2} (dash-dotted)]. Its magnitude can be of order of $\pm 10\%$, however, it can also be compatible with zero. In panel (b) we plot the leading twist-two asymmetry $\mathrm{CeA}^{\mathrm{unp}}_{c(0)}$, which shows that the BH amplitude dominates for small x_{B}. Also for HERMES there is a kinematical region in which the DVCS cross section overwhelms the BH one. This happens for the model A (B) at $x_{\mathrm{B}} \approx 0.2$ ($x_{\mathrm{B}} \approx 0.17$). The DVCS cross section only weakly depends on the D- and pion-pole term.

In Fig. 13 (c) we show the twist-three asymmetry $\mathrm{CoA}_{c(0),\mathrm{unp}}$, which can be rather sizeable, especially, at the kinematical boundary $\Delta_\perp \to 0$. The complexity of its shape partly emerges

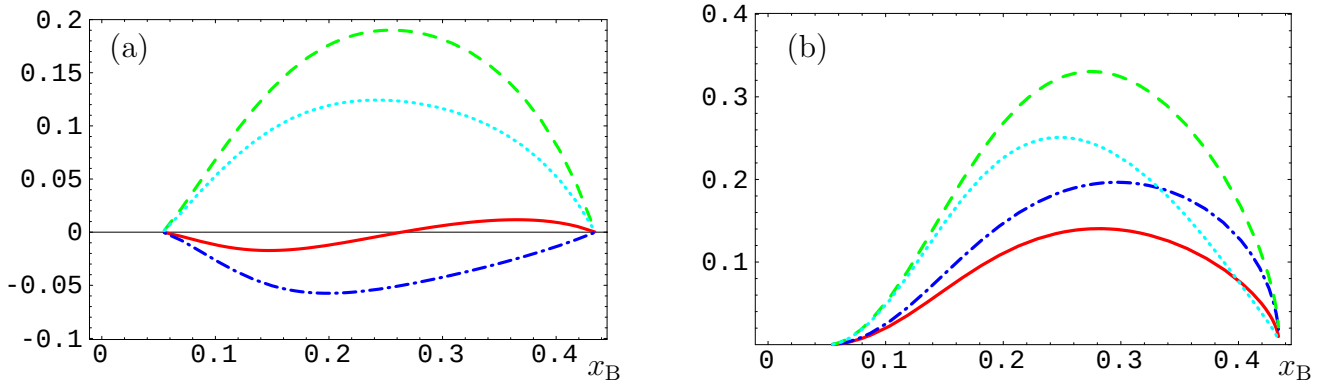

Figure 14: Twist-three azimuthal charge asymmetries of cos-harmonics $\mathrm{CoA}^{\mathrm{unp}}_{c(2)}$ (a) and $\mathrm{CeA}^{\mathrm{unp}}_{c(1)}$ (b) are plotted for the same kinematics as in Fig. 13. The model A with (without) the D-term in the WW-approximation and with the antiquark-gluon-quark correlation ($\phi^{qGq} = -\pi/3$) are displayed as dash-dotted (dotted) and solid (dashed) curves, respectively.

from the kinematical factors in Eq. (53). According to this equation and from the definition of the charge asymmetries in section 5.2.1, we have the constraint

$$\begin{aligned}\mathrm{CoA}^{\mathrm{unp}}_{\Delta} &\equiv \mathrm{CoA}^{\mathrm{unp}}_{c(0)} - \frac{\pi}{2}\frac{(1-x_{\mathrm{B}})(2-y)^3}{(2-2y+y^2)}\frac{-\Delta^2}{\mathcal{Q}^2 K}\left\{\left(1-\frac{\Delta^2_{\mathrm{min}}}{\Delta^2}\right) - \frac{(2-x_{\mathrm{B}})(1-y)}{(1-x_{\mathrm{B}})(2-y)^2}\right\}\mathrm{CoA}^{\mathrm{unp}}_{c(1)} \\ &= \frac{\pi}{2}\frac{(2-y)}{(2-2y+y^2)}\frac{\sqrt{-\Delta^2}}{\sqrt{\mathcal{Q}^2}K}(1-y)(2-x_{\mathrm{B}}) + \dots\,, \end{aligned} \tag{182}$$

where the ellipsis stand for terms generated by the addendum $\Delta\mathcal{C}^{\mathcal{I}}_{\mathrm{unp}}$, defined in Eq. (72). For large y this difference should vanish. Although, $\Delta\mathcal{C}^{\mathcal{I}}_{\mathrm{unp}}$ is suppressed by at least one power of x_{B}, we see in Fig. 13 (d) that it starts to be sizeable for $x_{\mathrm{B}} > 0.3$. This effect arises from the fact that for this kinematics in our model $|\widetilde{\mathcal{H}}| > |\mathcal{H}|$, and $\widetilde{\mathcal{H}}$ can contribute considerably both to $\mathrm{CA}^{\mathrm{odd}}_{c(1),\mathrm{unp}}$ and $\mathrm{CoA}^{\mathrm{unp}}_{c(0)}$. If one would measure a large deviation of $\mathrm{CoA}^{\mathrm{unp}}_{\Delta}$ from zero, it will indicate that $\Re\mathrm{e}\mathcal{H}$ is small and does not give the dominant contributions in the even harmonics.

Now we come to the dynamical twist-three effects, which show up in the charge asymmetries $\mathrm{CoA}^{\mathrm{unp}}_{c(2)}$ and $\mathrm{CeA}^{\mathrm{unp}}_{c(1)}$ displayed in Fig. 14 (a) and (b), respectively. In the WW-approximation with the model A (dash-dotted and solid curves) we find again the expected magnitude of asymmetries: the size of the charge-even asymmetry $\mathrm{CeA}^{\mathrm{unp}}_{c(1)}$ is larger than the twist-two charge-odd one $\mathrm{CoA}^{\mathrm{unp}}_{c(1)}$. Furthermore, we see that the shape of $\mathrm{CoA}^{\mathrm{unp}}_{c(2)}$ is correlated with the one of $\mathrm{CoA}^{\mathrm{unp}}_{c(1)}$. A large $\mathrm{CoA}^{\mathrm{unp}}_{c(2)}$ asymmetry can be generated by multi-parton correlation effects shown as dashed and dotted lines, respectively. Such correlation can even enhance the asymmetry $\mathrm{CeA}^{\mathrm{unp}}_{c(1)}$.

Let us add that the parameter dependence in the twist-two sector and twist-three effects for the polarized beam can also be discussed in a clear manner in terms of the charge asymmetries

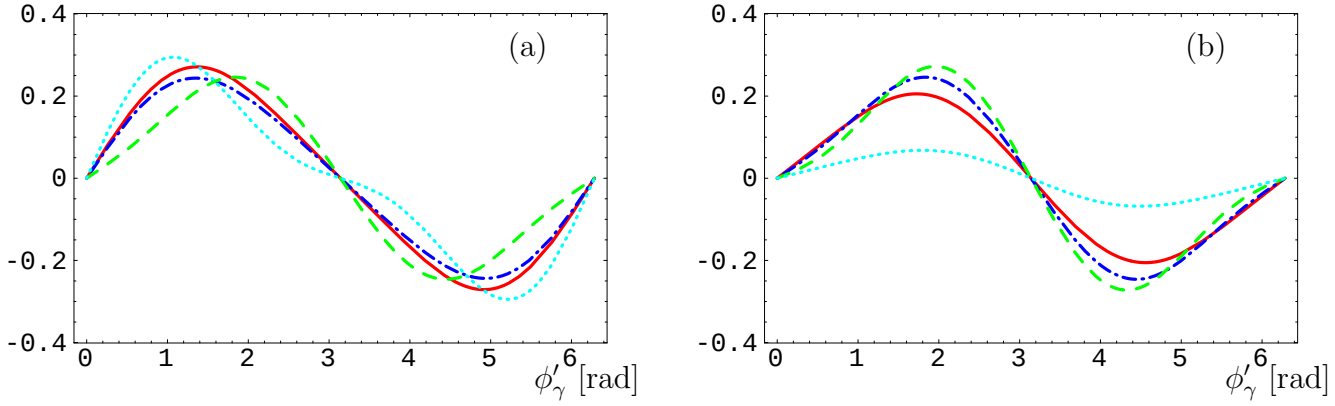

Figure 15: Estimates of the target spin asymmetry $A_{\rm UL}(\phi)$ for the E-01-113 experiment at Jefferson Lab [10] with the $E = 6$ GeV electron beam. Same models and kinematics as in Fig. 10 (a) and (b).

$\mathrm{CoA}^{\rm unp}_{s(1)}$, $\mathrm{CoA}^{\rm unp}_{s(2)}$, and $\mathrm{CeA}^{\rm unp}_{c(1)}$. However, since qualitatively they display the same effects as it has already been discussed for the beam-spin asymmetry in section 7.2.1, we will not repeat these considerations here.

7.3 Numerical estimates for longitudinally polarized target

Finally, we provide quantitative estimates for the cross sections of polarized electron scattering off the longitudinally polarized proton target. In these settings there are two further observables, which can be used to unravel GPDs from data.

The first one is the target-spin asymmetry with unpolarized lepton beam

$$A_{\rm UL}(\phi) = \frac{d\sigma^{\Uparrow}(\phi) - d\sigma^{\Downarrow}(\phi)}{d\sigma^{\Uparrow}(\phi) + d\sigma^{\Downarrow}(\phi)}\,, \tag{183}$$

where the up (down) arrow stands for $\Lambda = +(-)1$ longitudinal polarization. Completely analogous to the beam-spin asymmetry, the BH cross section cancels and one is left with the leading- and higher-twist contributions from the interference term and power-suppressed effects from the squared DVCS amplitude. From the explicit expressions for the Fourier coefficients one can qualitatively understand the magnitude of the asymmetry. For instance, comparing the main term in the asymmetry $\mathcal{C}^{\mathcal{I}}_{\rm LP}$, see Eq. (70), with $\mathcal{C}^{\mathcal{I}}_{\rm unp}$, previously analyzed in section 7.2.1, one observes that the CFF $\mathcal{H}$, dominating the latter at moderate and small $x_{\rm B}$, now enters the amplitude with an additional power of $x_{\rm B}$. It becomes parametrically of the same order as the parity-odd CFF $\widetilde{\mathcal{H}}$: $|\widetilde{\mathcal{H}}| \sim x_{\rm B}|\mathcal{H}|$. Thus both of them play a distinctive role in building up the nucleon-spin asymmetry which is displayed in Fig. 15 for the kinematics of the E-01-113 experiment at Jefferson Lab with

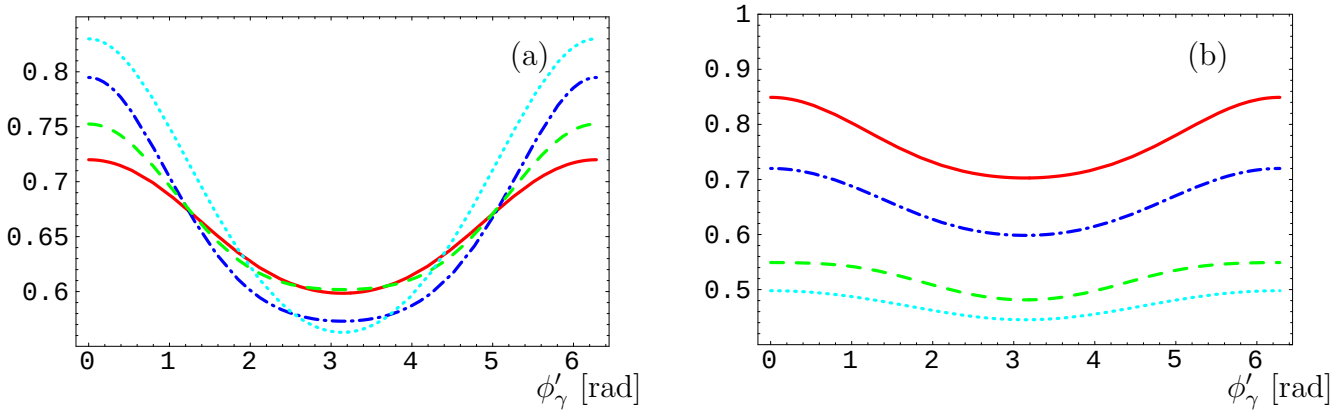

Figure 16: Estimates of the double spin asymmetry $A_{\rm LL}(\phi)$ for the E-01-113 experiment at Jefferson Lab [10] with a $E = 6$ GeV electron beam. Predictions for the model A (solid) with $B_{\rm D} = B_{\rm sea}$ in the WW-approximation and model B in the same approximation without D-term (dash-dotted) as well as with D-term and antiquark-gluon-quark contributions with $\phi^{qGq} = \pi$ (dashed) are plotted in (a) for $x_{\rm B} = 0.3$, $\Delta^2 = -0.25$, and $\mathcal{Q} = 2.5$ GeV^2. The dotted curve shows the BH contribution alone. In (b) we show the model A estimates for the same kinematics as in Fig. 10(b).

$E = 6$ GeV electron beam [10]. On the left panel (a) we give the estimates with the models A and B for the kinematical variables chosen as $x_{\rm B} = 0.3$, $\Delta^2 = -0.25$ GeV^2, and $\mathcal{Q}^2 = 2.5$ GeV^2. While on the panel (b) we display the asymmetry for several settings of the kinematical variables with the model B, which gave the best agreement with the unpolarized proton data.

The second interesting observable is the double lepton-nucleon spin asymmetry. The combination of the cross section which picks out only the $\lambda\Lambda$-part, bilinear in the nucleon and lepton helicity, is achieved by the following combination of the leptoproduction cross sections

$$A_{\rm LL}(\phi) = \frac{d\sigma^{\uparrow\Uparrow}(\phi) - d\sigma^{\downarrow\Uparrow}(\phi) - d\sigma^{\uparrow\Downarrow}(\phi) + d\sigma^{\downarrow\Downarrow}(\phi)}{d\sigma^{\uparrow\Uparrow}(\phi) + d\sigma^{\downarrow\Uparrow}(\phi) + d\sigma^{\uparrow\Downarrow}(\phi) + d\sigma^{\downarrow\Downarrow}(\phi)}\,. \tag{184}$$

Since the double-spin asymmetry is not protected from the contribution of the BH process, one expects that it overwhelms the DVCS signal inasmuch as it dominates the cross section for the CLAS kinematics. Indeed, this is what one finds in Fig. 16 (a), where the BH cross section alone generates a large asymmetry[13], displayed as dotted curve. Obviously, the interference and squared DVCS term produce a significant signal on its background. Due to rather good knowledge of the BH process its subtraction from the data should not present an obstacle of principle. However, what is more troublesome is the contamination of the asymmetry by the DVCS cross section and

[13]Note that we set in the asymmetry $A_{\rm LL}$ the DVCS amplitude in both the numerator and denominator to zero.

the fact that three CFFs, i.e., $\mathcal{H}$, $\widetilde{\mathcal{H}}$, and the pion-pole term of $\widetilde{\mathcal{E}}$, can contribute on the same footing to the interference term. This makes the disentanglement of separate components and, therefore, GPDs unmanageable from such an experiment alone. The expectations for the same kinematical settings as in Fig. 15 (b) are given in Fig. 16 (b) for the model A.

8 Summary and conclusions

Our present study has resulted into a complete analytical structure of the real-photon leptoproduction cross section with power accuracy. Although these results are quite complex, they allow for a qualitative discussion of observables in dependence of the kinematics and GPD parameters. Thus, in contrast to a purely numerical approach, our analysis tolerates a careful examination of experimental data. The most accurate information on GPDs can be deduced from the part of the total cross section, which stems from the interference of the BH process with the DVCS amplitude. The main tool of experimental exploration of the latter is the use of diverse asymmetries involving charge and spin.

The leading contributions in the light-cone expansion of the DVCS amplitude give access to diverse properties of the nucleon constituents due to a non-zero orbital momentum carried by them. These include, the parton angular momentum, the helicity-flip polarized glue uncontaminated by quarks, the pion cloud of the proton etc., just to name a few.

Twist expansion of the DVCS amplitude finds its reflection in the dependence of the cross section on the azimuthal angle of the outgoing real photon (or recoiled proton). One of the main results of our analysis is the finding that the Fourier harmonics of the separate charge-even and -odd components of the complete cross section, expressed in terms of the lowest-twist GPDs, stay uncontaminated even if $1/\mathcal{Q}$-power effects are switched on. Thus, power corrections to the Fourier coefficients will be suppressed by $1/\mathcal{Q}^2$. This gives a hope for a clean exploration of individual contributions, provided the same settings will become available in experiments. This can be achieved by a combining use of charge and spin asymmetries together with a precise extraction of different Fourier coefficients. These procedures enable a separate measurement of all coefficients of the interference and squared DVCS term. Extraction of the latter requires the subtraction of the squared BH amplitude from data.

For a lepton beam with a definite charge, high precision data may also result into a separation of the interference and squared DVCS terms made feasible by a Fourier analysis. Albeit, in this case the leading twist $\cos(\phi)/\sin(\phi)$ dependence in the cross section, stemming from the interference term, gets corrected by the twist-three contribution of the squared DVCS amplitude.

The magnitude of higher-order corrections strongly depends on the models assumed for GPDs.

The minimization of the radiative effects is possible within the so-called DVCS scheme. It is defined by the condition of absorption of gluonic higher-order corrections into the factorization scale, dividing short and long distances. This procedure results into a moderate modification of LO predictions, advocating the neglect of NLO terms for a crude estimate. Once a more accurate data will become available, a NLO analysis, similar to the one that is customarily performed nowadays for deeply inelastic scattering, will be necessary. Moreover, by measuring the scale dependence at small $x_{\rm B}$, one can get a deeper insight into the structure of gluonic GPDs.

There are several theoretical problems that should be answered in the future.

The most crucial one is the magnitude of higher-twist corrections, especially, of the target mass corrections. Let us mention that the resummation of target mass effects from the twist-two operators performed in Ref. [17] takes into account only a part of the entire tower of mass corrections, which are generated also by multi-particle operators in the off-forward Compton amplitude. They can be transformed into operators containing total derivatives by means of QCD equations of motion. Therefore, at any given nth order in the mass expansion, operators up to twist-n will contribute to the total correction. Therefore, the resummation cannot be handled in this situation, and it is sensible to address the problem order by order in the hadron mass.

A deeper insight into the structure of perturbative series can be achieved by means of conformal symmetry [71, 18]. This formally requires to set the QCD β-function to zero and to choose a special renormalization scheme, the so-called conformal scheme. With these simplifications the Wilson coefficients of deeply inelastic scattering, known in next-to-next-to-leading order (NNLO), allow a numerical evaluation of the twist-two DVCS amplitude to NNLO in the valence quark region. Moreover, the corrections proportional to the β-function have been calculated to the same order and can, therefore, be taken into account [72].

If experiments can measure twist-three effects, one certainly needs their better theoretical understanding. Let us mention that the LO evolution of the antiquark-gluon-quark GPDs is governed by known two-particle kernels. Since the one-loop corrections to the short distance twist-two coefficient functions are important, one could anticipate that NLO effects can be as sizable in the twist-three amplitudes. This requires a detailed study of radiative corrections to the latter along the line similar to the computations done for the transversely polarized structure function g_2 of deeply inelastic scattering in Refs. [73, 74, 75, 76].

After these issues are addressed, their consequences and impact on the amplitudes have to be quantitatively analyzed in order to demonstrate the regions of the phase space, which are less sensitive to their presence and where an accurate determination of the parameters of the twist-two and -three GPDs can be performed. Of course, such studies are model-dependent. Thus, one should incorporate as much as possible information from perturbative QCD. This requires

modeling the GPDs at a low normalization point, e.g., $\mathcal{Q}_0 \sim 0.5$ GeV, and their evolution upwards to experimental scales.

In the most favorable situation, which means high enough $\mathcal{Q}^2$ required to discard power suppressed contributions and limit the analysis to the twist-two approximation in LO, the imaginary part of DVCS with real photon can give access to the GPDs on the diagonal $x = \pm\xi$ only, i.e., it becomes a function of a single scaling variable $F(\xi, \xi, \Delta^2)$. The only way one can measure it as a function of two variables, momentum fraction and skewedness, is in the deeply leptoproduction (virtual photoproduction) of a lepton pair,

$$N\gamma^\star \to N'\gamma^\star \to N'\ell\bar{\ell}\,,$$

since the generalized Bjorken variable and skewedness are independent in this case, $\xi \neq \eta$.

To conclude, experimental facilities having electron and positron beams is an ideal place to disentangle and study GPDs, and, thus, to extract fundamental information about the spin structure of the nucleon. However, if one of them is not available, an accurate measurement with high momentum transfer probes will serve the purpose and will result into systematic tests of our understanding of the quark-gluon content of the nucleon.

Acknowledgements

We would like to thank S. Stepanyan for providing us experimental data on the DVCS measurement with CLAS and communications on the Jefferson Lab experiment E-01-113, and H. Avakian for help to access the HERMES data on the beam-spin asymmetry in DVCS. We are grateful to M. McDermott, M. Diehl, A. Freund, W.D. Nowak, A.V. Radyushkin, A. Schäfer, and M. Vanderhaeghen for discussions. This work was supported by the US Department of Energy under contract DE-FG02-93ER40762 (A.B.) and Studienstiftung des deutschen Volkes (A.K.). A.B. would like to thank the theory group at the University of Wuppertal for its hospitality.

References

[1] D. Müller, D. Robaschik, B. Geyer, F.M. Dittes, J. Hořejši, Fortsch. Phys. 42 (1994) 101.

[2] X. Ji, Phys. Rev. Lett. 78 (1997) 610.

[3] X. Ji, J. Phys. G 24 (1998) 1181.

[4] A.V. Radyushkin, Phys. Rev. D 56 (1997) 5524.

[5] J.C. Collins, L.L. Frankfurt, M. Strikman, Phys. Rev. D 56 (1997) 2982.

[6] M. Airapetian, et al. (HERMES Coll.), Phys. Rev. Lett. 87 (2001) 182001.

[7] P.R.B. Saull (ZEUS Coll.), *Prompt photon production and observation of deeply virtual Compton scattering*, hep-ex/0003030.

[8] C. Adloff et al. (H1 Coll.), Phys. Lett. B 517 (2001) 47.

[9] S. Stepanyan et al. (CLAS Coll.), Phys. Rev. Lett. 87 (2001) 182002.

[10] V. Burkert, L. Elouadrhiri, M. Garçon, S. Stepanyan (CLAS Coll.), *Deeply virtual Compton scattering with CLAS at 6 GeV*, E-01-113.

[11] J.P. Chen et al. (Hall A Jefferson Lab), *Deeply virtual Compton scattering at 6 GeV*, PCCF-RI-0013.

[12] V.A. Korotkov, W.D. Nowak, *Future measurements of deeply virtual Compton scattering at HERMES*, hep-ph/0108077;
W.D. Nowak, *European perspectives for electron-nucleon scattering at the luminosity frontier*, hep-ph/0111218.

[13] A.V. Belitsky, A. Kirchner, D. Müller, A. Schäfer, Phys. Lett. B 510 (2001) 117;
A.V. Belitsky, A. Kirchner, D. Müller, *Spin effects in deeply virtual Compton scattering*, hep-ph/0106228;
A.V. Belitsky, D. Müller, *Overview of deeply virtual Compton scattering*, hep-ph/0111037.

[14] A.V. Belitsky, D. Müller, Nucl. Phys. B 589 (2000) 611.

[15] N. Kivel, M.V. Polyakov, M. Vanderhaeghen, Phys. Rev. D 63 (2001) 114014.

[16] K. Goeke, M.V. Polyakov, M. Vanderhaeghen, Prog. Part. Nucl. Phys. 47 (2001) 401.

[17] A.V. Belitsky, D. Müller, Phys. Lett. B 507 (2001) 173.

[18] A.V. Belitsky, D. Müller, Phys. Lett. B 417 (1998) 129.

[19] X. Ji, J. Osborne, Phys. Rev. D 58 (1998) 094018.

[20] L. Mankiewicz, G. Piller, E. Stein, M. Vänttinen, T. Weigl, Phys. Lett. B 425 (1998) 186.

[21] A.V. Belitsky, D. Müller, Nucl. Phys. B 537 (1998) 397.

[22] A.V. Belitsky, A. Freund, D. Müller, Nucl. Phys. B 574 (2000) 347.

[23] A.V. Belitsky, D. Müller, L. Niedermeier, A. Schäfer, Phys. Lett. B 474 (2000) 163; Czech. J. Phys. 50/S1 (2000) 123.

[24] A. Freund, M.F. McDermott, *A next-to-leading order analysis of deeply virtual Compton scattering*, hep-ph/0106124.

[25] A. Freund, M.F. McDermott, *A next-to-leading order QCD analysis of deeply virtual Compton scattering amplitudes*, hep-ph/0106319; *A detailed next-to-leading order QCD analysis of deeply virtual Compton scattering observables*, hep-ph/0111472.

[26] M. Pentinen, M.V. Polyakov, A.G. Shuvaev, M. Strikman, Phys. Lett. B 491 (2000) 96.

[27] I.V. Anikin, B. Pire, O.V. Teryaev, Phys. Rev. D 62 (2000) 071501.

[28] A.V. Radyushkin, C. Weiss, Phys. Rev. D 63 (2001) 114012.

[29] C. Itzykson, J. Zuber, Quantum Field Theory, McGraw-Hill, (New York, 1980).

[30] A.P. Bukhvostov, G.V. Frolov, L.N. Lipatov, E.A. Kuraev, Nucl. Phys. B 258 (1985) 601.

[31] F.-M. Dittes, B. Geyer, D. Müller, D. Robaschik, J. Hořejši, Phys. Lett. B 209 (1988) 325.

[32] N. Kivel, M.V. Polyakov, Nucl. Phys. B 600 (2001) 334.

[33] A.V. Belitsky, D. Müller, A. Kirchner, A. Schäfer, Phys. Rev. D 64 (2001) 116002.

[34] N. Kivel, M.V. Polyakov, A. Schäfer, O.V. Teryaev, Phys. Lett. B 497 (2001) 73.

[35] I.V. Anikin, O.V. Teryaev, Phys. Lett. B 509 (2001) 95.

[36] I.V. Anikin, D. Binosi, R. Medrano, S. Noguera, V. Vento, *Single spin asymmetry parameter from DVCS of hadrons up to twist-three accuracy: pion case*, hep-ph/0109139.

[37] M. Diehl, Eur. Phys. J. C 19 (2001) 485.

[38] P. Hoodbhoy, X. Ji, Phys. Rev. D 58 (1998) 054006.

[39] A.V. Belitsky, D. Müller, Phys. Lett. B 486 (2000) 369.

[40] P. Kroll, M. Schürmann, P.A.M. Guichon, Nucl. Phys. A 598 (1996) 435.

[41] E.R. Berger, M. Diehl, B. Pire, *Time-like Compton scattering: exclusive photoproduction of lepton pairs*, hep-ph/0110062.

[42] M. Diehl, T. Gousset, B. Pire, J.P. Ralston, Phys. Lett. B 411 (1997) 193.

[43] A.V. Belitsky, D. Müller, L. Niedermeier, A. Schäfer, Nucl. Phys. B 593 (2001) 289.

[44] N. Kivel, L. Mankiewicz, Eur. Phys. J. C 21 (2001) 621.

[45] A. Freund, Phys. Lett. B 472 (2000) 412.

[46] J. Balla, M.V. Polyakov, C. Weiss, Nucl. Phys. B 510 (1998) 327.

[47] B. Geyer, D. Robaschik, M. Bordag, J. Hořejši, Z. Phys. C 26 (1985) 591.

[48] J. Breitweg et al. (ZEUS Coll.), Eur. Phys. J. C 6 (1999) 603.

[49] V.M. Braun, P. Górnicki, L. Mankiewicz, A. Schäfer, Phys. Lett. B 302 (1993) 291.

[50] M. Burkardt, Phys. Rev. D 62 (2000) 071503.

[51] J.P. Ralston, B. Pire, *Femto-photography of protons to nuclei with deeply virtual Compton scattering*, hep-ph/0110075.

[52] O.V. Teryaev, Phys. Lett. B 510 (2001) 125.

[53] M.V. Polyakov, C. Weiss, Phys. Rev. D 60 (1999) 114017.

[54] M. Diehl, T. Feldmann, R. Jakob, P. Kroll, Nucl. Phys. B 596 (2001) 33;
S.J. Brodsky, M. Diehl, D.S. Hwang, Nucl. Phys. B 596 (2001) 99.

[55] A.V. Radyushkin, Phys. Lett. B 449 (1999) 81.

[56] P.A.M Guichon, M. Vanderhaeghen, Prog. Part. Nucl. Phys. 41 (1998) 125;
M. Vanderhaeghen, P.A.M Guichon, M. Guidal, Phys. Rev. D 60 (1999) 094017.

[57] V.Yu. Petrov, P.V. Pobylitsa, M.V. Polyakov, I. Bornig, K. Goeke, C. Weiss, Phys. Rev. D 57 (1998) 4325.

[58] A.D. Martin, R.G. Roberts, W.J. Stirling, Phys. Lett. B 354 (1995) 155.

[59] N. Mathur, S.J. Dong, K.F. Liu, L. Mankiewicz, N.C. Mukhopadhyay, Phys. Rev. D 62 (2000) 114504.

[60] I.I. Balitsky, X. Ji, Phys. Rev. Lett. 79 (1997) 1225.

[61] T. Gehrmann, W.J. Stirling, Phys. Rev. D 53 (1996) 6100.

[62] L.B. Okun, *Leptons and quarks*, North-Holland, (Amsterdam, 1982).

[63] M. Penttinen, M.V. Polyakov, K. Goeke, Phys. Rev. D 62 (2000) 014024.

[64] I.I. Balitsky, E. Kuchina, Phys. Rev. D 62 (2000) 074004.

[65] A.G. Shuvaev, K.J. Golec-Biernat, A.D. Martin, M.G. Ryskin, Phys. Rev. D 60 (1999) 014015.

[66] A. Hebecker, T. Teubner, Phys. Lett. B 498 (2001) 16.

[67] A.V. Belitsky, D. Müller, L. Niedermeier, A. Schäfer, Nucl. Phys. B 546 (1999) 279.

[68] A.D. Martin, R.G. Roberts, W.J. Stirling, R.S. Thorne, Eur. Phys. J. C 4 (1998) 463.

[69] L.L. Frankfurt, A. Freund, M. Strikman, Phys. Rev. D 58 (1998) 114001, (E) D 59 (1999) 119901E.

[70] A. Donnachie, H.G. Dosch, Phys. Lett. B 502 (2001) 74.

[71] D. Müller, Phys. Rev. D 58 (1998) 054005.

[72] A.V. Belitsky, A. Schäfer, Nucl. Phys. B 527 (1998) 235,

[73] X. Ji, W. Lu, J.A. Osborne, X. Song, Phys. Rev. D 62 (2000) 094016.

[74] A.V. Belitsky, X. Ji, W. Lu, J.A. Osborne, Phys. Rev. D 63 (2001) 094012.

[75] V.M. Braun, G.P. Korchemsky, A.N. Manashov, Nucl. Phys. B 597 (2001) 370.

[76] X. Ji, J.A. Osborne, Nucl. Phys. B 608 (2001) 253.